February 5, 1969

To the Graduate Council:

I am submitting herewith a dissertation written by Ronald Nutt entitled "A Study of a NaI(Tℓ) Scintillator-Photomultiplier Timing System." I recommend that it be accepted in partial fulfillment of the requirements for the degree of Doctor of Philosophy, with a major in Electrical Engineering.

J. F. Pierce
Major Professor

We have read this dissertation
and recommend its acceptance:

John C. Biggerstaff

Z. Vaughn Blalock

L. H. Turner

J. W. Wallace

W. E. Deeds

Accepted for the Council:

Sutton A. Smith
Vice Chancellor for
Graduate Studies and Research

A STUDY OF A NaI(Tl) SCINTILLATOR-PHOTOMULTIPLIER TIMING SYSTEM

A Dissertation

Presented to

the Graduate Council of

The University of Tennessee

In Partial Fulfillment

of the Requirements for the Degree

Doctor of Philosophy

---

by

Ronald Nutt

March 1969

ACKNOWLEDGMENT

This research was performed at the Oak Ridge National Laboratory under the sponsorship of the U. S. Atomic Energy Commission under contract with Union Carbide Corporation.

The author is particularly indebted to his Major Professor, Dr. J. F. Pierce, and to Mr. C. J. Borkowski, Director of the Instrumentation and Controls Division of the Oak Ridge National Laboratory. The assistance of the entire staff of the Van de Graaff Laboratory where the research was conducted is deeply appreciated.

The author wishes to thank Dr. J. A. Biggerstaff for suggesting the thesis topic and for the many stimulating discussions during the course of this research.

A special note of appreciation is due my wife, Robbie, who patiently and skillfully typed the rough draft of the thesis.

861776

ABSTRACT

The timing resolution of a system composed of a NaI(Tℓ) scintillator and photomultiplier was studied. A model was developed to describe the timing resolution in terms of the probability density function of the photon transit time in the crystal and the electron transit time from the cathode to the anode of the photomultiplier. The timing resolution as a function of the individual system parameters was calculated and compared with experimental data to demonstrate the validity of the model.

The theoretical limit in time resolution for a small NaI(Tℓ) crystal and an ideal photomultiplier was established. The method is shown to be valid for a more practical scintillator-photomultiplier system.

TABLE OF CONTENTS

CHAPTER		PAGE
I.	INTRODUCTION	1
	Background	1
	Scope of the Thesis	5
II.	THE NaI(Tℓ) SCINTILLATOR TIMING CHARACTERISTICS	7
	Timing Characteristics of an Infinitesimally Small NaI(Tℓ) Scintillator	7
	Evidence of a single exponential decay in NaI(Tℓ)	7
	Order statistics for a single exponential probability density function	14
	First and second moment calculations for the single exponential case	22
	Theoretical Limit of the Time Resolution for the Single Exponential Case	28
	Photon Transit Time Calculations	34
	Computer program	34
	Summary of the photon transit time calculations	40
III.	PHOTOMULTIPLIER CHARACTERISTICS	54
	Sources of Time Variance	54
	Difference in photoelectron transit times for different generation points on the cathode	55
	Fluctuation in photoelectron transit times due to initial velocity differences	62
	Uncertainty in transit times of secondary electrons from the dynodes	66

CHAPTER PAGE

Photoelectron Yield of the Cathode 74

IV. TIMING CHARACTERISTICS OF THE SCINTILLATOR AND PHOTOMULTIPLIER SYSTEM 83

System's Response to Single Detected Photons 83

Influence of the Individual Parameters on the Time Resolution of the System 89

The influence of crystal size on time resolution . . . 90

The influence of the difference in photoelectron transit times for different generation points on the cathode 93

The influence of the fluctuation in photoelectron transit times due to initial velocity differences . . 94

The influence of the photoelectron yield on the time resolution 96

The influence of the detection level on time resolution 99

Time Resolution Measurement Techniques 101

Experimental Results 108

V. SUMMARY AND SUGGESTIONS FOR FURTHER STUDY 123

Summary 123

Suggestions for Further Study 126

CHAPTER PAGE

LIST OF REFERENCES 129

APPENDIXES 133

A. CALCULATION OF THE VARIANCE OF THE Jth PHOTOELECTRON FOR A SINGLE EXPONENTIAL DISTRIBUTION FUNCTION 134

B. COMPUTER PROGRAM LISTING FOR THE PHOTON TRANSIT TIME CALCULATIONS 140

C. CALCULATION OF THE WEIGHT OF THE REFLECTED AND TRANSMITTED LIGHT OF AN UNPOLARIZED PLANE WAVE 154

D. COMPUTER PROGRAM LISTING FOR THE PHOTOMULTIPLIER-SCINTILLATOR ORDER STATISTICS 159

VITA 166

LIST OF FIGURES

FIGURE		PAGE
1.	A Typical Neutron Time-of-Flight System	2
2.	The Bollinger-Thomas Technique for Measuring Scintillation Decay Time	9
3.	Block Diagram of the System Used to Measure the Shape of NaI(Tℓ) Scintillation Decay	11
4.	A Measured Probability Density Function of the NaI(Tℓ) Scintillator	12
5.	The Response of a Charge Sensitive System to an Ideal Photomultiplier Pulse	15
6.	The Probability Density Function for the First Eight Photoelectrons Where R = 100	21
7.	Standard Deviation in Time Versus Photoelectron Level for a Single Exponential Decay	27
8.	The Coordinate System and Dimensions of the Cylindrical Crystal Used in the Monte Carlo Calculations	35
9.	Computer Printout Showing a Typical Histogram of a Probability Density Function	39
10.	Probability Density Function of the Photon Path Length for a Crystal with Dimensions H = 0.6, r = 1	41
11.	Probability Density Function of the Photon Path Length for a Crystal with Dimensions H = 0.8, r = 1	42

FIGURE PAGE

12. Probability Density Function of the Photon Path Length for a Crystal with Dimensions H = 1, r = 1 43

13. Probability Density Function of the Photon Path Length for a Crystal with Dimensions H = 1.4, r = 1 44

14. Probability Density Function of the Photon Path Length for a Crystal with Dimensions H = 2.0, r = 1 45

15. Standard Deviation of Photon Path Length Versus Height-to-Radius Ratio of the Crystal 47

16. Probability Density Function of the Photon Path Length for a Crystal with Dimensions H = 1, r = 1 48

17. Probability Density Function of the Photon Path Length for a Crystal with Dimensions H = 2, r = 1 49

18. Standard Deviation of Photon Path Length Versus Index of Refraction Ratio of the Exit Window 51

19. Standard Deviation and Mean Photon Path Length Versus Position of Photon Generation 52

20. Block Diagram of System Used for Measuring the Photocathode Transit Time Difference 56

21. Transit Time Delay Versus Distance from Center of the RCA 8575 Photocathode 57

22. Transit Time Delay Versus Distance from Center of the XP-1020 Photocathode 58

FIGURE PAGE

23. Transit Time Delay Versus Distance from Center of the XP-1040 Photocathode 59

24. System for Measuring the Transit Time Distribution for a Photomultiplier 64

25. A Typical Transit Time Distribution for the RCA 8575 Photomultiplier 67

26. A Typical Transit Time Distribution for the XP-1020 Photomultiplier 68

27. System for Measuring Photoelectron Yield in NaI(Tℓ) 77

28. Block Diagram of a Scintillator and Photomultiplier System Showing the Individual Sources of Time Variance . . 84

29. Typical Shape of a Time Distribution Function Calculated for the RCA-8575 Photomultiplier and a Crystal Height of One Inch 91

30. Calculated Time Resolution Versus Crystal Height 92

31. Calculated Time Resolution Versus the Photocathode Transit Time Difference Parameter, K 95

32. Calculated Time Resolution Versus the Transit Time Parameter K_1 97

33. Calculated Time Resolution Versus the Photoelectron Yield 98

34. Calculated Time Resolution Versus Photoelectron Level . . . 100

35. The Optimum Photoelectron Detection Level Versus the Scintillator Decay Time 102

FIGURE PAGE

36. A Measured Amplitude Noise Spectrum for a Typical RCA-8575 Photomultiplier 103

37. Block-Diagram of a Two-Level Recognization Scheme 105

38. Schematic of a Two-Level Electronic Discriminator 107

39. System for Measuring the Time Resolution of the NaI(Tℓ) Scintillator and Photomultiplier System 109

40. Comparison of the Measured and Calculated Time Distribution for a Crystal with h = 1 112

41. Comparison of the Measured and Calculated Time Distribution for a Crystal with h = 2 113

42. Comparison of the Measured and Calculated Time Distribution for a Crystal with h = 3 114

43. Comparison of the Measured and Calculated Time Distribution for a Crystal with h = 4 115

44. Time Resolution Versus Crystal Height Using the RCA-8575 Photomultiplier 117

45. Time Resolution Versus Crystal Height Using the XP-1020 Photomultiplier 118

46. Comparison of the Measured and Calculated Time Resolution as a Function of Photoelectron Yield 119

47. Photoelectron Level Versus Potentiometer Setting for the Low Level Discriminator 120

48. Comparison of Calculated and Measured Time Resolution as a Function of Photoelectron Level 121

FIGURE PAGE

49. Reflection and Refraction of a Plane Polarized Wave with Electric Field Parallel to the Incident Plane 155

CHAPTER I

INTRODUCTION

I. BACKGROUND

The use of a sodium iodide scintillator and photomultiplier in a time-of-flight system has been described by Neiler and Good[1] and also by Rae and Bowery.[2] The NaI(Tℓ) crystal detects the gamma rays resulting from the neutron bombardment of boron in the time-of-flight system. A schematic of the system is shown in Figure 1 which illustrates the use of a pulsed accelerator for generating neutrons. The objective of a time-of-flight experiment is usually to measure the neutron energy. The objective is accomplished by measuring the flight time of the neutrons along a prescribed path. The use of NaI(Tℓ) in other timing experiments has advantages over gamma ray detectors of other types[3,4], but the time-of-flight system is sufficient for illustrating the desired properties of the detector.

The background radiation level in the vicinity of a time-of-flight system, as shown in Figure 1, is often very high. A desirable characteristic of the detector is that it be able to distinguish to some extent between the background and the signal. The NaI(Tℓ) scintillator detects the 478-Kev gamma rays resulting from the reaction $B^{10}(n,\alpha\gamma)$ and establishes the time of arrival of the neutrons. Since the NaI(Tℓ) scintillator has a pulse height resolution of better than 10 percent at

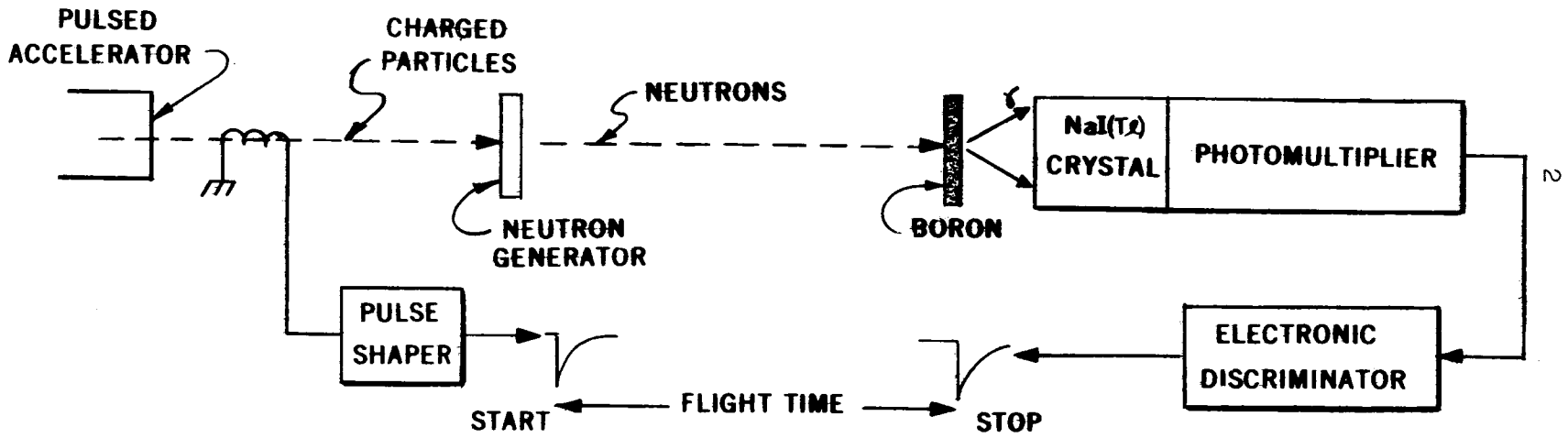


Figure 1. A typical neutron time-of-flight system.

the 478-keV gamma ray energy,[5] discrimination against much of the background can be achieved.

Another desirable characteristic of the detector is a high gamma ray detection efficiency. To achieve a high detection efficiency, the volume of the NaI(Tℓ) is usually in the order of several hundred to a few thousand cubic centimeters. Although the pulse height resolution is not degraded appreciably because of the large volume,[6] some of the information about the initial time of a scintillation event is lost. The loss of timing information in the large detector is due to the differences in photon transit times from the generation points to the photocathode.[7] This timing difference, in addition to the differences in the photon generation time, limits the amount of timing information available from the detector. One of the objectives of this thesis is to determine the limitation imposed by the photon transit time on the overall time resolution of the system.

Several sources of time variance are known to exist in the photomultiplier.[8,9,10] As a general rule the sources are divided into three classes. One source occurs because electrons which originate at different points on the photocathode have different transit times to the first dynode. This source of time variance is due primarily to geometrical problems at the photocathode. Another source of time variance is associated with the different velocities that electrons have as they emerge from the photocathodes. A third source occurs because of the variance associated with the multiplication process of the dynodes.

Gatti and Svelto[9] first described the time characteristics of photomultipliers in terms of the shape of the current pulse appearing at the anode as a result of the single electron response (SER). This approach has gained wide acceptance in predicting the photomultiplier response to fast scintillators. In a later paper Gatti and Svelto[11] included with the SER the effect of transit time variance of the electrons from the photocathode and performed several Monte Carlo[12] computer calculations to determine the response of the system. In the computer calculations the basic assumption was that the number of photoelectrons generated in a time interval Δt follows a Poisson distribution. With the assumption of Poisson statistics the authors also attempted an analytical treatment of the system in which the multiplication process was assumed to be a delta function in time.

El-Wahab and Kane[10] also approached the photomultiplier system from an analytical viewpoint. The assumption of Poisson statistics made by Gatti and Svelto do not appear in this treatment; however, the assumption of a delta function in time of the multiplication process is inferred beyond the first dynode. The results, assuming a single exponential distribution function, are presented in closed form and appear to represent the correct mathematical treatment of the processes involved. When a second distribution is considered, namely the transit time distribution convoluted with the distribution of light from the crystal, the result is not simple. In fact, the result is a sum of N-1 complicated terms where N is the number of photoelectrons resulting from a scintillation event.

The single electron approach introduced by Gatti and Svelto together with the analysis presented by El-Wahab and Kane represent a significant advancement in understanding the timing characteristics of the detector system, although the results of the analysis are lacking in simplicity and in general applicability.

II. SCOPE OF THE THESIS

The objectives of this thesis are:

1. To develop the statistical equations needed for describing the timing characteristics of a photomultiplier-scintillator system.

2. To characterize the transit time distribution of the photons inside a cylindrical crystal.

3. To determine experimentally the transit time distribution between photocathode and first dynode for some of the fast photomultipliers, and also the distribution resulting from the geometrical problems of the photocathode.

4. To apply the statistical equations using the results of objectives 2 and 3 to describe the timing characteristics of the NaI(Tℓ) detector.

The first part of Chapter II presents the analysis of a single exponential distribution function using the concept of order statistics. The analysis is expanded to a general case including any number of cascaded distribution functions. The second part of Chapter II presents the Monte Carlo calculations of the photon transient times inside the crystal.

Chapter III presents the experimental investigation of the photoelectron transit time distribution and the time distribution due to the photocathode geometry problems. In addition, this chapter contains both a discussion of the techniques used to determine the photoelectron yield of NaI(Tℓ) and also the introduction of a new technique which is used in Chapter IV.

Chapter IV presents the calculation pertaining to the NaI(Tℓ) scintillator and the photomultiplier as a system. A comparison is made between the results of these calculations and the experimental results obtained by using several crystals having different sizes.

Chapter V includes a summary of the thesis and suggestions for further study.

CHAPTER II

THE NaI(Tℓ) SCINTILLATOR TIMING CHARACTERISTICS

In this chapter the timing information available from a NaI(Tℓ) scintillator is determined. In Section I the scintillator is assumed to be infinitesimally small so that the photon generation statistics determine the timing characteristics of the scintillator. Furthermore, the photocathode is assumed to be an ideal photon-to-electron converter which introduces no additional time variance to the system. The mean electron generation time and the variance in the electron generation time at the photocathode are calculated for the ideal system using the concept of order statistics. In Section II a mathematical procedure for determining the lower limit on the time variance of a system is presented. The procedure is applied to the ideal system defined in Section I. In Section III the calculation of the distribution of photon transit times in a cylindrical crystal is presented.

I. TIMING CHARACTERISTICS OF AN INFINITESIMALLY SMALL NaI(Tℓ) SCINTILLATOR

Evidence of a Single Exponential Decay in NaI(Tℓ)

In the NaI(Tℓ) scintillator at least three basic mechanisms are responsible for the photon generation.[13] All three processes produce the same pulse shape, but not the same light amplitude. The pulse shape of the light is the most important parameter in determining the time

resolution of the scintillator. In more precise terms, the rate of photon generation as a function of time is the important relationship in the study of the timing properties of the scintillator. If the scintillation event is composed of R independent photons, then the rate of photon generation as a function of time is simply the unnormalized probability-per-unit time that a single photon will be generated at time t. This function is usually referred to as the probability density function (p.d.f.). The importance of the p.d.f. will be more evident after the function is used to determine the important characteristics of the system.

Bollinger and Thomas[14] devised a technique for measuring the p.d.f. for individual photoelectrons from a scintillation event. A diagram demonstrating this technique is shown in Figure 2. Many photoelectrons are associated with a single scintillation event, each of which has the same p.d.f. in time. The total probability-per-unit time that a photoelectron will be generated at time t is

$$P_T = \sum_{i=1}^{R} P_i \quad , \tag{1}$$

where P_i is the p.d.f. for a single photoelectron and R is the total number generated per event. The density function P_T can be measured by repeating a multiple time-sampling of the photoelectrons from a single event or by sampling once per event for a number of events. The latter technique is based on the assumption that the p.d.f. does not change from event to event. The Bollinger-Thomas technique (Figure 2) is based

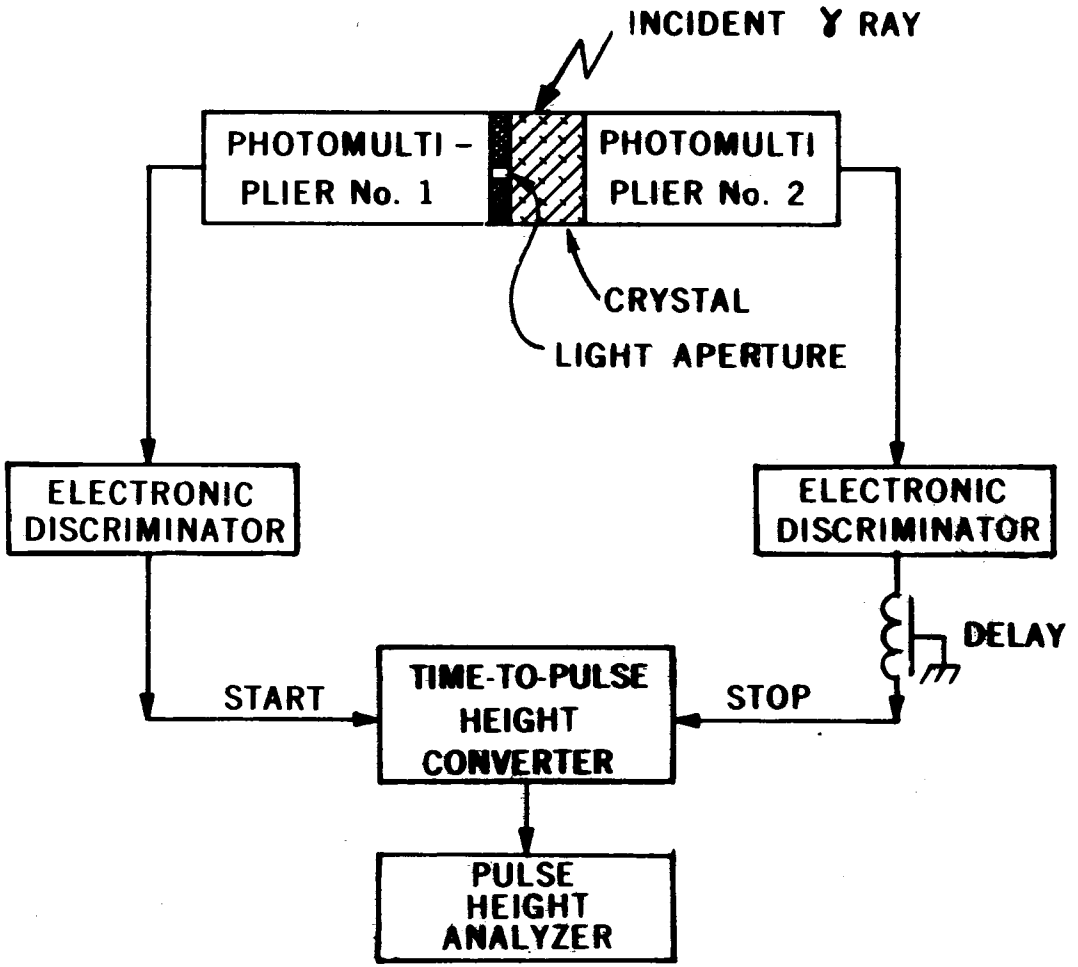


Figure 2. The Bollinger-Thomas technique for measuring scintillation decay time.

on the single sample per event technique. A time reference signal is developed in photomultiplier number 1 and starts the time-to-pulse height converter (TPHC). The stop signal for the TPHC is developed in photomultiplier number 2. Since the TPHC is limited to a single stop for a given start signal, a small aperture is placed between the crystal and photomultiplier number 2 so that the probability of generating a photoelectron per event is approximately 0.01. If this condition is imposed, the probability of obtaining two photoelectrons per event is 1×10^{-4} and can be neglected.

A block diagram of the system used to measure the shape of the probability density function for several NaI(Tℓ) crystals is shown in Figure 3. This system differs only slightly from the one shown in Figure 2. The crystals used for the experiment were cylindrical with only one end open. For this reason a light pipe was used to couple the light from the scintillator to both photomultipliers. The diameter of the light pipe leading to photomultiplier "B" was made small enough so that the probability per event of a photoelectron being generated is approximately 0.01. The time reference signal was developed in photomultiplier "A." Also, an energy signal was taken from the tenth dynode of photomultiplier "A" to determine the range of R, the number of photoelectrons, that would be accepted. This restriction is placed on the system to eliminate some of the timeing uncertainties associated with the reference signal.

A time spectrum is shown in Figure 4 which is the unnormalized p.d.f. for a typical NaI(Tℓ) crystal. The shape is approximately

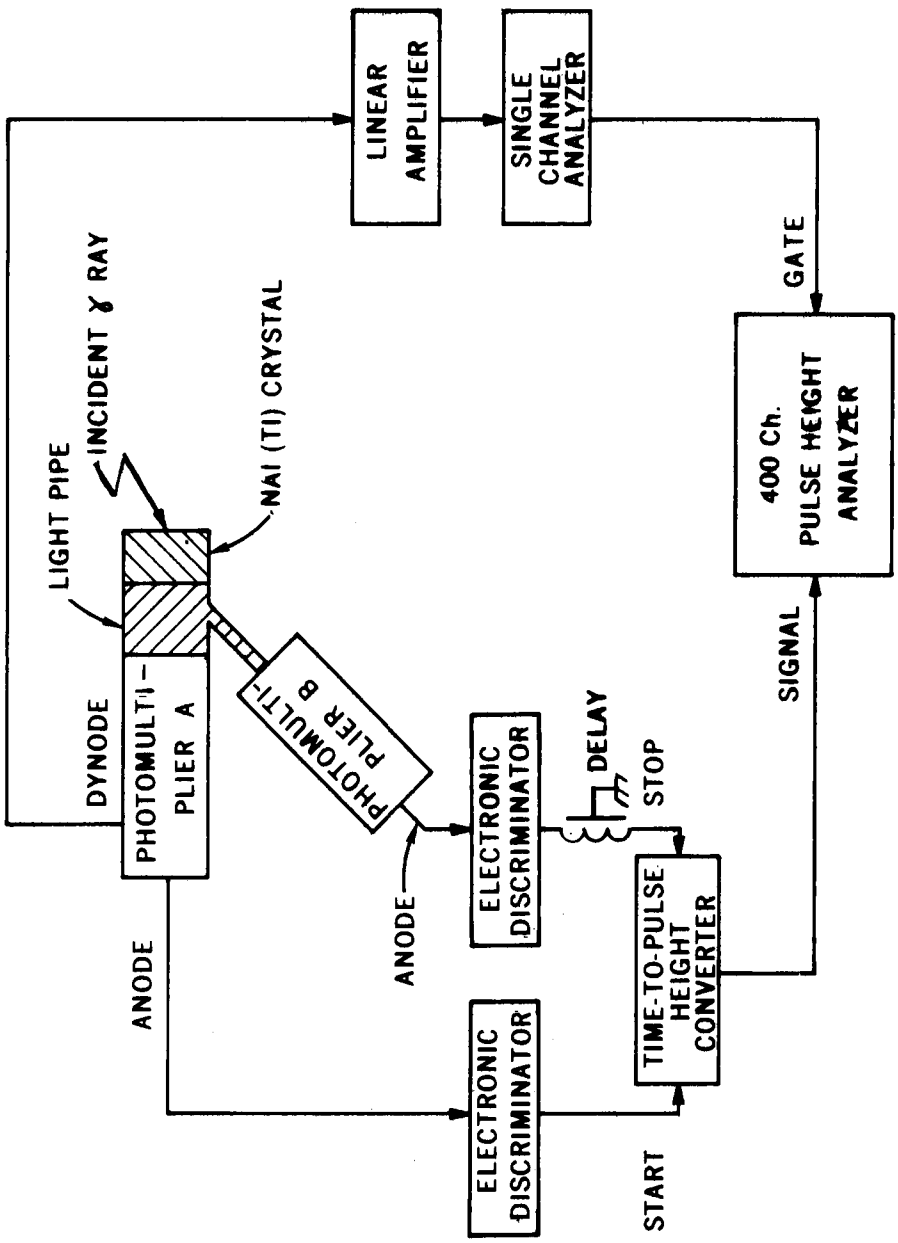


Figure 3. Block diagram of the system used to measure the shape of NaI(Tl) scintillation decay.

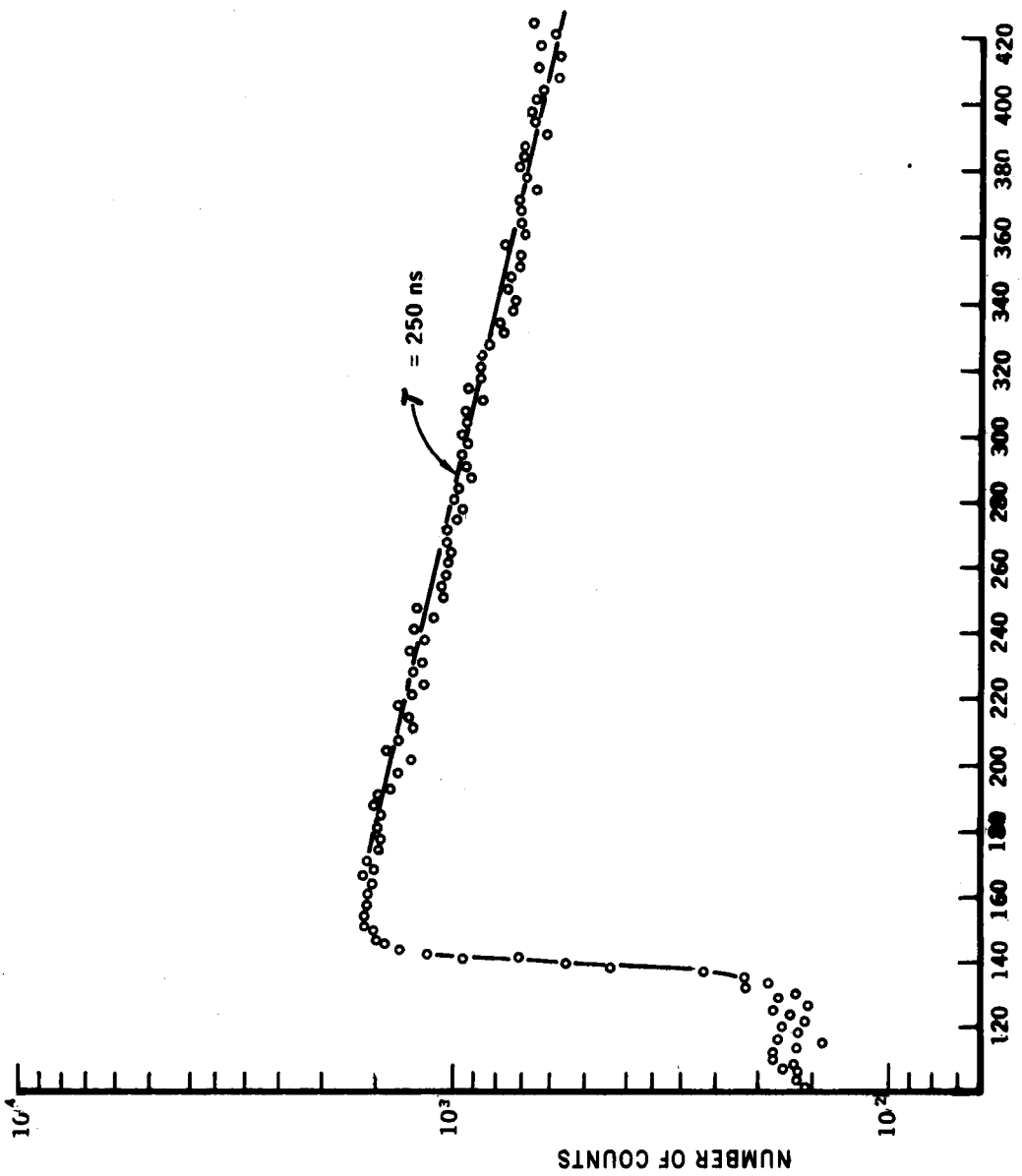


Figure 4. A measured probability density function of the NaI(Tl) scintillator.

exponential with a decay time constant of approximately 250 nsec ± 10 nsec. One of the major problems with this test is the severe background shown in the first few channels of the spectrum of Figure 4. The background is caused by the discriminator in channel B triggering on the single electron noise of the photomultiplier. Since the discriminator level must be below the single-electron level to detect the photons from the NaI(Tℓ), the only means for reducing the background is to use an extremely low-noise photomultiplier in channel B. Another problem associated with the system of Figure 3 is the relatively slow response time of the system. An indication of the response time can be obtained from the rise-time of the spectrum in Figure 4. Since the time response of the photomultiplier and discriminator is known to be much faster than the rise-time of the spectrum, the photon transit time in the crystal is considered to be the cause of the slow time response of the system. The photon transit time in the crystal is increased because of the small aperture at the entrance to photomultiplier "B" in Figure 3.

The Bollinger-Thomas measurement was performed for several crystals all of which exhibited an exponential shape for the p.d.f. Other experimenters[15] have made similar measurements which indicate that the p.d.f. is exponential with a decay time constant of approximately 250 nsec. Thus the prediction made by W. J. Van Sciever[16] that a fast decay component exists in NaI(Tℓ) at a temperature of 25°C remains unconfirmed. Since the Bollinger-Thomas system has a relatively slow response time, the expected fast components would not be detectable. Although the results of the Bollinger-Thomas measurements are not

suitable evidence of the absence of a fast component, the assumption of a single exponential p.d.f. will be assumed for the remainder of this paper. Stronger evidence for the validity of the assumption will be presented in Chapter IV.

Order Statistics for a Single Exponential Probability Density Function

In general, the electronic discrimination system establishes the arrival time of photoelectrons at the anode of the photomultiplier by establishing the time when the current or charge pulse exceeds a certain level. For an ideal photomultiplier with an infinite bandwidth, each photon would produce a current pulse at the anode characterized by a delta function in time. The response of a charge sensitive system to such an ideal pulse is shown in Figure 5.

Consider the problem of determining the p.d.f. of the arrival time of the $j^{\underline{th}}$ photoelectron at the anode for the ideal system. This time corresponds to the time when the charge level changes from the $(j-1)^{\underline{th}}$ to the $j^{\underline{th}}$ state in Figure 5. To determine the p.d.f. for the $j^{\underline{th}}$ photoelectron, the events must be ordered in time. The following definitions are to be used in the ordering process:

R = the total number of photoelectrons produced due to a single gamma ray interaction in the scintillator.

j = the number associated with the $j^{\underline{th}}$ photoelectron after the first photoelectron.

t_j = the time associated with the $j^{\underline{th}}$ photoelectron.

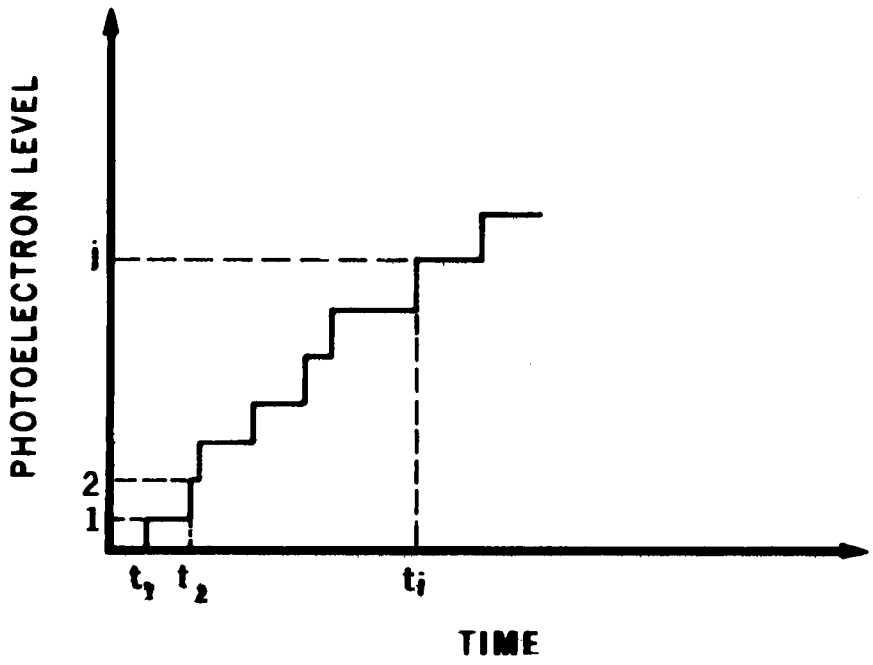


Figure 5. The response of a charge sensitive system to an ideal photomultiplier pulse.

$f(t)$ = probability-per-unit time that a photoelectron will be generated at time t (p.d.f.).

$F(t)$ = probability distribution function associated with each photoelectron, $F(t) = \int_{-\infty}^{t} f(\tau)\, d\tau$.

Let t_1', t_2', ... , t_R' be a random sample in time from the p.d.f., $f(t)$, for $0 \leq t' < \infty$, and let t_1, t_2, ..., t_R be the time at which the first, second, ..., $R^{\underline{th}}$ photoelectron appears at the anode. The events associated with t_1, t_2, ..., t_R are then ordered in time.[17,18] The joint p.d.f. of the ordered events is

$$g(t_1, t_2, \ldots, t_R) = [f(t_1)f(t_2) \cdots f(t_R)]J \quad , \qquad (2)$$

where J is the Jacobian of the transformation. Hog and Craig[18] shows that J=R! for such a transformation. Using this fact the joint p.d.f. of the ordered events is

$$g(t_1, t_2, \ldots, t_r) = R![f(t_1)\, f(t_2)\, f(t_3) \cdots f(t_R)] \quad , \qquad (3)$$

where $0 < t_1 < t_2 < \ldots < t_R < \infty$.

The marginal p.d.f. of t_j is given by,

$$g_j(t_j) = \int_0^{t_j} \cdots \int_0^{t_2} \int_{t_j}^{\infty} \cdots \int_{t_{R-1}}^{\infty} R!\, \{f(t_1)\, f(t_2) \cdots f(t_R)\} x$$

$$\{dt_R \cdots dt_{j+1}\, dt_1 \cdots dt_{j-1}\} \quad . \qquad (4)$$

The marginal p.d.f., $g_j(t_j)$, is the probability-per-unit time that the $j^{\underline{th}}$ photoelectron will be generated at time t_j with all other time variables integrated over their respective domains. The first integral in Eq. (4) is

$$\int_{t_{R-1}}^{\infty} f(t_R)\, dt_R = F(\infty) - F(t_{R-1}) \quad .$$

Since $F(t_R)$ is defined as unity at infinity for a p.d.f.,

$$\int_{t_{R-1}}^{\infty} f(t_R)\, dt_R = 1 - F(t_{R-1}) \quad . \tag{5}$$

The second integral in Eq. (4) is

$$\int_{t_{R-2}}^{\infty} f(t_{R-1})\, [1 - F(t_{R-1})]\, dt_{R-1} \quad . \tag{6}$$

By the definition of F(t), Eq. (6) can be put in the form,

$$\int_{t_{R-2}}^{\infty} \frac{dF(t_{R-1})}{dt_{R-1}} [1 - F(t_{R-1})] dt_{R-1} = \frac{[1 - F(t_{R-1})]^2}{2} \quad . \tag{7}$$

If this procedure is repeated (R - j) times, the result is

$$\int_{t_j}^{\infty} \left[\frac{dF(t_{j+1})}{dt_{j+1}} \right] \frac{[1 - F(t_{j+1})]^{(R-j-1)}}{(R - j - 1)!}\, dt_{j+1} = \frac{[1 - F(t_j)]^{R-j}}{(R - j)!} \quad . \tag{8}$$

There are (j - 1) terms remaining to be integrated in Eq. (4). The first of the remaining terms is

$$\int_0^{t_2} f(t_1)\, dt_1 = F(t_2) - F(0) \quad .$$

Since f(t) is defined to be zero for t < 0, F(0) is equal to zero and the first term reduces to

$$\int_0^{t_2} f(t_1)\, dt_1 = F(t_2) \quad . \tag{9}$$

The second integral is

$$\int_0^{t_3} f(t_2)\, F(t_2)\, dt_2 = \int_0^{t_3} \frac{dF(t_2)}{dt_2} F(t_2)\, dt_2 \quad .$$

The result of the integration is

$$\int_0^{t_3} \frac{dF(t_2)}{dt_2} F(t_2)\, dt_2 = \frac{F(t_2)^2}{2} \quad . \tag{10}$$

After repeating this procedure (j - 2) times, the final integral of the group is

$$\frac{1}{(j-2)!} \int_0^{t_j} \frac{dF(t_{j-1})}{dt_{j-1}} F(t_{j-1})\, dt_j = \frac{F(t_j)^{j-1}}{(j-1)!} \quad . \tag{11}$$

Substituting Eq. (8) and (11) for the appropriate integrals in Eq. (4) yields the marginal p.d.f. for the $j^{\underline{th}}$ photoelectron,

$$g_j(t_j) = \frac{R!}{(j-1)!(R-j)!} [1 - F(t_j)]^{R-j} F(t_j)^{j-1} f(t_j) \quad . \qquad (12)$$

The only restrictions placed on Eq. (12) are that the original samples, t_1', t_2', ..., t_n' be stochastically independent, and each event be governed by the same p.d.f. For samples to be stochastically independent means that their joint p.d.f. can be written as a product of their respective marginal p.d.f.'s, or

$$g(t_1', t_2' --t_R') = g_1(t_1') \; g_2(t_2') \ldots g_R(t_R') \quad . \qquad (13)$$

The general shape of the p.d.f. governing the photon generation was shown in a previous section to be

$$f(t) = \frac{1}{\tau} e^{-t/\tau} \quad . \qquad (14)$$

For NaI(Tℓ) the decay time-constant was determined from Figure 3, page 11, to be approximately 250 nsec. The distribution function in time is

$$F(t) = \frac{1}{\tau} \int_0^t e^{-t'/\tau} \, dt' = (1 - e^{-t/\tau}) \quad . \qquad (15)$$

If Eqs. (14) and (15) are substituted into Eq. (12), the marginal p.d.f. for the $j^{\underline{th}}$ photoelectron becomes

$$g_j(t_j) = \frac{R!}{(j-1)!(R-j)!\tau} e^{-\frac{t_j(R-j+1)}{\tau}} (1 - e^{-t/\tau})^{j-1} \quad . \qquad (16)$$

Equation (16) indicates the probability-per-unit time that the $j^{\underline{th}}$ photoelectron will be generated at the cathode of the photomultiplier at a time t_j. The restrictions on Eq. (16) are that each photoelectron be represented by the same exponential p.d.f. and that each photon before the ordering process be time independent as previously defined. The density function $g_j(t_j)$ is plotted in Figure 6 for a total number of 100 photoelectrons. The curve labeled j=1 is the p.d.f. for the first photoelectron, j=2 for the second photoelectron, and out to j=8 for the eighth photoelectron. The general shapes of the distributions of Figure 6 are identical to the calculated distributions of El-Wahab and Kane.[10]

The fact that Eq. (16) appears in a much simpler form than the results of El-Wahab and Kane is not so important. The significant difference between the two developments is the generality of the mathematical procedures used in the present development. To illustrate this point, consider a single photoelectron distribution which is much more complex than the distribution given by Eq. (14). For example, the complex distribution might be the result of several cascade processes. In such a case, the procedure for going from Eq. (12), which is the general expression, to Eq. (16) remains the same. The results will always be in a closed form similar to Eq. (16) if f(t) is a continuous, integrable function.

The procedure for analyzing the scintillator and photomultiplier system is precisely defined by the application of the general order equation. The distribution associated with each independent process

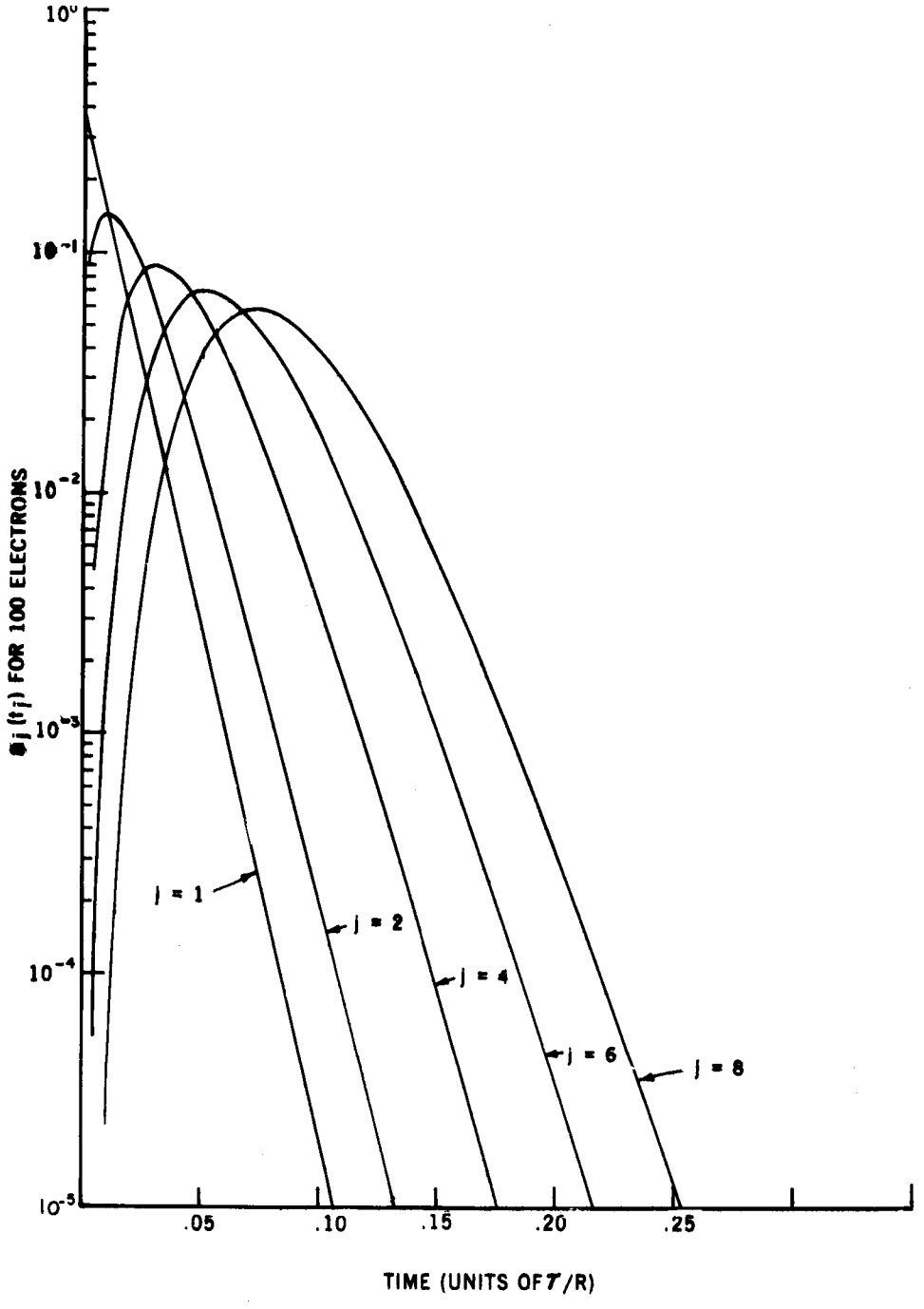


Figure 6. The probability density function for the first eight photoelectrons where R = 100.

will be determined separately, and then the convolution of all the distributions will be performed. The procedure as outlined between Eq. (12) and (16) will then be used to obtain $g_j(t_j)$. Before going to the more general case, some important characteristics of the single exponential system will be investigated.

First and Second Moment Calculations for the Single Exponential Case

The first moment or the mean time of the $(j + 1)^{\underline{th}}$ photoelectron by definition is

$$\bar{t}_{j+1} = \int_0^\infty t\, g_{j+1}(t_{j+1})\, dt_{j+1} \quad . \tag{17}$$

For simplicity a normalized time, t/τ, is defined so that Eq. (17) becomes

$$\bar{X}_{j+1} = \frac{\bar{t}_{j+1}}{\tau} = \int_0^\infty x_{j+1} g_{j+1}(x_{j+1})\, dx_{j+1} \quad . \tag{18}$$

Substituting Eq. (16) into Eq. (18) yields

$$\bar{X}_{j+1} = \frac{R!}{(j-1)!(R-j)!\tau} \int_0^\infty e^{-x_{j+1}(R-j)} \left(1 - e^{-x_{j+1}}\right)^j x_{j+1} dx_{j+1}$$

$$= \frac{B(R,j)}{A(R,j)} \quad . \tag{19}$$

The definitions of $A(R,j)$ and $B(R,j)$ are

$$A(R,j) = \frac{(j-1)!(R-j)!\tau}{R!} \tag{20}$$

and

$$B(R,j) = \int_0^\infty x_{j+1}\, e^{-Rx_{j+1}}\, (e^{x_{j+1}} - 1)^j\, dx_{j+1} \quad .$$

After dropping the subscripts from the dummy variable, B(R,j) becomes

$$B(R,j) = \int_0^\infty x\, e^{-Rx}\, (e^x - 1)^j\, dx \quad . \tag{21}$$

Integrating by parts

$$B(R,j) = x(e^x - 1)^j(-\tfrac{1}{R}\, e^{-Rx})\,\Big|_0^\infty + \tfrac{1}{R}\int_0^\infty e^{-Rx}(e^x - 1)^j\, dx$$

$$+ \tfrac{j}{R}\int_0^\infty x\, (e^x - 1)^{j-1}\, e^{-(R-1)x}\, dx \quad . \tag{21a}$$

By substituting (R-1) for R and (j-1) for j in B(R,j), Eq. (21a) reduces to

$$B(R,j) = \tfrac{1}{R}\int_0^\infty e^{-Rx}(e^x - 1)^j\, dx + \tfrac{j}{R}\, B(R-1,\, j-1) \quad .$$

Also, since the function

$$\frac{1}{A(R,j)}\int_0^\infty e^{-Rx}\, (e^x - 1)^j\, dx$$

is a p.d.f. integrated over the entire domain, then

$$\int_0^\infty e^{-Rx}\, (e^x - 1)^j\, dx = A(R,j) \quad . \tag{22}$$

Substituting Eq. (22) into Eq. (21) yields

$$B(R,j) = \frac{A(R,j)}{R} + \frac{j}{R} B(R-1, j-1) \quad . \tag{23}$$

The second term of Eq. (23) is

$$B(R-1, j-1) = \int_0^\infty x e^{-(R-1)x} (e^x - 1)^{j-1} \, dx$$

$$= \frac{A(R-1, j-1)}{R-1} + \frac{j-1}{R-1} B(R-2, j-2) \quad . \tag{23a}$$

Eqs. (23) and (23a) outline the reduction procedure for reducing Eq. (21) to a sum of (j - 1) terms. Substituting Eq. (23a) into Eq. (23) yields

$$B(R,j) = \frac{A(R,j)}{R} + \frac{jA(R-1,j-1)}{R(R-1)} + \frac{j(j-1)}{R(R-1)} B(R-2,j-2) \quad . \tag{24}$$

If the procedure outlined between Eq. (22) and Eq. (24) is repeated j times, the result is

$$B(R,j) = A(R,j) \sum_{P=0}^{j} \left(\frac{1}{R-P} \right) \quad .$$

Substituting the expression for B(R,j) back into Eq. (19) yields

$$\overline{X}_{j+1} = \sum_{P=0}^{j} \left(\frac{1}{R-P} \right) \quad . \tag{25}$$

The mean time is obtained by substituting Eq. (25) into Eq. (18).

$$\bar{t}_{j+1} = \tau \sum_{P=0}^{j} \frac{1}{R-P} \quad . \tag{26}$$

The sum in Eq. (26) can be replaced by an integral for large values of R without excessive error. Equation (26) becomes,

$$\bar{t}_{j+1} \approx \int_{\ell=R}^{R-j} (-\frac{1}{\ell})\, d\ell = \tau \ell n \left(\frac{R}{R-j} \right) \quad . \tag{27}$$

A further approximation for small values of j is

$$\bar{t}_{j} \approx \left(\frac{j}{R} \right) \tau \quad . \tag{28}$$

The second moment is calculated in Appendix A using a similar procedure. The result is given by Eq. (107) of Appendix A as

$$\overline{x^2_{j+1}} = 2 \sum_{k=0}^{j} \left(\frac{1}{R-k} \right) \sum_{P=k}^{j} \left(\frac{1}{R-P} \right) \quad . \tag{107}$$

The variance is

$$\sigma^2_{j+1} = \tau^2 \left\{ \left[\sum_{k=0}^{j} \left(\frac{1}{R-k} \right) \sum_{P=k}^{j} \frac{2}{R-P} \right] - \left(\sum_{P=0}^{0} \frac{1}{R-P} \right)^2 \right\}$$

$$= \tau^2 \left\{ \left[\sum_{k=0}^{j} \left[\frac{1}{R-k} \sum_{P=k}^{j} \frac{2}{R-P} \right] \right] - \left(\sum_{k=0}^{j} \frac{1}{R-k} \right) \left(\sum_{k=0}^{j} \frac{1}{R-k} \right) \right\} . \tag{109}$$

By factoring Eq. (109) the time variance of the $(j + 1)^{\underline{th}}$ photoelectron is

$$\sigma_{j+1}^2 = \tau^2 \left\{ \sum_{k=0}^{j} \left[\left(\frac{1}{R-k} \right) \left(2 \sum_{p=k}^{j} \left(\frac{1}{R-p} \right) - \sum_{R=0}^{j} \frac{1}{R-k} \right) \right] \right\}$$

$$= \tau^2 \left\{ \sum_{k=0}^{j} \left[\frac{1}{R-k} \left(\sum_{p=k}^{j} \frac{1}{R-p} - \sum_{p=0}^{k-1} \frac{1}{R-p} \right) \right] \right\}$$

$$= \tau^2 \left\{ \sum_{k=0}^{j} \left(\frac{1}{R-k} \right)^2 \right\} \quad . \tag{110}$$

In the limit for large values of R and R-j, the variance can be expressed in integral form as

$$\sigma_{j+1}^2 \approx \tau^2 \int_{R-j}^{R} \left(\frac{1}{q^2} \right) dq = \frac{\tau^2 j}{R(R-j)} \quad . \tag{111}$$

A further approximation yields

$$\sigma_j \approx \frac{\tau \sqrt{j}}{R} \quad . \tag{29}$$

This agrees with Gatti's[9] calculation for the limiting conditions only. The standard deviation in time, σ_j, is then proportional to the square root of j and inversely proportional to R, the total number of photoelectrons. Therefore, σ_j is inversely proportional to the incident energy. The standard deviation in time as a function of the photoelectron level j is plotted in Figure 7 for three values of R and for the decay time constant corresponding to a NaI(Tℓ) crystal.

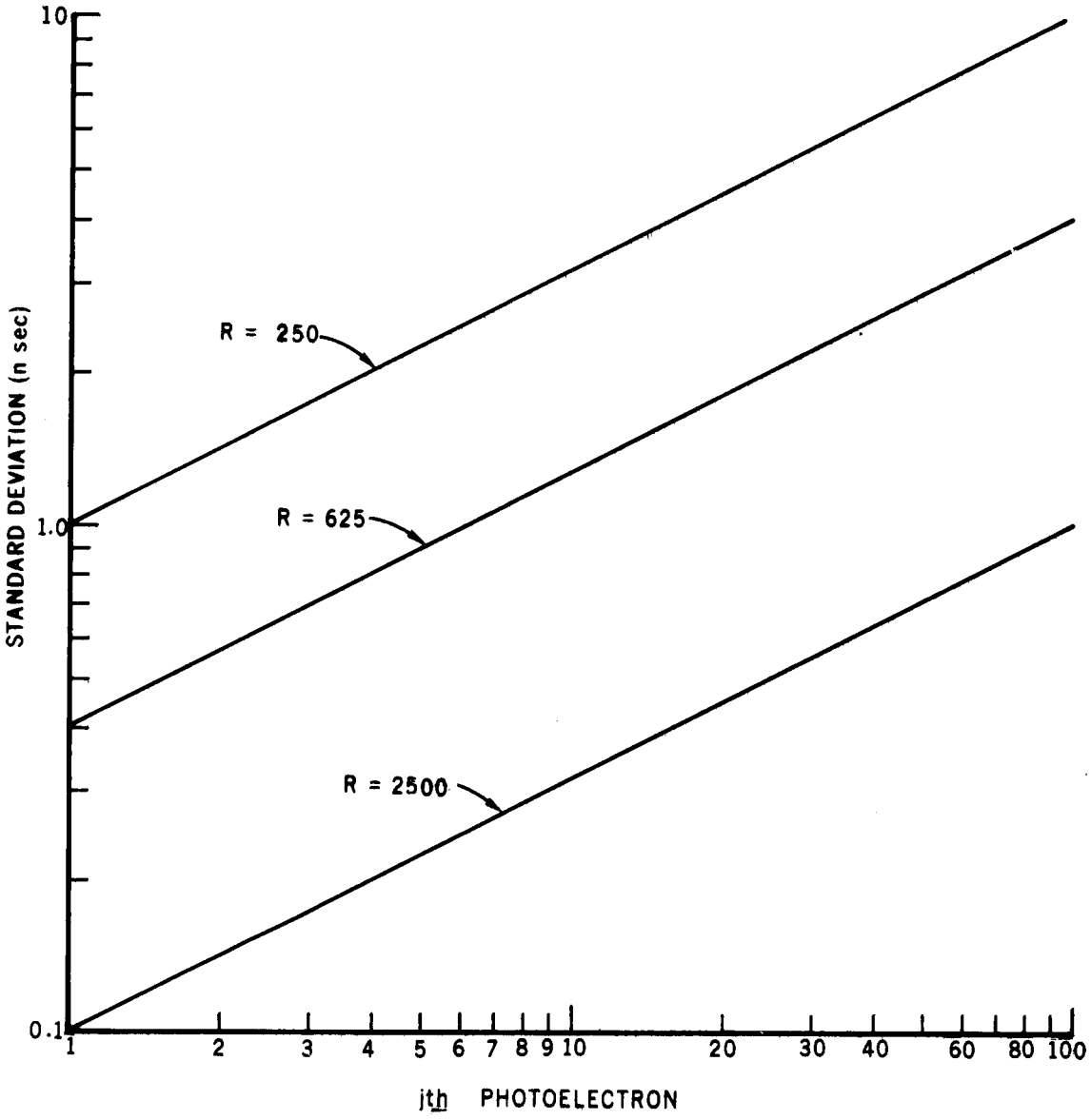


Figure 7. Standard deviation in time versus photoelectron level for a single exponential decay.

II. THEORETICAL LIMIT OF THE TIME RESOLUTION FOR THE SINGLE EXPONENTIAL CASE

In order to establish the theoretical limit of the time resolution, two statistical definitions are necessary. The first concept is that of a "sufficient"[18] statistic for a parameter. Let $x_1, x_2, \ldots, x_R$ be R random samples from the distribution $f(x;\theta)$, where θ is the parameter to be estimated. Further consider R statistics for the R random samples as,

$$Y_1 = U_1(x_1, x_2, \ldots, x_R)$$

$$Y_2 = U_2(x_1, x_2, \ldots, x_R)$$

$$\vdots \qquad\qquad \vdots$$

$$Y_R = U_R(x_1, x_2, \ldots, x_R) \quad .$$

The functions, Y_1 through Y_R, must satisfy the definition of a statistic. A statistic is a function of one or more random variables, but not a function of any unknown parameter. Consider the conditional probability

$$h(Y_2, Y_3, \ldots, Y_R | Y_1; \theta) = \frac{g(Y_1, \ldots, Y_R; \theta)}{g_1(Y_1; \theta)} \quad . \qquad (30)$$

This function is the probability-per-unit time of the statistics Y_2 through Y_R given that Y_1 has already occurred. If the conditional probability, Eq. (30), is not a function of the parameter θ, the function $g_1(Y_1;\theta)$ is said to be the p.d.f. of the sufficient statistic Y_1. The term "sufficient" implies that $g_1(Y_1;\theta)$ contains all the information

available about the parameter θ. The relationship given by Eq. (30) states simply that if Y_1 is specified, the p.d.f. of Y_2, Y_3, ..., Y_R contains no additional information about the unknown parameter. Therefore, the statistic Y_1 is "sufficient" for estimating θ in the sense that no other statistic can improve the estimate.

The second definition to be considered is the concept of a "complete" family of p.d.f.'s. Consider again the family of p.d.f.'s, $f(x;\theta)$, where θ is the parameter to be estimated and is defined for any range of real numbers. Let $U(x)$ be any continuous function of the variable x over the defined range. The p.d.f., $f(x;\theta)$, is a "complete" family if the function $U(x)$ is required to be identically zero for the expectation of $U(x)$ to be zero. More precisely, $U(x)$ must be zero at each point x where at least one member of the family, $f(x;\theta)$, is greater than zero. The expectation of $U(x)$ is

$$E[U(x)] = \int_{-\infty}^{+\infty} f(x;\theta)\, U(x)\, dx \quad .$$

Thus for $f(x;\theta)$ to be a complete family, the condition

$$\int_{-\infty}^{+\infty} f(x;\theta)\, U(x) dx = 0$$

must require that $U(x)$ be zero for each point x where at least one member of the family of p.d.f.'s is positive. The remaining problem is to show that the detected time, t_1, of the first photoelectron is a sufficient statistic and that $g_1(t_1;t_0)$ is a complete family. The

unknown parameter, t_0, is the initial time of the scintillation event. After these two properties are demonstrated, the statistic t_1 will be used to determine an unbiased estimator for the parameter t_0. An unbiased estimator is a statistic with an expectation of the parameter t_0. Furthermore, the unbiased estimator will have a minimum variance and will be unique. Thus, the unbiased estimator will contain all the information about the parameter to be estimated.

The Fisher-Neyman Theorem defines an easy method for determining whether or not a statistic is sufficient.[18] This theorem states that if the joint p.d.f. can be factored as

$$f(x_1;\ )f(x_2;\theta)\ \ldots,\ f(x_R;\theta) = g_1(Y_1;\theta)\left[h(x_1,\ x_2,\ \ldots,\ x_3)\right] \tag{31}$$

where $h(x_1, x_2, \ldots, x_R)$ is not a function of and where $Y_1 = U(x_1, x_2, \ldots, x_R)$ is a statistic, then $g_1(Y_1)$ is a p.d.f. of the sufficient statistic Y_1. The joint p.d.f. for the single exponential case is

$$\prod_{i=1}^{R} f(t_i)t_0) = \frac{R!}{(\tau)^R}\ \exp\left\{-\left[\sum_{i=1}^{R}\frac{t_i - t_0}{\tau}\right]\right\} \quad . \tag{32}$$

According to Eq. (16), the p.d.f. for the first order statistic is

$$g_1(t_1;t_0) = \frac{R}{\tau}\, e^{-(t_1-t_0)R/\tau}, \quad t_0 \leq t_1 < \infty \quad .$$

In Eq. (16), t_0 was zero, but here t_0 is the initial time of the event and the unknown parameter to be estimated. After rearranging Eq. (32),

the joint p.d.f. becomes

$$\prod_{i=1}^{R} f(t_i;t_0) = \left[\frac{R}{\tau} e^{-(t_1-t_0)R/\tau}\right] \left[\frac{(R-1)!}{(\tau)^{R-1}}\right] x$$

$$\exp\left\{-\left[\sum_{i=2}^{R} \frac{t_i}{\tau}\right] + \frac{(R-1)t_1}{\tau}\right\} . \qquad (33)$$

Equation (33) can be factored as follows,

$$\prod_{i=1}^{R} f(t_i;t_0) = g_1[\ (t_1;t_0)]\ h(t_1, t_2, \ldots, t_R) \quad ,$$

where

$$g_1[\,U(t_1;t_0)] = g_1(t_1;t_0) = \frac{R}{\tau} e^{-R(t_1-t_0)/\tau} \quad .$$

The conclusion is that the joint p.d.f. satisfies the condition stated in the Fisher-Neyman Theorem, Eq. (31). Therefore, t_1 is a sufficient statistic.

The next problem is to determine whether or not the family of p.d.f.'s, $f(t_1;t_0)$, is a "complete" family. By the definition of "completeness" the expectation

$$E(\mu_{(t)}) = \int_{t=t_0}^{\infty} U(t)f(t_1;t_0)dt = 0, \qquad t_0 \leq t_1 < \infty \quad .$$

The expectation being zero must require that $U(t)$ be zero for all values of t, where $f(t_1;t_0)$ is greater than zero for at least one

value of t_0. For the single exponential p.d.f. the expectation is

$$E(\mu_{(t)}) = \frac{R}{\tau} \int_{t_1=t_0}^{\infty} U(t)\, e^{-(t_1-t_0)R/\tau}\, dt_1 = 0 \quad .$$

Dividing through by the exponential containing t_0, the integral becomes

$$\int_{t_1=t_0}^{\infty} U(t_1)\, e^{-t_1 R/\tau}\, dt_1 = 0 \quad .$$

The derivative of the expectation with respect to t_0 is

$$\frac{d}{dt_0} \int_{t_1=t_0}^{\infty} U(t_1)\, e^{-t_1 R/\tau}\, dt = U(t_0)\, e^{-t_0 R/\tau} = 0 \quad .$$

Since the exponential is not zero except when t_0 is infinity, then $U(t_0)$ is zero and, therefore, $U(t_1)$ must be zero. The first order statistic is then a "complete" and "sufficient" statistic for the parameter t_0.

The next part of the problem is to determine whether or not the expectation of the first order statistic is the desired parameter t_0. By the definition of expectation (Eq. 30),

$$E(t_1) = \frac{R}{\tau} e^{t_0 R/\tau} \left\{ \left[-\frac{t\tau}{R} e^{-t_1 R/\tau} - \left(\frac{\tau}{R}\right)^2 e^{-t_1 R/\tau} \right]_{t_0}^{+\infty} \right\}$$

$$E(t_1) = t_0 + \frac{\tau}{R} \quad . \tag{34}$$

The expectation of t_1 is not t_0, but the expectation of the statistic $(t_1 - \frac{\tau}{R})$ is t_0. A special case of a general theorem by Lehniann and Scheffe[18] states that if a statistic is sufficient and if the family, $g_1(t_1;t_0)$, is complete, any unbiased linear function of the statistic will exhibit minimum variance. In this theorem an unbiased statistic is one whose expectation is the unknown parameter. The conclusion then from this theorem is that the statistic $(t_1 - \frac{\tau}{R})$ has a variance less than any other unbiased estimation of t_0. In practice subtraction of the small ratio, $\frac{\tau}{R}$, from t_1 is unnecessary since the contribution to the variance is extremely small. In summary, the first photoelectron contains all the information about t_0, the initial time of the scintillation event. Therefore, no additional measurements exist that will improve the time measurement for the single exponential case.

The problem of determining an optimum single or multiple sample measurement for t_0 is very complex as demonstrated by this example. In the example just presented the measurement of t_1 was logically selected as a good estimate of t_0, and was later found to be the best estimate. Even in this simple case the process of trial and error was used. The example of the single exponential case has served to demonstrate the fact that optimizing a multiple sampling detector will only become feasible after the system is completely characterized. An optimum single sample other than the first photoelectron will be necessary in the more practical case to obtain all the information about the initial time. This fact will be demonstrated in Chapter IV.

III. PHOTON TRANSIT TIME CALCULATIONS

Computer Program

Several investigators[19,20] of the timing characteristics of scintillators have implied that the time variance associated with photon transit time inside the crystal significantly affects the overall resolution of the system. More recently Braunsfurth and Koner[21] observed a 15 percent decrease in the time resolution of a NaI(Tℓ) system going from a crystal with a 38 mm. diameter and 25 mm. height to a crystal with a 38 mm. diameter and 51 mm. height.

The purpose of this section is to calculate the photon transit time distribution to be used in Chapter III to calculate the overall time resolution of the scintillator-photomultiplier system. The effect of such parameters as the height-to-radius ratio, the index of refraction of exit window, and the photon generation point in the crystal on the transit time distribution are considered separately. Calculations are made for the boundary conditions resulting from a specular and nonspecular surface.

The cylindrical crystal is shown in Figure 8 with the coordinate system and dimensions used in the calculations. The photomultiplier is connected to the base end of the crystal. To determine the probability-per-unit time associated with the travel of a photon in the crystal, a computer program was written to trace photons from a specified origin in the crystal to the exit at the base end. A detail listing of the computer program is given in Appendix B. After choosing an origin, a random

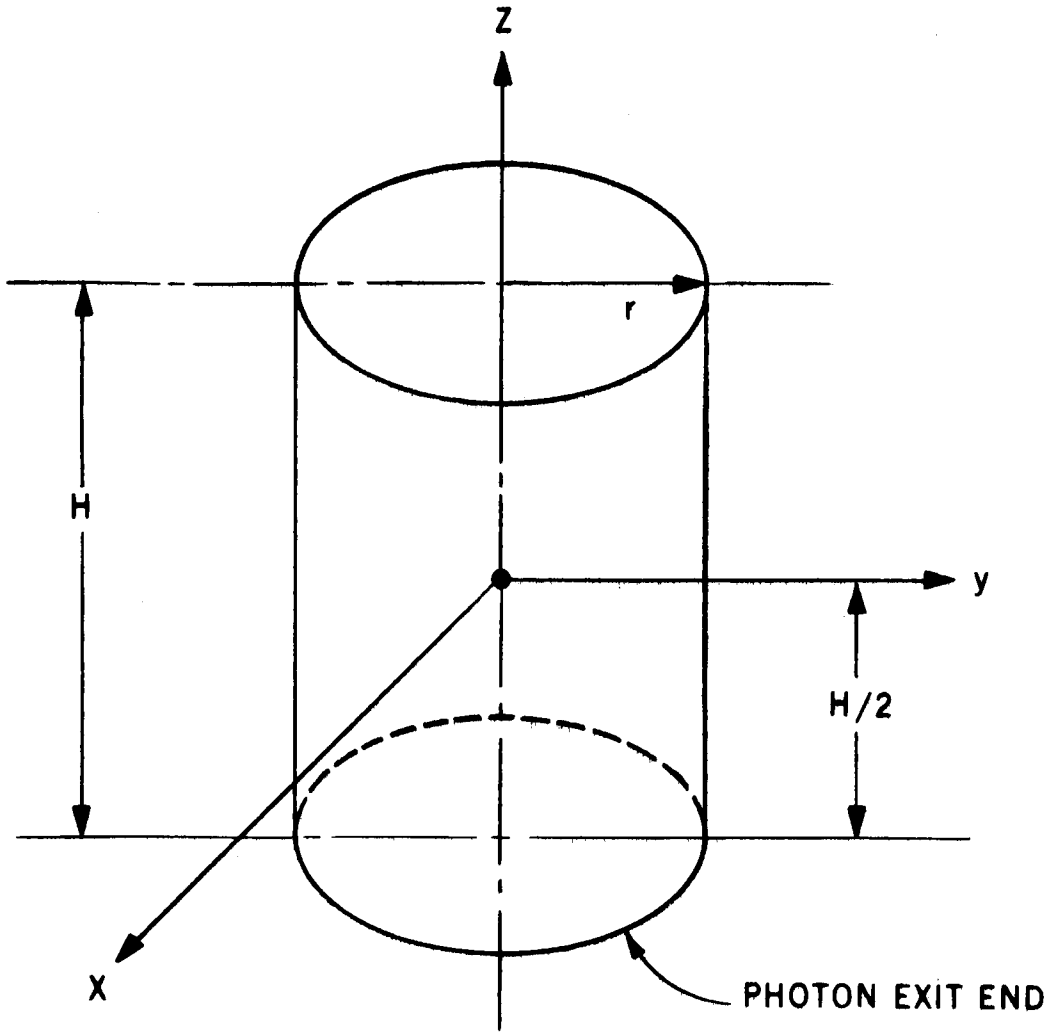


Figure 8. The coordinate system and dimensions of the cylindrical crystal used in the Monte Carlo calculations.

direction is assigned to a photon. Depending on the assigned direction, the photon encounters one of two boundary conditions:

1. The base where unmatched indices of refraction causes the photon to have a probability of being either transmitted or reflected.
2. The cylindrical wall and top where one or more interfaces may be encountered.

The photon has a probability of being transmitted and also a probability of being reflected when it strikes the base. The weight of the transmitted light (the probability of transmission) is assumed to be equal to the percentage transmission of an unpolarized plane wave incident at the same angle. The calculation of the transmission of an unpolarized plane wave is made in Appendix C. The distance traveled is multiplied by the transmitted weight and stored. The light reflected at the base having weight of W_R (W_R = 1 - probability of transmission) is tracked by the program until it encounters another boundary. The boundary encountered after reflection will be either the cylindrical wall or top.

The photon may encounter one or more interfaces at the walls or top of the cylinder shown in Figure 8. The program is written so that either or both interfaces can be used in the calculation. The first interface is a polished surface with NaI(Tℓ) on one side and air on the other side. The second interface is the nonspecular surface which is usually aluminum oxide (Al_2O_3). All the light can be reflected if the critical angle is exceeded or partially reflected for angles less than

the critical angle. If partial reflection exists at the first interface, the program traces the reflected portion keeping up with its weight and distance traveled. After finishing the trace of the reflected part of the light, the program returns to the light transmitted to the aluminum oxide surface. The direction of reflection from the nonspecular (Al_2O_3) surface is considered to be independent of the incident angle. Thus, the direction is chosen from a random number generator with the restriction that the light re-enter the crystal at an angle less than the critical angle of the specular surface. The program continues until all the light exits through the base or until the weight of the light is less than a preset lower limit. If the weight associated with a given portion of the light becomes less than the lower limit, that portion of light is not accumulated in the output. The purpose in establishing the lower limit is to restrict the program to a reasonable running time.

For each photon started, the computer calculates the mean distance traveled and the weight of exited photon. The mean distance is calculated by

$$L_j = \frac{\sum_i W_{ij} L_{ij}}{\sum_i W_{ij}} \quad , \tag{35}$$

where the i subscript refers to the individual exits associated with the $j^{\underline{th}}$ photon. The mean length L_j is registered in a class according to its magnitude. Each class has a width of one unit of crystal radius. The number of photons registered in a class is referred to as the

frequency. A histogram showing the number of photons in each class is shown in the computer printout of Figure 9. The histogram can be interpreted as the probability-per-unit distance that a photon will travel a distance L before exiting at the base end. In the final analysis the distance will be transformed to photon transit time.

The input parameters are shown at the top of the computer printout of the program. All the input parameters listed are self explanatory except the "Index of Refraction of Base" which is really the ratio of the index of refraction of the scintillator to that of the photomultiplier. The "Total Weight Exited Through the Base" is the only entry at the very top of the printout that is not an input parameter.

In the row containing the output data of Figure 9 is a column labeled annulus. The base of the crystal is divided into ten annuli for which five separate calculations are made. The first is the exit probability which is defined as,

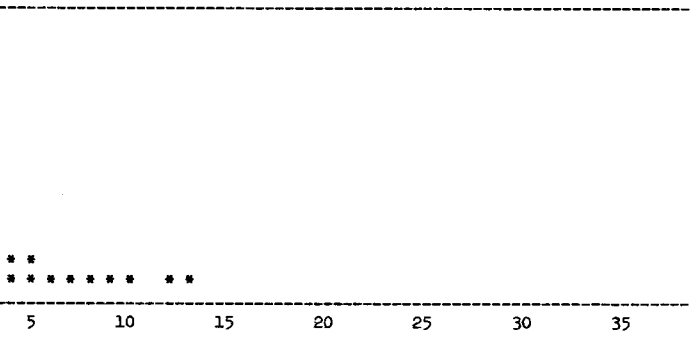
$$P_x = \frac{\sum_{ij} (W_{ijx})}{\sum_{ijx} (W_{ijx})} \qquad (36)$$

where the subscript x refers to a particular annulus. The effective distance for an annulus is calculated by averaging L_j, Eq. (35), for that portion of light that exits in the $x^{\underline{th}}$ annulus. The column labeled "Deviation" is calculated from the variance given by

```
RADIUS OF CYLINDER = 1.00000          HEIGHT OF CYLINDER = 1.00000          INDEX OF REFRACTION OF BASE = 0.98000
NUMBER OF ANNULI = 10                 NUMBER OF PHOTONS = 1000              NUMBER OF SOURCE POINTS = 1
LOWER LIMIT ON WEIGHT = 0.1000D-02    TOTAL WEIGHT EXITED THROUGH BASE = 0.9950D 03
XO = 0.0     YO = 0.0     ZO = -0.050
```

ANNULUS	EXIT PROBABILITY	EFFECTIVE DISTANCE	DEVIATION	ANNULAR ENERGY	WEIGHT PER EXIT
1	0.31437D 01	0.26277D 01	0.42843D 01	193	0.16207D 00
2	0.65156D 01	0.35506D 01	0.53876D 01	445	0.14569D 00
3	0.93599D 01	0.36826D 01	0.50513D 01	613	0.15193D 00
4	0.13637D 00	0.35263D 01	0.47056D 01	872	0.15560D 00
5	0.12789D 00	0.42201D 01	0.49946D 01	1014	0.12550D 00
6	0.12550D 00	0.48216D 01	0.55640D 01	1076	0.11606D 00
7	0.11931D 00	0.48293D 01	0.49821D 01	970	0.12238D 00
8	0.10831D 00	0.48646D 01	0.56460D 01	987	0.10919D 00
9	0.10973D 00	0.47527D 01	0.49835D 01	893	0.12226D 00
10	0.82699D 01	0.56666D 01	0.55715D 01	819	0.10047D 00
BASE	0.10000D 01	0.43775D 01	0.48645D 01	7882	0.12624D 00

CLASS	FREQUENCY
1.0	0.29000
2.0	0.18200
3.0	0.11400
4.0	0.05900
5.0	0.05700
6.0	0.03900
7.0	0.02900
8.0	0.03500
9.0	0.03500
10.0	0.02300
11.0	0.01900
12.0	0.02100
13.0	0.02100
14.0	0.00900
15.0	0.01400
16.0	0.01000
17.0	0.01000
18.0	0.00700
19.0	0.00900
20.0	0.00600
21.0	0.00400
22.0	0.0
23.0	0.00100
24.0	0.00200
25.0	0.00300
26.0	0.0
27.0	0.00100




```
SUM OF MIDPOINTS AND NUMBER IN CLASS = 0.43530D 01

NCCL =   37302     NPART =   20365

         0  0.0              0        0        0
```

Figure 9. Computer printout showing a typical histogram of a probability density function.

$$\sigma_x^2 = \frac{\sum_j W_j L_j^2}{\sum_j W_j} - (\bar{L}_x)^2 \quad , \tag{37}$$

where $\bar{L}_x$ is the effective distance for the $x^{\underline{th}}$ annulus. Also, the weights and lengths apply only to that portion of light which exits at the $x^{\underline{th}}$ annulus. The next column on the computer printout (Figure 9) is labeled "Annular Energy." The annular energy is the total number of exits resulting from all photons. The next column labeled "Weight per Exit" is calculated by dividing the exit probability by the annular energy.

Summary of the Photon Transit Time Calculations

The first part of the calculation was concerned with determining the effect of crystal size on the p.d.f. of the photon path length. To investigate the size effect, the starting point (X_0, Y_0, Z_0) of the light generation was fixed a constant distance from the photomultiplier end of the crystal and on the cylindrical axis ($X_0 = 0$, $Y_0 = 0$). The ratio of the index of refraction of the crystal to that of the photomultiplier window was fixed for each case. Attenuation of light in the crystal was assumed to be zero which for NaI(Tℓ) is justified.

Two sets of calculations were performed for each crystal size. First, the crystal was assumed to have a nonspecular surface everywhere except at the photomultiplier end. Histograms for the nonspecular case are shown in Figures 10 through 14. The height of the crystals was varied from 0.6 to 2.0 while the radius was held constant. Since the histograms are plotted using the crystal radius as the unit of length,

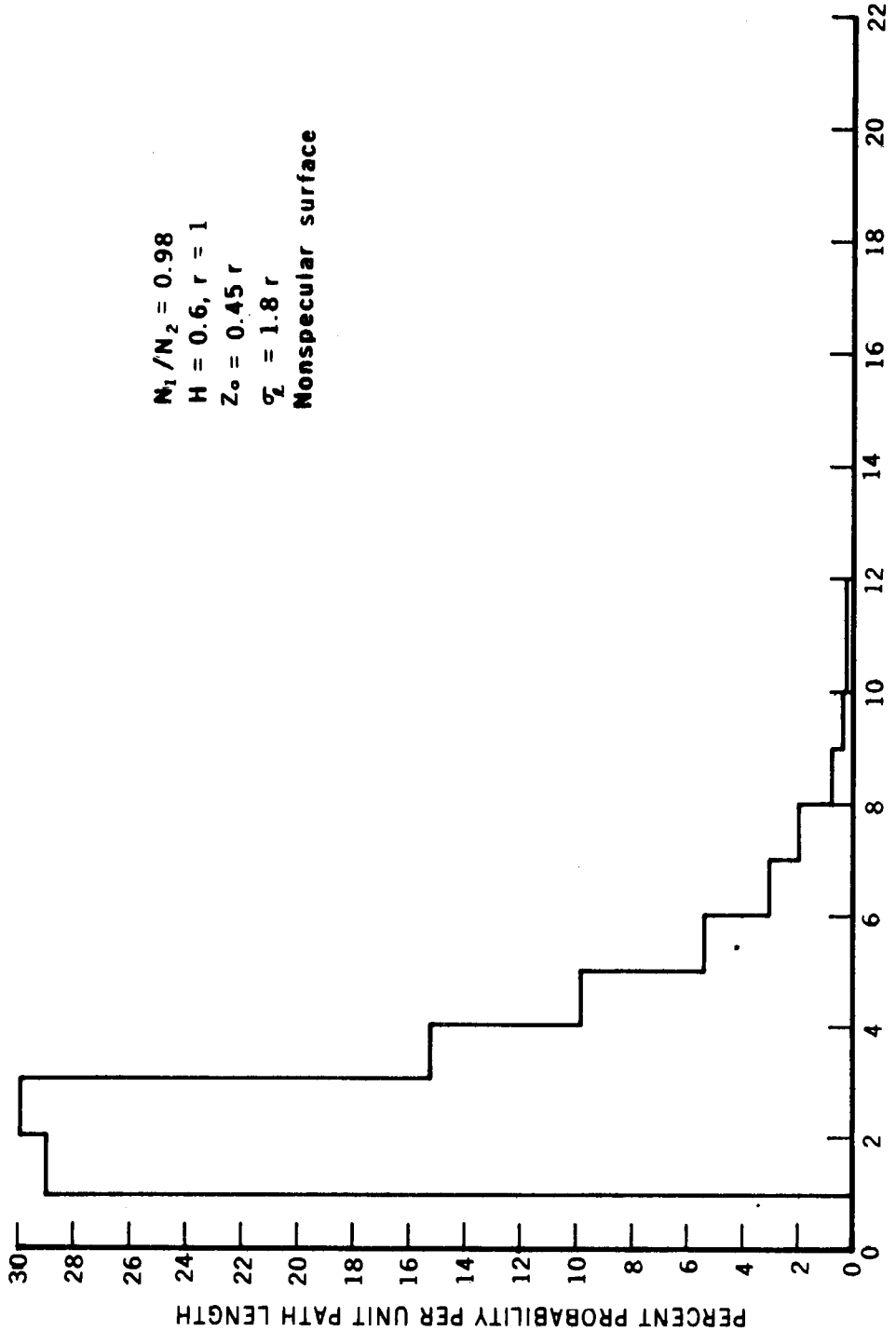


Figure 10. Probability density function of the photon path length for a crystal with dimensions H = 0.6, r = 1.

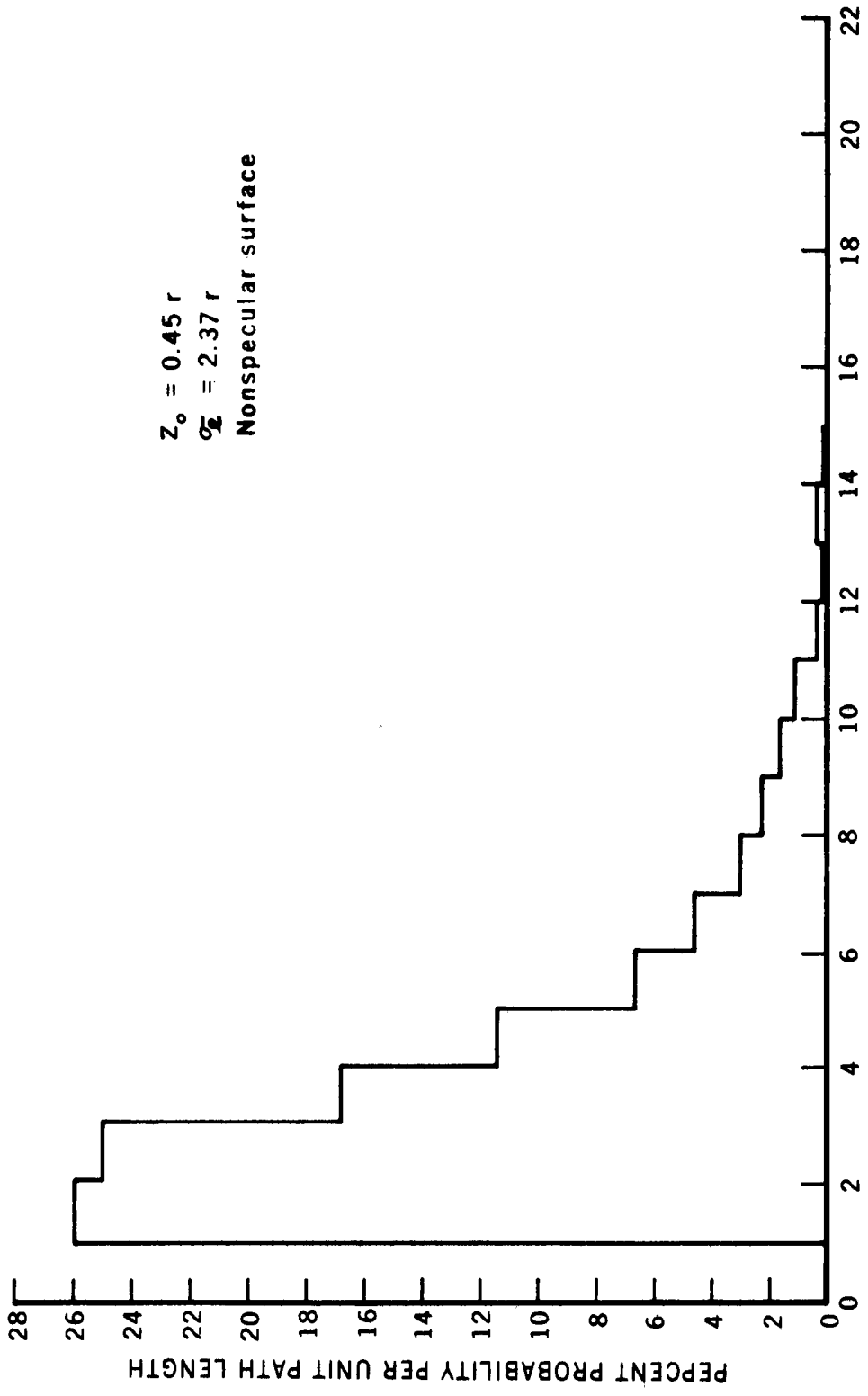


Figure 11. Probability density function of the photon path length for a crystal with dimensions H = 0.8, r = 1.

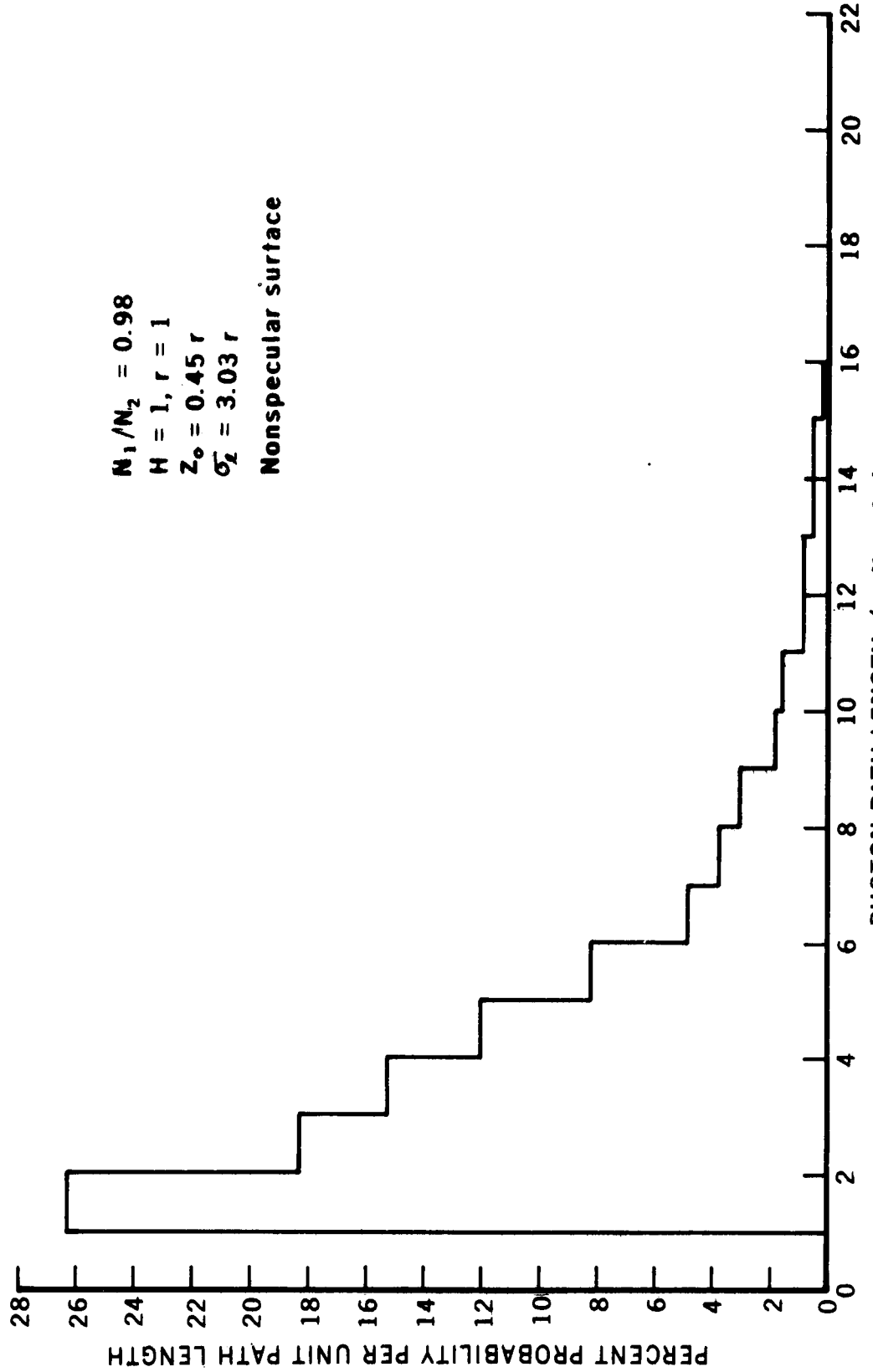


Figure 12. Probability density function of the photon path length for a crystal with dimensions H = 1, r = 1.

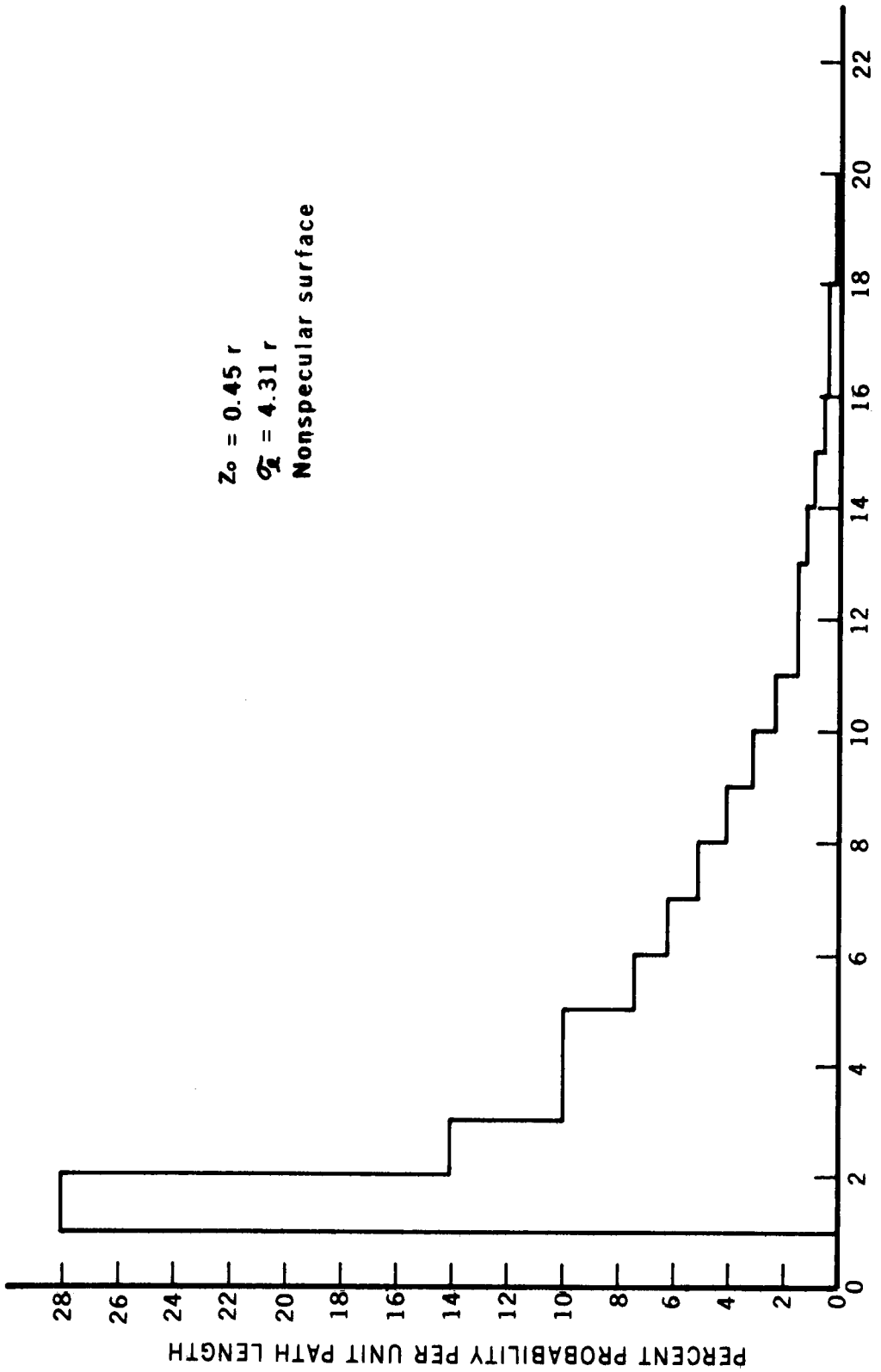


Figure 13. Probability density function of the photon path length for a crystal with dimensions H = 1.4, r = 1.

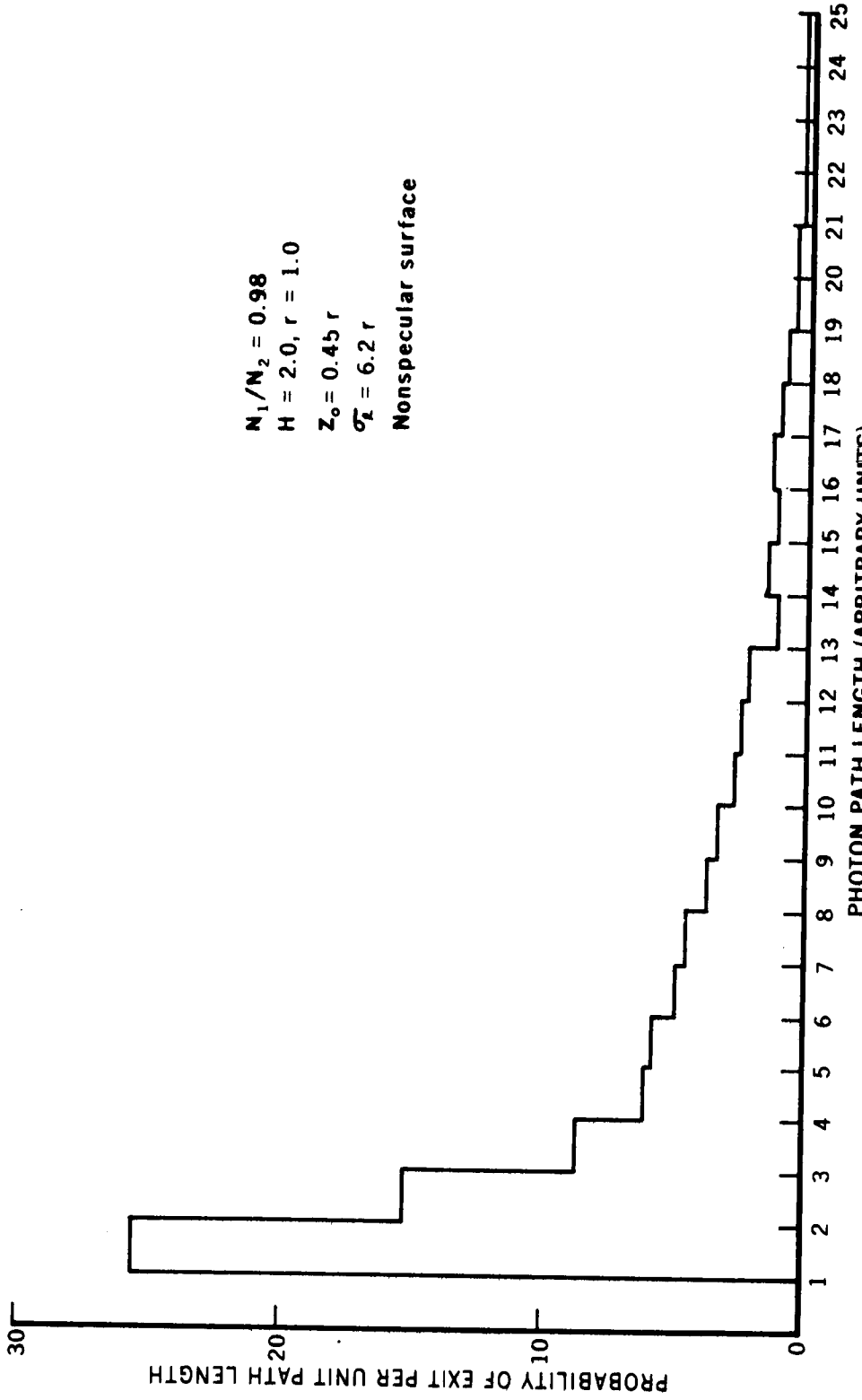


Figure 14. Probability density function of the photon path length for a crystal with dimensions H = 2.0, r = 1.

each histogram is valid for a family of crystals having the specified height-to-radius ratio. The standard deviation (σ) increases progressively from Figure 9, page 39, through Figure 14 which corresponds to a height-to-radius ratio range of 0.6 to 2.0. The variation of the standard deviation with the height-to-radius ratio is shown in Figure 15. In this figure one curve is for an index of refraction ratio of 0.98 and the other corresponds to the practical case of 0.85 as labeled. The index of refraction of NaI(Tℓ) is 1.77 and the photomultiplier window is approximately 1.5. The ratio of approximately 0.85 fits very closely the experimental system.

The boundary of the crystal was assumed to consist of a specular surface with a nonspecular backing in the second case. This boundary represents a rather unrealistic case, but may be of interest in some systems. Typical histograms of the p.d.f. for the second set of calculations are shown in Figures 16 and 17. The shape of the histograms for the two different sets of calculations are very similar, but the standard deviation is significantly smaller for the nonspecular surface. The difference in standard deviation is very apparent in Figure 15 where the standard deviation in photon path length is plotted as a function of height-to-radius for both boundary conditions. This calculation shows that a completely nonspecular surface is superior to that of a specular surface with nonspecular backing.

The effect of an optical mismatch between the crystal and the photomultiplier was investigated by changing the index of refraction of the photomultiplier window while holding the other input parameters

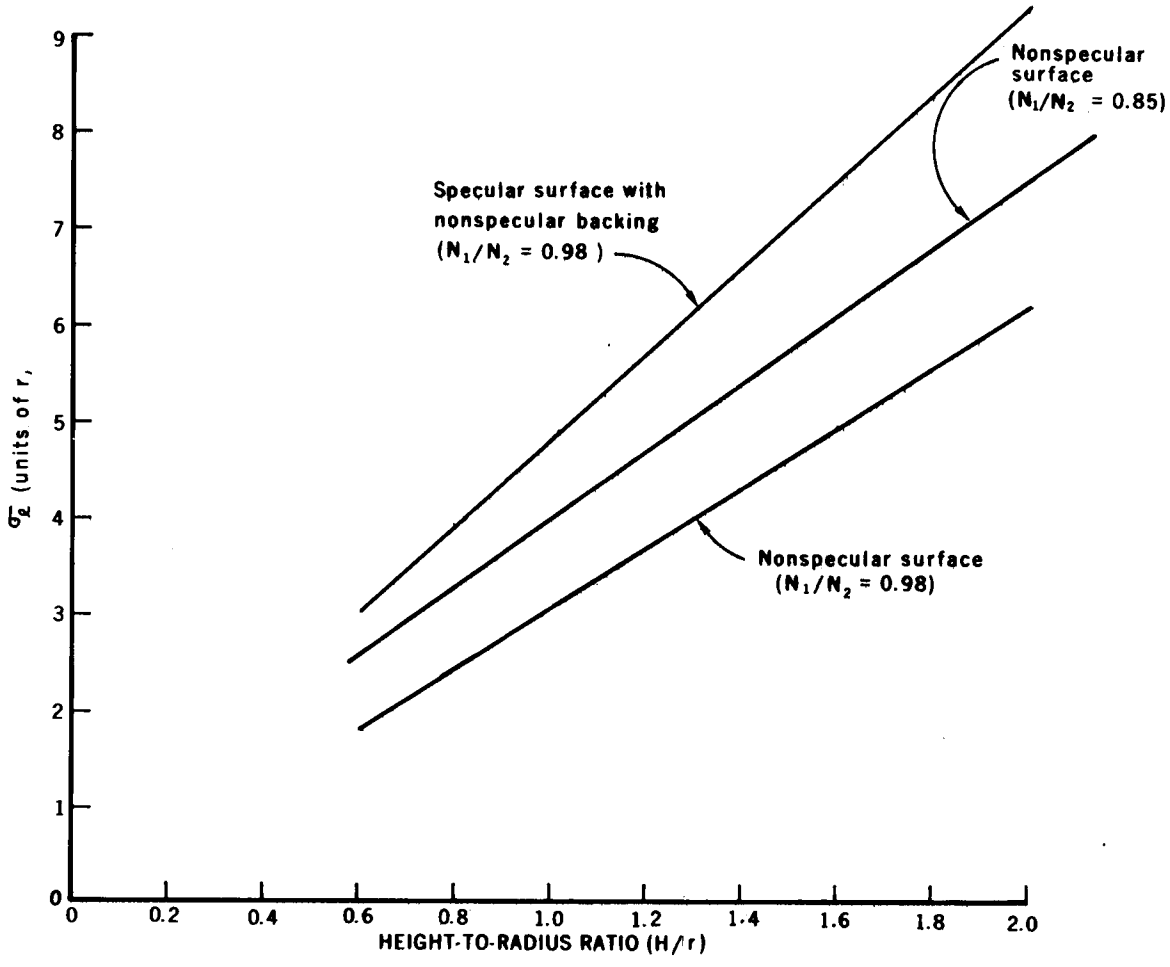


Figure 15. Standard deviation of photon path length versus height-to-radius ratio of the crystal.

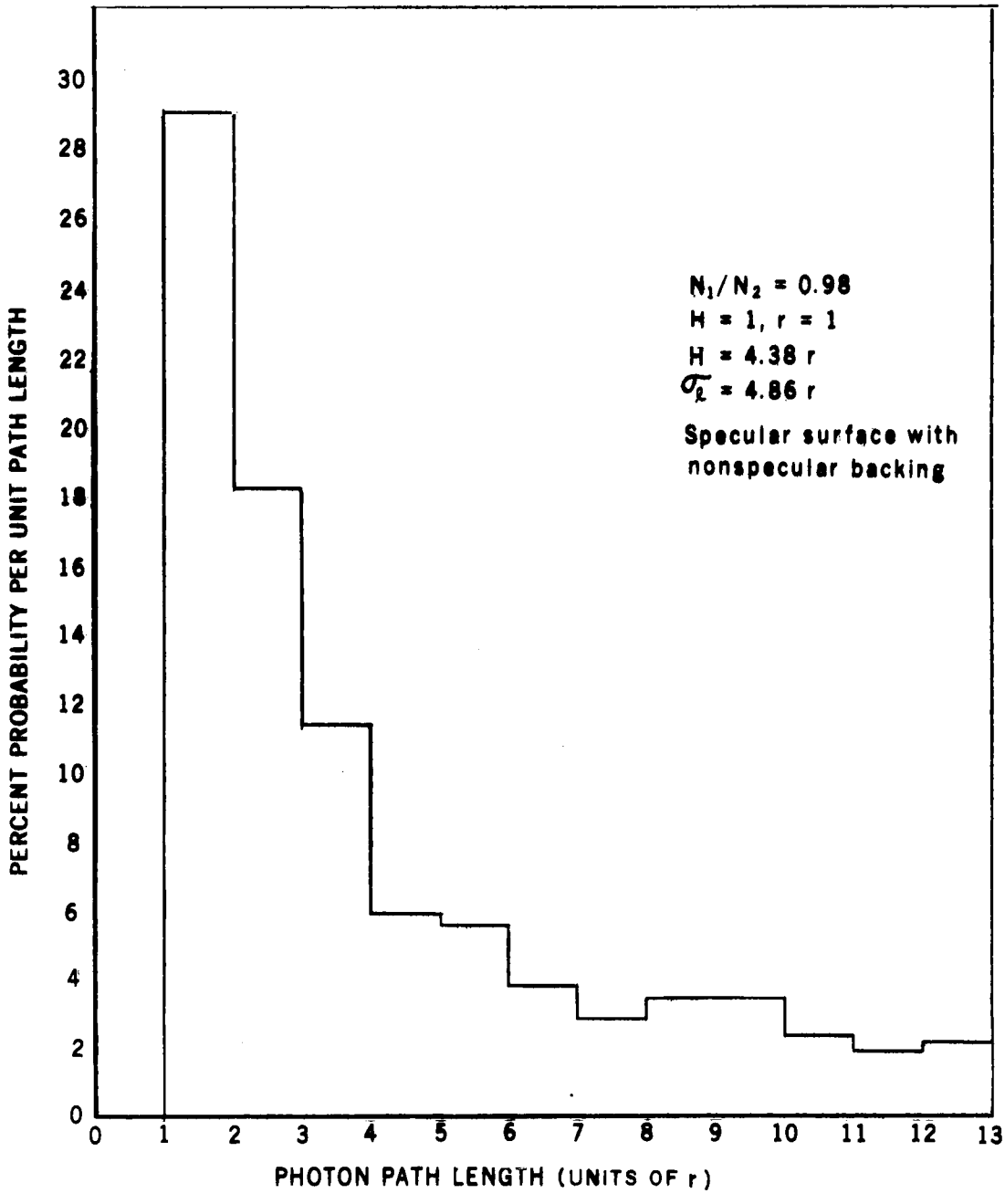


Figure 16. Probability density function of the photon path length for a crystal with dimensions H = 1, r = 1.

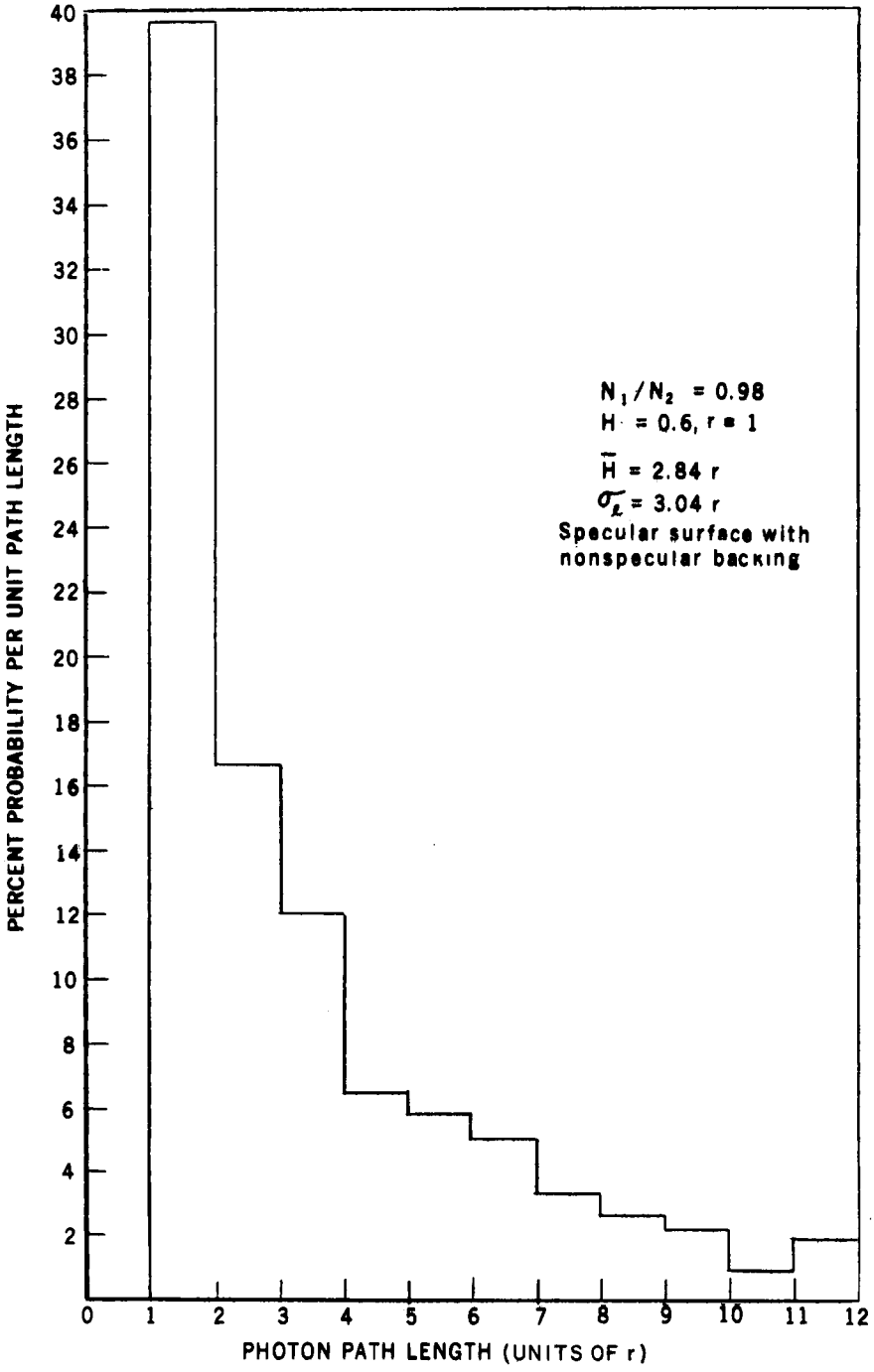


Figure 17. Probability density function of the photon path length for a crystal with dimensions H = 2, r = 1.

constant. The calculations (Figure 18) reveal that the standard deviation increases from 5 to 13.5 as the ratio of indices of refraction decreases from 0.98 to 0.85 for the specular surface with nonspecular backing. Although this is not a good measure of the effect on the overall response of the system, the calculation demonstrates the importance of a well-matched interface between the crystal and the photomultiplier. The effect is not as important for the crystal with the nonspecular surface.

The calculations presented thus far were based on the assumption that the light was generated at a single point in the crystal. Figure 19 shows how the standard deviation (σ) and the mean distance ($\bar{L}$) varies as a function of position of the light source along the cylindrical axis of the crystal. The standard deviation increases approximately 10 percent as the source position is changed from 0.1 unit to 0.9 unit from the bottom of the crystal. The mean distance ($\bar{L}$) changes approximately 2 units for the same change in source position. Since the mean distance calculation does not take into consideration the distance traveled by the incoming gamma ray, the distance from the top of the crystal to the source point should be added to the $\bar{L}$ curve. The result of this addition is the dashed curve of Figure 19 which indicates an approximate change of 20 percent in the corrected mean distance ($\bar{L}'$) for the specified change in position of the light source. Since both the mean and standard deviation change with position, the exact time distribution of light from the crystal cannot be determined from a single light source.

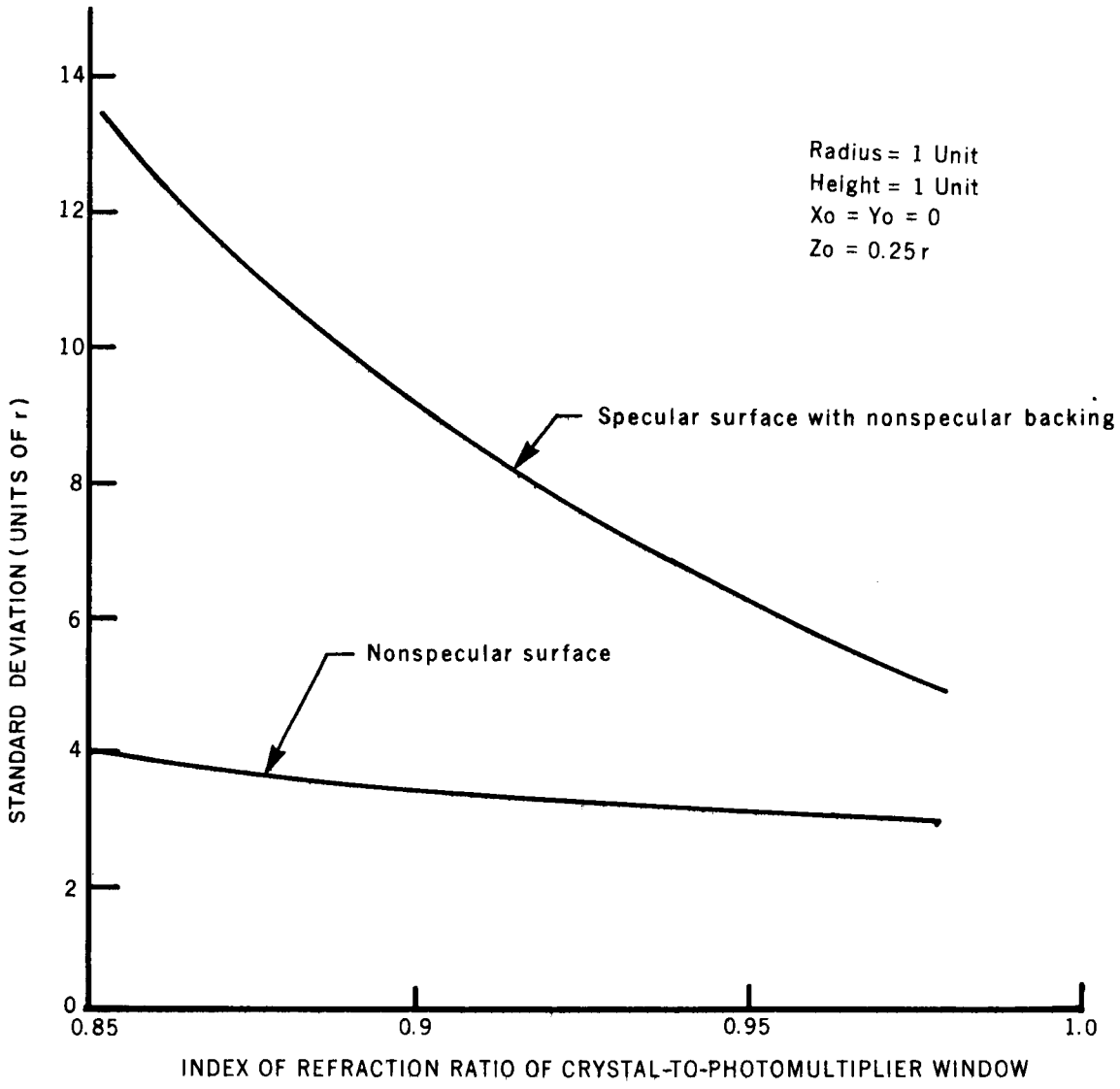


Figure 18. Standard deviation of photon path length versus index of refraction ratio of the exit window.

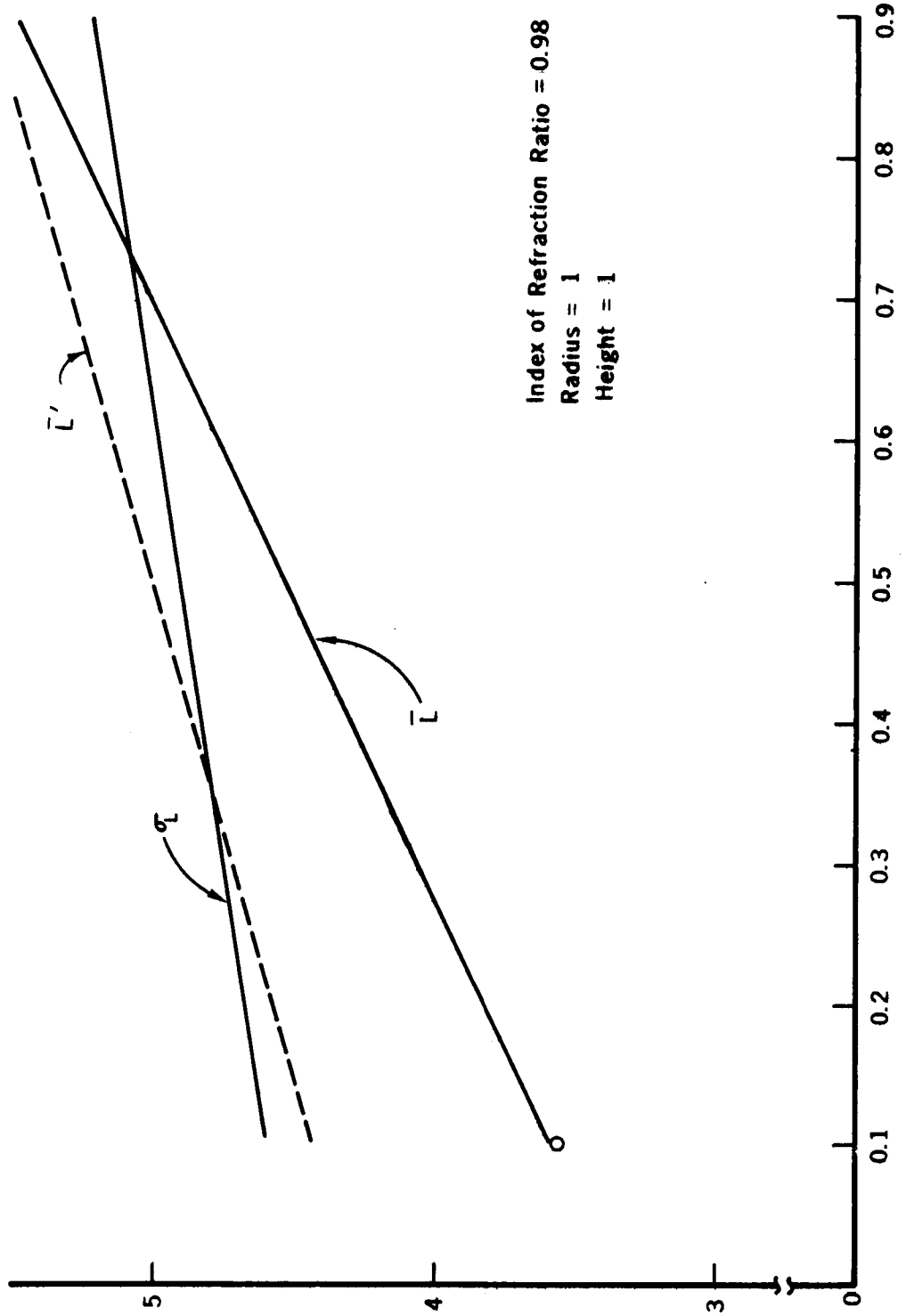


Figure 19. Standard deviation and mean photon path length versus position of photon generation.

To a first order approximation the histograms shown in Figures 10 through 17 (pages 41-45, 47, 48) can be represented by an exponential function with a single decay time-constant. The p.d.f. in transit time is

$$f(t) = \frac{1}{\sigma} e^{-t/\sigma} \quad , \tag{38}$$

where σ is the standard deviation in time. The standard deviation is different for the two sets of calculations. For the specular surface with a nonspecular backing the standard deviation from Figure 15, page 47, is

$$\sigma = \frac{4.8H}{V_0} \quad , \tag{39}$$

where V_0 is the velocity of light with dimensions consistent with those of the crystal, and H is the height of the crystal. Equation (38) can be rewritten as

$$f(t) = \frac{V_0}{4.8H} e^{-V_0 t/4.8H} \quad . \tag{40}$$

For the case of the nonspecular surface the standard deviation is

$$\sigma = \frac{4H}{V_0} \quad . \tag{41}$$

The offset time, as indicated in the histograms, is not important in the system calculations and is ignored in the analysis.

CHAPTER III

PHOTOMULTIPLIER CHARACTERISTICS

I. SOURCES OF TIME VARIANCE

The photomultiplier is usually considered to have three major sources of time variance.[22,23,24,25] The three major sources are:

1. Difference in photoelectron transit times for different generation points on the cathode,
2. Fluctuation in photoelectron transit times due to initial velocity differences,
3. Uncertainty in transit times of secondary electrons from the dynodes.

The first source of time variance is due to the geometry of the photocathode. Photoelectrons generated at different points on the photocathode encounter different path lengths and also different potential gradiants. The potential gradient and path length variation causes the transit times of the photoelectrons to be different.

The second source is a result of the photoelectrons leaving the surface of the photocathode with different velocities. The time variance resulting from the spread of photoelectron velocities accounts for an appreciable part of the overall time variance of a system using NaI(Tℓ) as the scintillator.

The third source of time variance is due to secondary electrons at the first dynode being emitted with different velocities. Also, included in the third source is the variation in multiplication gain of the dynodes.

Difference in Photoelectron Transit Times for Different Generation Points on the Cathode

A fast mercury relay light pulser[26] was used to measure the transit time difference for different electron generation points on the cathode. The light pulser had a pulse width much less than one nanosecond when operated at an extremely low voltage.[27] The full width at half maximum (FWHM) of the light distribution from the pulser was reported to be less than 1.5 nsec when the relay was operated at 1,000 volts.[26] The pulser had an electrical trigger pulse that was time synchronized to the light pulse with a timing uncertainty of only a few picoseconds. The trigger pulse was used to trigger a Tektronix type 661 sampling oscilloscope as shown in Figure 20.

In operation the light is focused on the center of the photocathode and a zero time reference is established on the oscilloscope. A large number of photoelectrons are produced for each light pulse in order to reduce the time variance due to the other sources. After the time reference is established, the photomultiplier's position with respect to the small aperture (Figure 20) is changed and the position recorded. The transit time difference along a single axis is shown in Figures 21, 22, and 23 for three types of fast tubes.

The transit time difference is transformed to a distribution in time by assuming that the photons are evenly distributed over the entire area of the photocathode. The probability that a photon will generate a photoelectron at a distance x from the center of the cathode and within the annulus Δx is given by

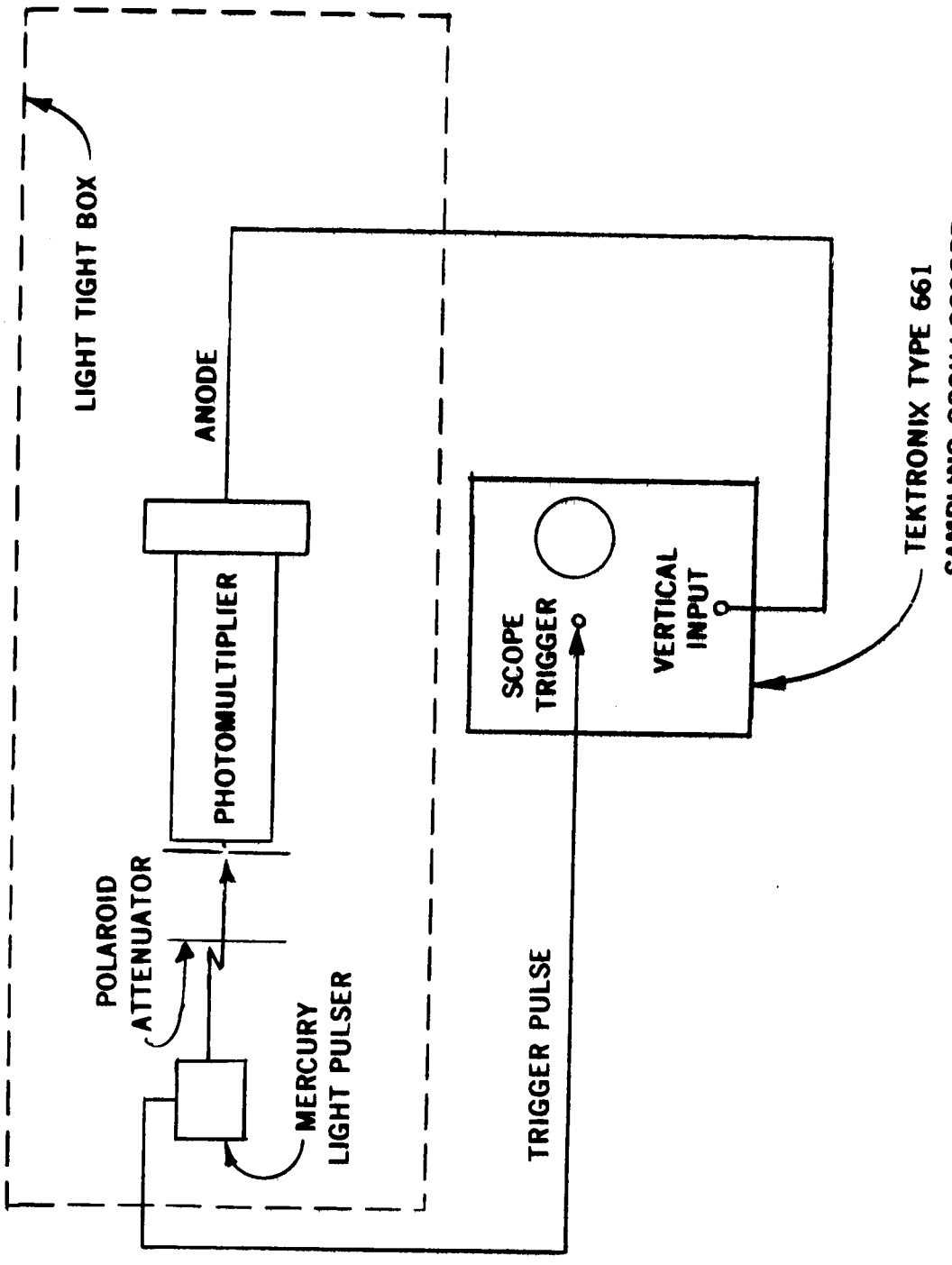


Figure 20. Block diagram of system used for measuring the photocathode transit time difference.

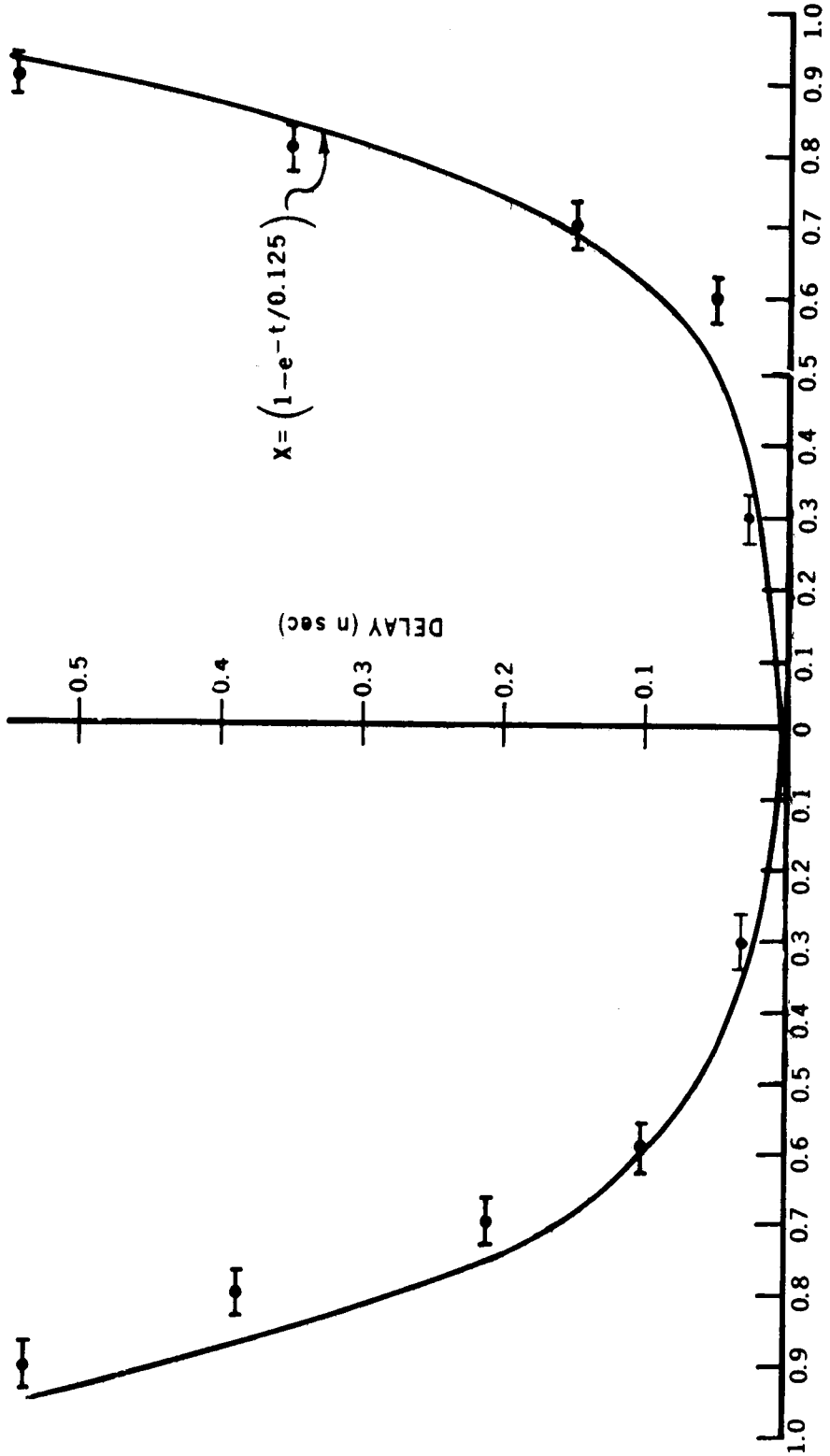


Figure 21. Transit time delay versus distance from center of the RCA 8575 photocathode.

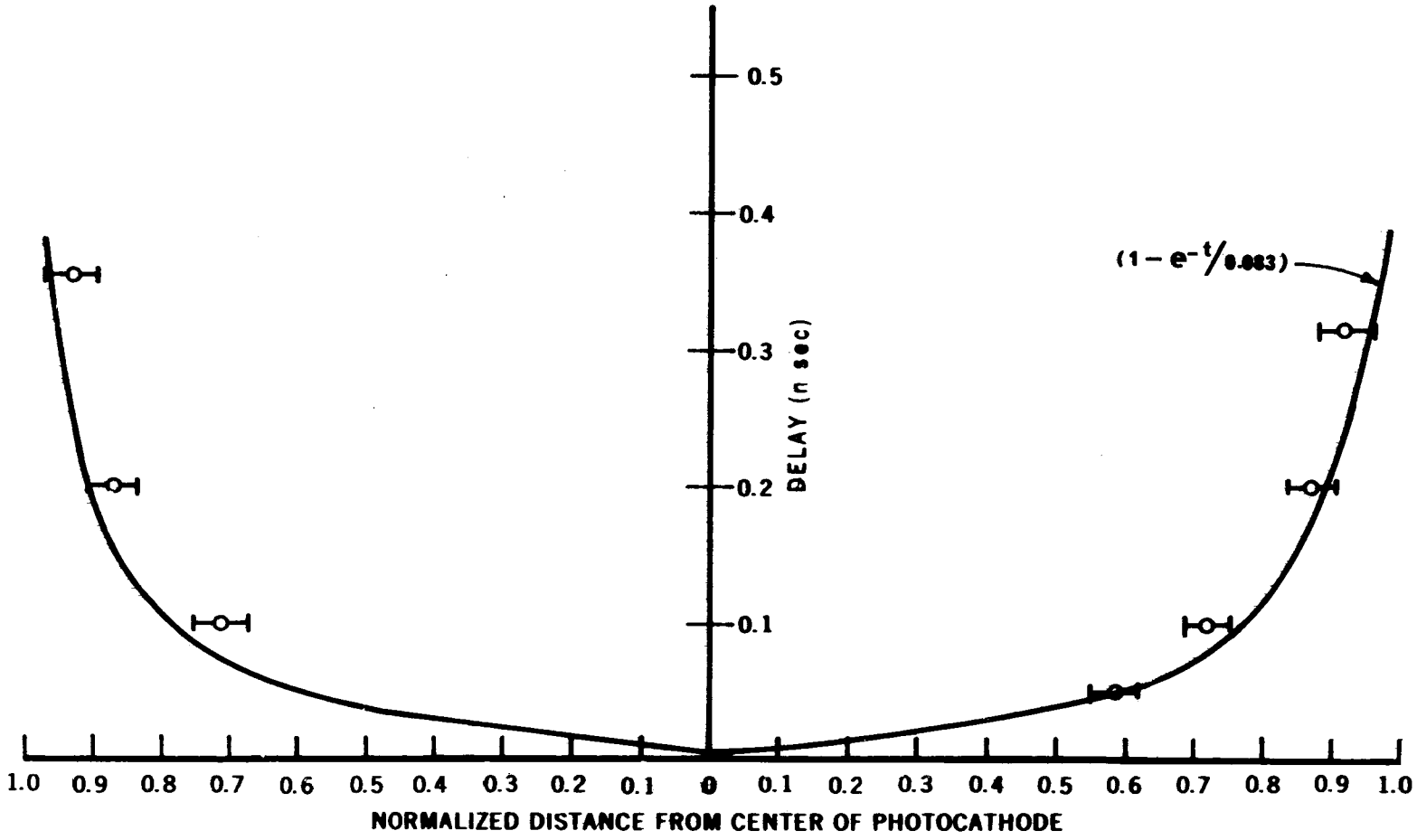


Figure 22. Transit time delay versus distance from center of the XP-1020 photocathode.

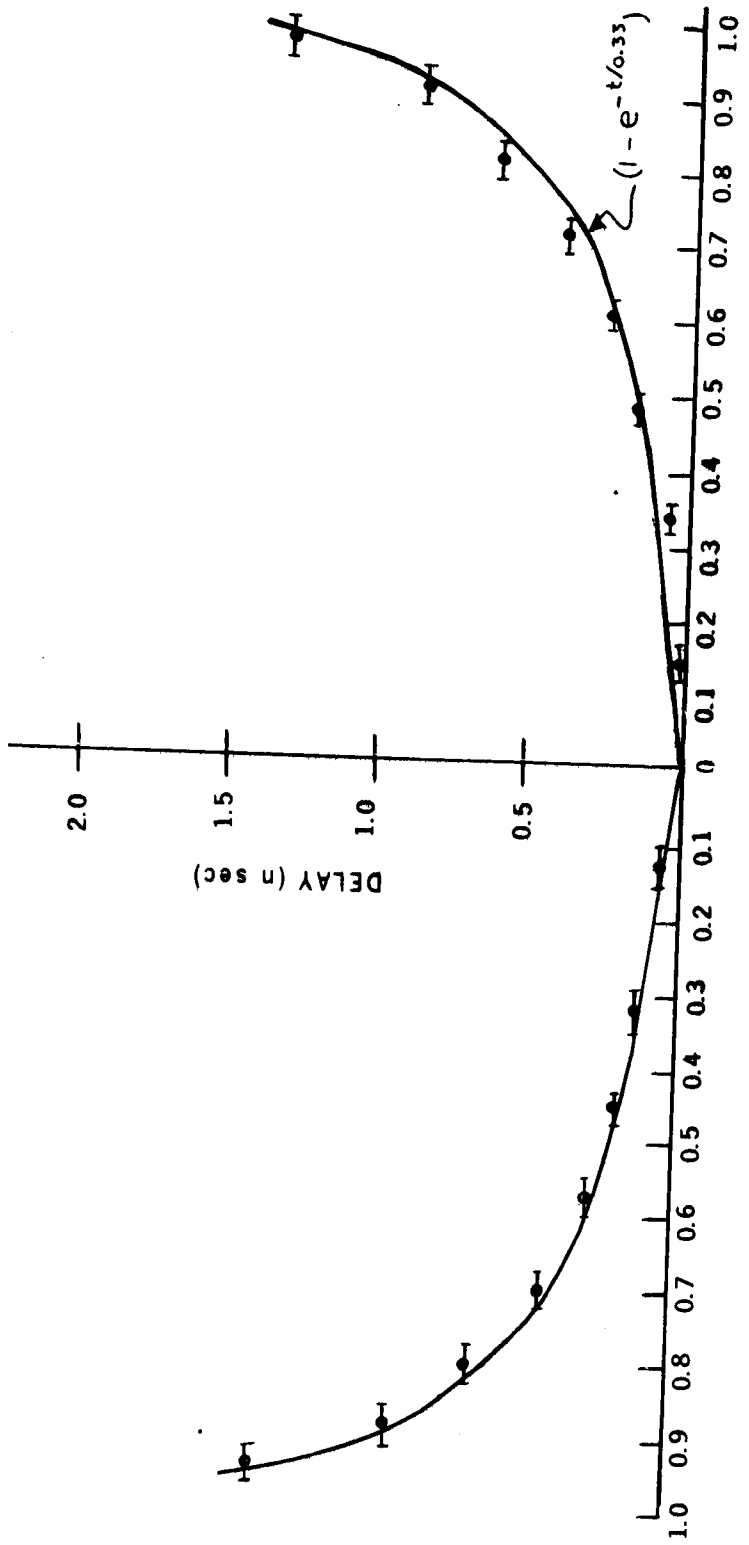


Figure 23. Transit time delay versus distance from center of the XP-1040 photocathode.

$$P(x) = 2x\Delta x \quad , \quad 0 \leq x \leq 1 \quad . \tag{42}$$

The relationship between transit time difference and the normalized distance (x) for the two tubes as shown in Figures 21 and 22 can be approximated by

$$t = k \, \ell n(1 - |x|) \quad , \quad -1 \leq x \leq +1 \quad , \tag{43}$$

where t is measured in nanoseconds. Typical values of the constant k are 0.125 for the RCA-8575 and 0.08 for the XP-1020. Solving for the distance, Eq. (43) becomes

$$|x| = (1 - e^{-t/k}) \equiv g(t) \quad . \tag{44}$$

To compare this particular source of time variance with the other sources, Eq. (44) will be used to describe the transit time difference at any position on the cathode. For the RCA-8575 tube Eq. (44) becomes

$$|x| = (1 - e^{-t/0.125}) \quad .$$

The p.d.f. in time is obtained by substituting $|x|$ into Eq. (42). The resulting p.d.f. for the RCA-8575 tube is

$$P(t) = 2g(t) \frac{dg(t)}{dt}$$

$$= \frac{2e^{-t/0.125}}{0.125} (1 - e^{-t/0.125}) \quad . \tag{45}$$

The mean transit time difference is

$$\bar{t} = \frac{2}{0.125} \int_0^\infty t(e^{-t/0.125} - e^{-2t/0.125})dt$$

which reduces to

$$\bar{t} \approx 0.19 \text{ nsec} \quad . \tag{46}$$

The general expression for the standard derivation in time is

$$\sigma_t = \overline{t^2} - (\bar{t})^2 = 2k \quad .$$

For the RCA-8575 the standard deviation is

$$\sigma_t \approx 0.17 \text{ nsec.} \tag{47}$$

The RCA-8575 and the Amperex XP-1020 have an effective cathode diameter of 42 millimeters. The transit time difference versus the normalized distance from the center of an XP-1040 photomultiplier tube is shown in Figure 23, page 59. The XP-1040 has an effective diameter of 110 millimeters. At an operating voltage of 2200 volts the maximum difference in transit time is approximately 1.5 nanoseconds. The relationship between the transit time difference and the distance from the center can be approximated by

$$|x| = (1 - e^{-t/0.33}) \quad . \tag{48}$$

Assuming radial symmetry, the p.d.f. in time becomes

$$P_{(t)} = 6(1 - e^{-t/0.33})e^{-t/0.33}, \quad 0 \leq t \leq \infty \quad . \tag{49}$$

The mean transit time difference expected for the XP-1040 is

$$\bar{t} = 6 \int_0^{\infty} (te^{-3t} - te^{-6t}) \approx 0.5 \text{ nsec.} \tag{50}$$

The standard deviation in time for the XP-1040 tube is

$$\sigma_t = \overline{t^2} - (\bar{t})^2 \approx 0.47 \text{ nsec.} \tag{51}$$

These calculations (Eqs. 50 and 51) are only valid for a single photoelectron and, therefore, have no significance with respect to the overall system. The calculations are presented here so that the time variance contribution of the photoelectron transit time difference can be compared with the other sources of time variance. For example, the transit time difference for an RCA-8575 would be equivalent to the photon transit time spread in a NaI(Tℓ) crystal with a height of 0.29 inch. The transit time difference of the XP-1040 (110 mm diameter) would be equivalent to the photon transit time spread in a crystal with a height of 0.8 inch.

Fluctuation in Photoelectron Transit Times Due to Initial Velocity Differences

After overcoming the photoelectric work function at the surface of the photocathode, the electrons emerge with a statistical spread in

velocity. This spread in velocity gives rise to the source of time variance often referred to as photocathode-to-first dynode transit time fluctuation.

Figure 24 is a block diagram of a system for measuring the distribution of the transit times of single electrons. The critical part of the system is the light pulser which must have a narrow pulse width compared with the width of the transit time distribution that is to be measured. The mercury relay pulser used in the transit time difference measurement has a pulse width much less than one nsec when the relay is operated at approximately 300 volts.[27] At this voltage, a measurement of the full width at half-maximum of the time distribution was 320 picoseconds. This measurement included the transit time spread associated with a fast photomultiplier. The light output of the pulser, operating at 300 volts, is only a few hundred photons. Since the light pulse is too small for a time measurement using photodiodes or any known photographic technique, the indirect measurement using the fast photomultiplier of reference 27 is accepted as an upper limit of the pulse width.

Other sources of statistical spread in the transit time measurement are the photocathode geometric effect as described in the previous section, the spread due to the multiplication process at the dynodes, and the tunnel diode discriminator. The first of these, the geometric effect, is eliminated by masking all the photocathode except a small sperture in the center as shown in Figure 24. The second source, the multiplier spread, cannot be eliminated from this transit-time measurement.

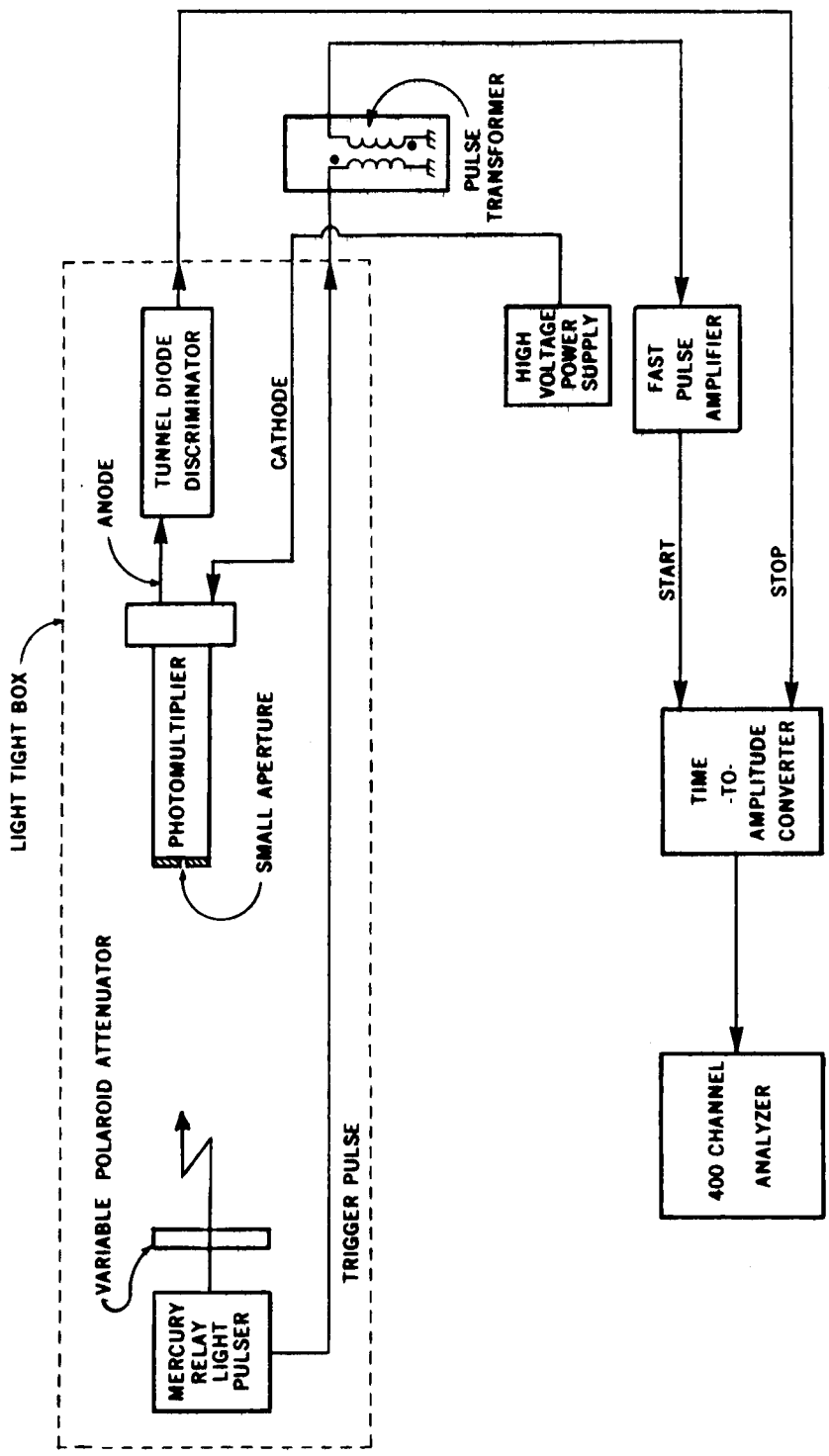


Figure 24. System for measuring the transit time distribution for a photomultiplier.

In the next section, the effect of the transit time spread of electrons traveling from the first to the second dynode will be calculated using realistic assumptions about the multiplication process.

The third source of time variances in the transit time measurement is the tunnel diode discriminator. The tunnel diode operating in a switching mode contributes only slightly to the time variance when a large signal current is applied to the input.[28] Since the mean current amplitude at the anode of an RCA-8575 tube due to a single photoelectron is approximately 12 ma, no appreciable time variance is expected due to the tunnel diode discriminator. Therefore, the width of the time distribution measured by the system of Figure 24 is the result of the variation of transit times of electrons from the cathode to the anode. The primary contribution is shown in the next section to be the variance due to variations in the transit times of photoelectrons between the cathode and the first dynode.

The photoelectron transit time distribution measurement is based on the same concept as the scintillator decay time measurement of Chapter II. The light pulser output is adjusted, by means of polaroid attenuator (Figure 24), so that the probability of a single electron being generated at the photocathode is much less than unity. With this condition imposed, the probability of the time interval measured by the time-to-amplitude converter of Figure 24 being between zero and time t is

$$F(t) = \int_0^t f(t')dt' \quad , \tag{52}$$

where f(t) is the p.d.f. of the statistical distribution F(t). Several thousand single electron transit time measurements were made and stored in the pulse-height analyzer. A plot of the number of counts versus time represents then the unnormalized p.d.f.

A typical p.d.f. representing the transit time spread of single electrons in the RCA-8575 tube is shown in Figure 25 and for the XP-1020 in Figure 26. The function,

$$f(t) = \frac{t^2}{2(k_1)^2} e^{-t/k_1} , \quad 0 \leq t < \infty , \tag{53}$$

is shown in Figures 24 (page 64) and 25 to be a reasonable fit to the measured p.d.f. The relationship between the FWHM of the measured p.d.f. and the constant k_1 in Eq. (53) is given by

$$k_1 = \frac{\Delta t}{3.395} , \tag{54}$$

where Δt is the FWHM of measured p.d.f. (Figures 25 and 26). Equation (53) will be used in Chapter IV as the single electron transit time p.d.f. to determine the time resolution of the overall system.

Uncertainty in Transit Times of Secondary Electrons from the Dynodes

The time variance of the dynode multiplication process was included in the measurements of the previous section. The purpose of this section is to calculate an upper limit of the contribution of the dynode multiplier to the overall cathode-to-anode transit time spread.

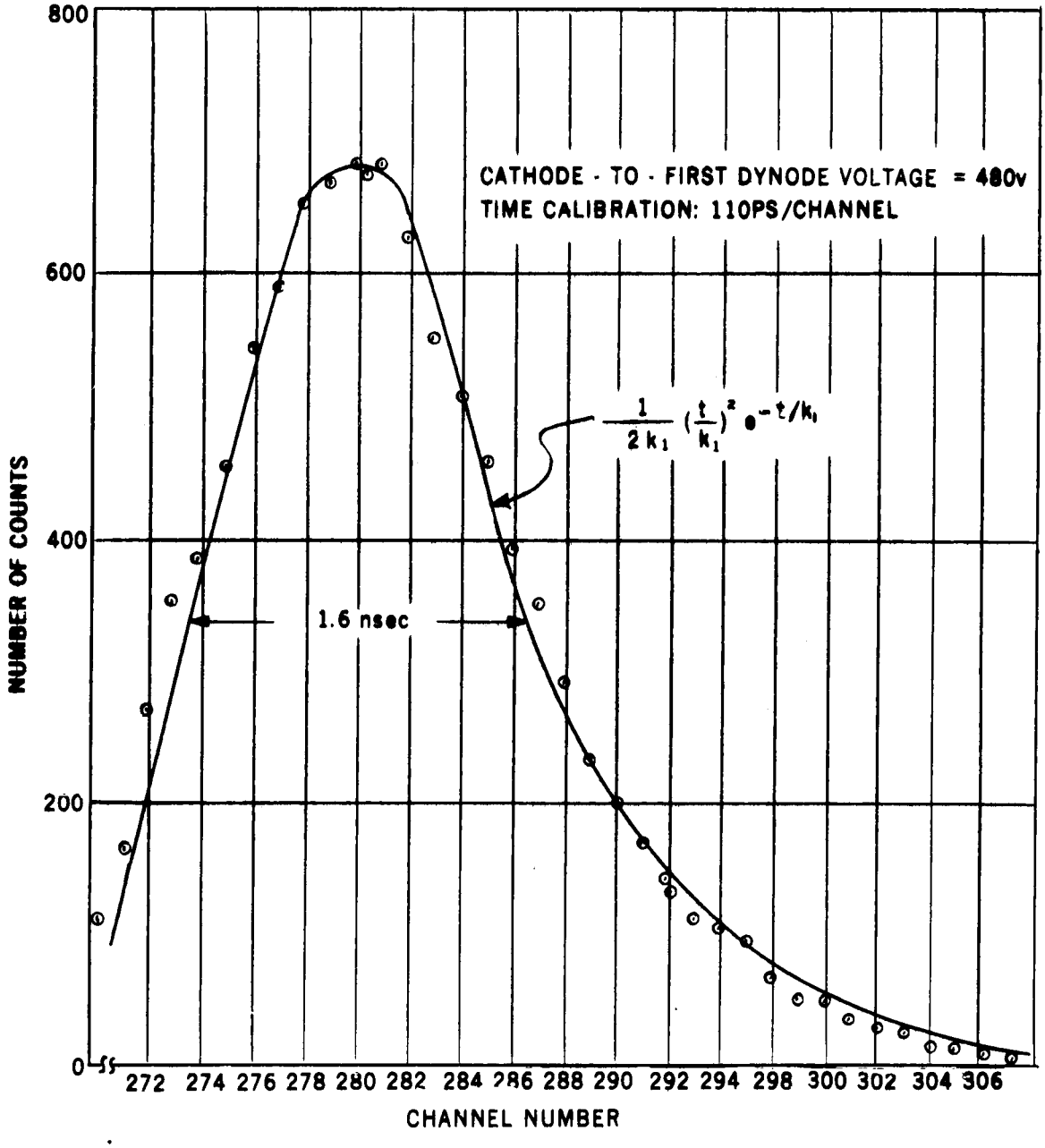


Figure 25. A typical transit time distribution for the RCA 8575 photomultiplier.

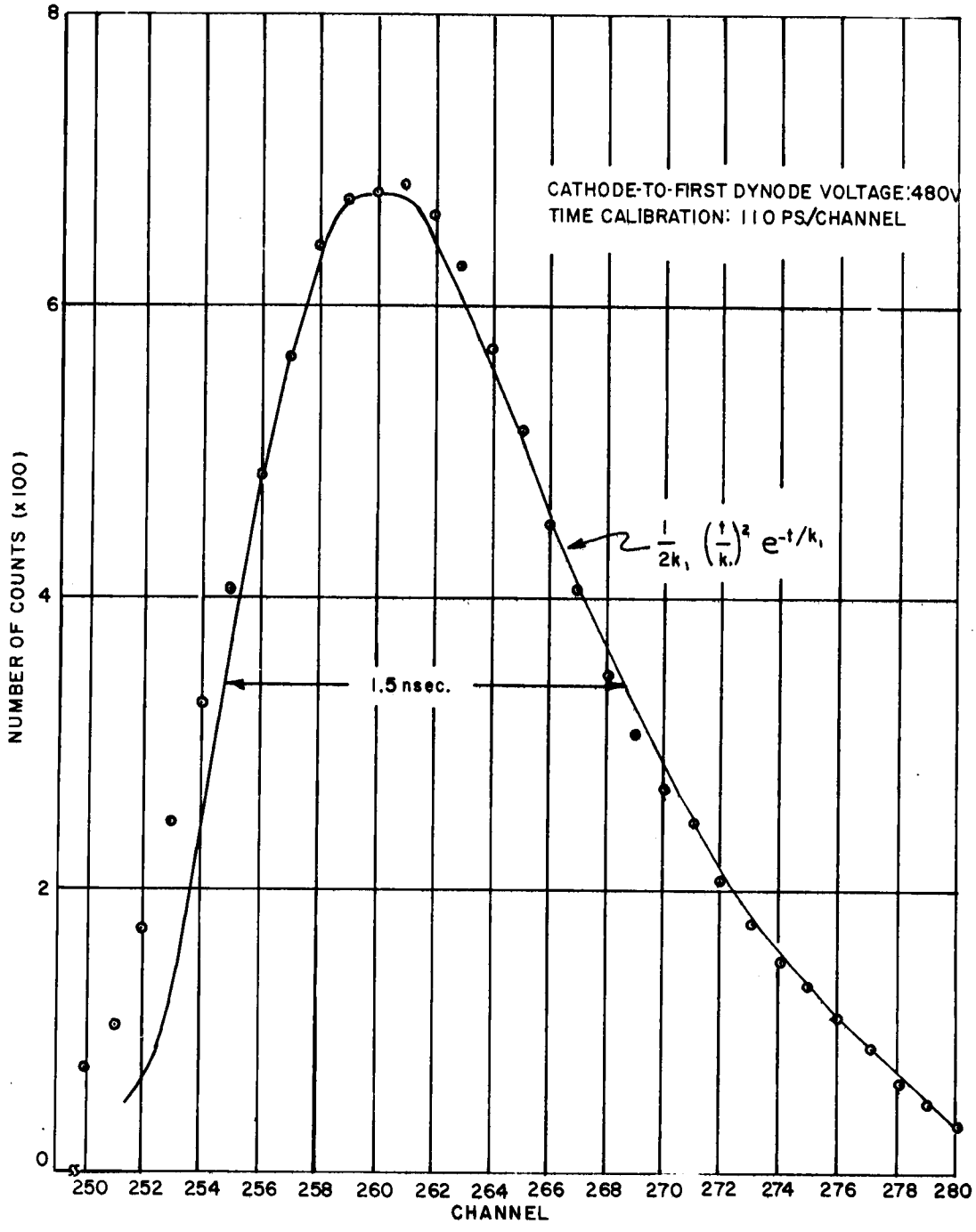


Figure 26. A typical transit time distribution for the XP-1020 photomultiplier.

To establish an upper limit, the p.d.f. of the transit time between the cathode and first dynode is assumed to be exponential with a variance of σ^2. Furthermore, individual electrons from the first dynode is assumed to have the same p.d.f. as electrons from the cathode. This assumption is justified by the fact that the field between the cathode and the first dynode is normally less than the field between the dynodes. As a result of the relative amplitudes of electric fields, the time variance is expected to be greater for electrons from the cathode.[23] Therefore, the assumption of p.d.f.'s with equal variance is realistic for establishing an upper limit on the contribution to the total variance of electrons from the first dynode. The assumed p.d.f. for individual electrons from the cathode and also from the first dynode is

$$f(t) = \frac{1}{\sigma} e^{-t/\sigma} \quad . \tag{55}$$

Since the first dynode has a mean multiplication gain greater than unity, the effective transit time variance between the first and second dynode will be substantially less than the time variance of single electrons. If the gain were constant, the problem of determining the effective time variance would be simpler. The fluctuation in gain obeys a Poisson distribution

$$f(k) = \frac{(\bar{k})^k \, e^{-\bar{k}}}{k!} \quad , \quad k = 0,1,2,\ldots, \tag{56}$$

where k is the gain of the first dynode. The mean gain is $\bar{k}$ and the variance in gain is also $\bar{k}$.

Let a fictitious observer be placed on the second dynode who is instructed to record the mean time of arrival of the electrons from the first dynode. An argument could be made that the mean time of arrival is not as important, for example, as the time when the first, second, or third electron arrives at the dynode. The variance increases as the electron level increases as indicated by Eq. (29) for a single exponential p.d.f. Therefore, the variance of the mean arrival time is larger than the variance of any electron arriving before the mean time. The detection of the mean arrival time then should be realistic for determining the upper limit on the contribution of the transit times of electrons between the first and second dynode to the overall system. The first part of the calculation is to determine the distribution of the mean transit times of k independent electrons. For k equal to unity, the distribution is given by Eq. (55). For two electrons, the distribution is slightly more complicated. Let t_1 and t_2 be the times of arrival at the second dynode of two electrons. The joint p.d.f., assuming stochastic independence, is

$$f(t_1,t_2) = \frac{1}{\sigma} e^{-t_1/\sigma} \cdot \frac{1}{\sigma} e^{-t_2/\sigma} \quad . \tag{57}$$

The sample mean of t_1 and t_2 is defined as

$$\hat{t} = \frac{t_1 + t_2}{2} , \quad 0 \leq \hat{t} < \infty \quad . \tag{58}$$

The distribution of the sample mean will contain the desired information for the two electrons. Since the transformation of the variables t_1 and t_2 to the variable t must be one-to-one, t_1 and t_2 must be transformed to two variables. For the second variable let

$$\hat{\hat{t}} = \frac{t_1}{t_1 + t_2} \quad , \; 0 \leq \hat{\hat{t}} \leq 1 \quad .$$

The desired transformation is

$$f(\hat{t},\hat{\hat{t}}) = f(t_1,t_2)|J| \quad , \tag{59}$$

where the Jacobian is given by

$$J = \begin{vmatrix} \frac{\partial t_1}{\partial \hat{t}} & \frac{\partial t_1}{\partial \hat{\hat{t}}} \\ \\ \frac{\partial t_2}{\partial \hat{t}} & \frac{\partial t_2}{\partial \hat{\hat{t}}} \end{vmatrix} \quad ,$$

or

$$J = \begin{vmatrix} 2\hat{\hat{t}} & 2\hat{t} \\ \\ 2-2\hat{\hat{t}} & -2\hat{t} \end{vmatrix} \quad . \tag{60}$$

After reducing the determinant,

$$J = 2\hat{\hat{t}}(-2\hat{t}) - 2\hat{t}(2 - 2\hat{\hat{t}}) = - 4\hat{t} \quad . \tag{61}$$

Substituting Eq. (61) into Eq. (59) yields

$$f(\hat{t},\hat{\hat{t}}) = \frac{4\hat{t}}{\sigma^2} e^{-(2\hat{t}\hat{\hat{t}}+2\hat{t}-2\hat{t}\hat{\hat{t}})/\sigma}$$

$$= \frac{4\hat{t}}{\sigma^2} e^{-(2\hat{t})/\sigma} \quad . \tag{62}$$

The marginal p.d.f. of $\hat{t}$ is obtained from Eq. (62) by integrating over the domain of $\hat{\hat{t}}$.

$$f_2(\hat{t}) = \int_{\hat{\hat{t}}=0}^{1} \frac{4\hat{t}}{\sigma^2} e^{-2\hat{t}/\sigma} \, d\hat{\hat{t}}$$

$$f_2(\hat{t}) = \frac{\hat{t}}{(\sigma/2)^2} e^{-\hat{t}/(\sigma/2)} \quad . \tag{63}$$

Equation (63) is the marginal p.d.f. for the mean arrival time of two electrons. For three electrons, a similar procedure is used to determine the p.d.f. The resulting p.d.f. for three electrons is

$$f_3(\hat{t}) = \frac{(\hat{t})^2}{2!(\sigma/3)^3} e^{-\hat{t}/(\sigma/3)} \quad . \tag{64}$$

The p.d.f. for 4 electrons is

$$f_4(\hat{t}) = \frac{(\hat{t})^2}{3!(\sigma/4)^4} e^{-\hat{t}/(\sigma/4)} \quad . \tag{65}$$

The p.d.f. for k electrons is

$$f_k(\hat{t}) = \frac{(\hat{t})^{k-1}}{(\sigma/k)^k} e^{-\hat{t}/(\sigma/k)} \quad . \tag{66}$$

This p.d.f. is a gamma distribution in the parameter tk/σ. Let

$$x = (tk)/\sigma \quad ,$$

so that Eq. (66) becomes,

$$f_k(x) = \frac{x^{k-1}}{(k-1)!} e^{-x} \quad . \tag{67}$$

The variance of x is k and, also, the mean of x is k. Therefore, the variance of t is

$$\sigma_t^2 = \left(\frac{\sigma}{k} \right)^2 \sigma_x^2 = \frac{\sigma^2}{k} \quad . \tag{68}$$

The weighted variance expected by repeating the experiment a large number of times is

$$\sigma_{W_{\hat{t}}}^2 = \sum_{k=1}^{\infty} W_k \, \sigma_t^2 \quad , \tag{69}$$

where W_k is the probability of exactly k electrons arriving at the second dynode. Thus, W_k is given by Eq. (66). Combining Eqs. (66) and (69), the weighted variance is

$$\sigma_{\hat{t}W}^2 = \sum_{k=1}^{\infty} \frac{(\bar{k})^k e^{-\bar{k}}}{k(k!)} \, \sigma^2 \quad . \tag{70}$$

The mean gain $\bar{k}$ is assumed to be 4 which is low in comparison with the gain of the first stage of a typical photomultiplier. For the mean gain of 4,

$$\sigma^2_{\hat{t}W} = 4e^{-4}(1 + 1 + \frac{16}{18} + \ldots + \frac{(4)^P}{4P(P!)} + \ldots)\sigma^2 \simeq 0.32\sigma^2 \quad .$$

Assuming that the variance of two cascade processes can be added linearly, the width of the time distribution is increased due to the first dynode by a factor of

$$\frac{\sigma_t}{\sigma} = \frac{\sqrt{\sigma^2 + 0.32\sigma^2}}{\sigma} \simeq 1.15 \quad . \qquad (71)$$

Under the worst operating conditions the transit times of electrons from the first dynode contribute only 15 percent of the total cathode-to-anode transit time spread. The contribution of the other dynodes to the transit time spread is much less than 15 percent. Therefore, under normal operating conditions the transit time spread of electrons from the cathode to the first dynode is expected to be the major source of transit time spread in the photomultiplier.

II. PHOTOELECTRON YIELD OF THE CATHODE

The number of photoelectrons produced at the cathode for a single event has a strong influence on the timing information available about the initial time of that event. This influence can be seen from the standard deviation in time (Eq. 29) of the $j^{\underline{th}}$ photoelectron for the

single exponential p.d.f. system. The standard deviation in time is

$$\sigma_j = \frac{\tau\sqrt{j}}{R} \quad . \tag{29}$$

where τ is the light decay time of the scintillator and R is the total number of electrons emitted from the cathode for a single scintillation event. The minimum standard deviation in time obtainable from the single exponential p.d.f. system was shown in a previous section to be

$$\sigma_1 = \frac{\tau}{R} \quad . \tag{72}$$

Since the single exponential p.d.f. is considered to be the ultimate limit for the more practical scintillator-photomultiplier system, the importance of the yield for determining the timing characteristics is evident from Eqs. (29) and (72). The purpose of this section is to outline a useful technique for determining R, the photoelectron yield, for a NaI(Tℓ) scintillator and photomultiplier. The technique to be introduced is considered useful in determining the relative photocathode efficiency even when a NaI(Tℓ) scintillator is not the scintillator to be used in a particular application.

Several techniques have been used to determine the photoelectron yield. Onno and Bell[30] calculated the yield from a measurement of the pulse height resolution resulting from a monoenergetic gamma ray. Borkowski[31] compared the pulse height distribution of a 46 keV gamma ray with known single photoelectron pulse heights to determine the yield. Electron yields ranging from a low of 1.1 to a high of 11 photoelectrons

per keV have been reported.[32,33] The yield of 11 photoelectrons per keV was obtained using the most direct of the known techniques. A charge sensitive preamplifier was connected to the first dynode of the photomultiplier and a known pulse height spectrum from Na^{22} was recorded. The gain of the system was calibrated by injecting a pulse of known charge into the input of the charge sensitive preamplifier. Thus, a measurement was made of the number of electrons appearing at the preamplifier input corresponding to a known gamma ray energy. A necessary assumption in this experiment is that all the photoelectrons leaving the cathode reach the first dynode. Only a small error is introduced by this assumption since the collection efficiency of the first dynode is typically much larger than 90 percent. In comparing the results from all the experiments, a possible conclusion is that NaI(Tℓ) yields vary from scintillator to scintillator. Also, recently the photocathode efficiency has been improved remarkably by the use of a bialkali material. The variation in cathode efficiency and scintillator yield probably accounts for most of the differences in the measured yields. The fact that the yield varies from one experiment to another serves to further illustrate the need to measure the parameter for each combination of scintillators and photomultipliers used.

A block diagram of a system used to determine the yield is shown in Figure 27. The charge signal which is proportional to energy, is taken from a dynode of the photomultiplier and fed to a 2 μsec double delay line amplifier (DDL). A single channel analyzer is used to select a very narrow energy range and to generate a timing signal coincident

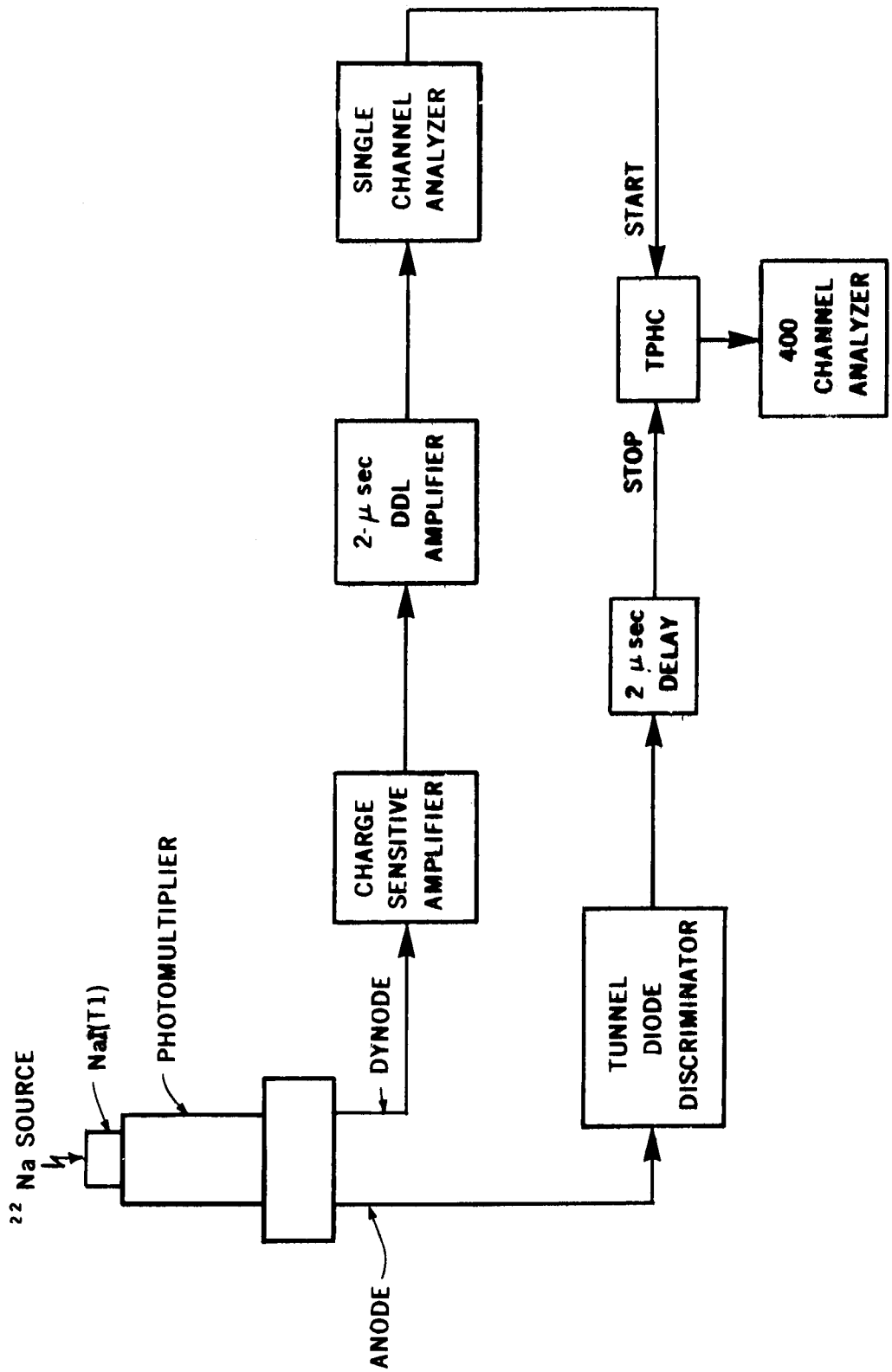


Figure 27. System for measuring photoelectron yield in NaI(Tl).

with the zero crossing of the DDL amplifier output. This signal starts a Time-to-Height Converter (TPHC) which is stopped by the delayed signal from the anode discriminator. An equation describing the essential part of the DDL amplifier is

$$f(t) = q_0 G(t) - 2q_0 U(t-d), \quad 0 \leq t \leq 2D \quad , \tag{73}$$

where q_0 is the charge corresponding to the energy selected by the single channel analyzer and D is length in time of the two delay lines used in the amplifier. The time interval measured by the system of Figure 27 is the time between the initial rise of the charge pulse and the time when f(t) equals zero. For f(t) equals zero, Eq. (73) becomes

$$0 = q_0 G(t_x + D) - 2G(t_x) q_0 U(t_x) \quad . \tag{74}$$

From Eq. (74), t_x is the time of the zero crossing of the DDL shaped charge pulse. If the delay time, D, is sufficiently long so that all the charge is collected in the time interval $t_x + D$, then

$$G(t_x + D) = 1 \quad .$$

After making this assumption, Eq. (74) can be solved for $G(t_x)$. The result is

$$G(t_x) = 1/2 \quad .$$

Therefore, t_x is the time when G(t) is half of its final value or the time when half the charge has been collected.

The system of Figure 27, page 77, measures the difference between the time of the first photoelectron and the time, t_x, of the $(R/2)^{th}$ photoelectron. The single exponential p.d.f. is sufficient for describing the crossover time t_x, since the standard deviation in time resulting from the 250 nsec scintillator decay is an order of magnitude larger than the deviation due to any other source. This is true only for gamma ray energies of 500 keV or less. The standard deviation in time is

$$\sigma_t = \frac{\tau\sqrt{j}}{\sqrt{R(R - j)}} \quad . \tag{111}$$

Substituting $j = R/2$ into Eq.(111) yields

$$\sigma_t = \frac{\tau\sqrt{R/2}}{\sqrt{(R)(R - R/2)}} = \frac{\tau}{\sqrt{R}} \quad . \tag{75}$$

The observed shape of the time spectrum for $j = R/2$ is almost normal as expected. The conversion from standard deviation to full width at half maximum (FWHM) for a normal distribution is

$$\Delta t_{FWHM} \approx 2.35\ \sigma_t \quad . \tag{76}$$

After combining Eqs. (75) and (76) the yield becomes,

$$R = \left(\frac{\tau 2.35}{\Delta t} \right)^2 \quad . \tag{77}$$

The uncertainty in detecting the $R/2^{th}$ photoelectron is calculated from the p.d.f. $g_t(j)$. This function is the probability per photoelectron

that the $j^{\underline{th}}$ photoelectron will be detected at time t_j. The p.d.f. is given by the transformation

$$g_t(j) = g_j(t_j)\left|\frac{dt_j}{dj}\right| \quad ,$$

where $g_j(t_j)$ is given by Eq. (16). The result, assuming the scintillator statistics dominate, is

$$g_t(j) = \frac{(R-1)!}{(j-1)!(R-j)!} e^{-t_j(R-j)/\tau} \left(1 - e^{-t_j/\tau}\right)^{j-1}$$

The expected deviation in the yield measurement is

$$\sigma^2_{(R-j)} = (R-1)e^{-t_j/\tau}\left(1 - e^{-t_j/\tau}\right) \quad ,$$

$$\sigma^2_{R/2} \simeq R/4 \quad .$$

The expression for the yield (Eq. 77) plus or minus one standard deviation is

$$R = \left[\frac{(2.35\tau)}{\Delta t}\right]^2 \mp \frac{\sqrt{R}}{2} \quad .$$

After the decay time-constant and the FWHM of the arrival time of $R/2^{\underline{th}}$ photoelectron is measured, the mean photoelectron yield can be determined. The assumptions in the development of Eq. (77) should be justified for each experiment before the equation is used to determine the yield. The width of the time spectrum (FWHM) for the $R/2^{\underline{th}}$ photoelectron should be

much larger than the width of the single electron time response of the system. Also, a gamma ray energy should be chosen so that R and R/2 are large enough for Eq.(111) to be valid.

The crossover time spectrum for the 511 keV gamma using NaI(Tℓ) was measured for the RCA-8575 and the XP-1020 photomultipliers. The time resolution (FWHM) for the RCA-8575 was 10.9 nsec and 17 nsec for the XP-1020. The shapes of the measured distributions could not be distinguished from a normal p.d.f. The measured resolutions were typical for the two types of tubes. Using Eq. (77) the yield for the RCA-8575 is

$$R = \left(\frac{250 \times 10^{-9} \times 2.35}{10.9 \times 10^{-9}} \right)^2 \pm 28 \qquad (78)$$

$$= 2950 \pm 28 \text{ photoelectrons/511 keV.}$$

This number (Eq. 78) converts to a photoelectron yield per keV of 5.8 which is lower than the maximum of 11 obtained by Hondayer *et al.*[33] The yield for the XP-1020 is

$$R = \left(\frac{250 \times 10^{-9} \times 2.35}{17 \times 10^{-9}} \right) \pm 17 \qquad (79)$$

$$= 1200 \pm 17 \text{ photoelectrons/511 keV} \quad ,$$

which converts to approximately 2.4 photoelectrons per keV. The advertized typical efficiencies of the RCA-8575 and the XP-1020 cathodes are 28 percent and 12 percent respectively. The difference in the

measured yield of the two tubes can be accounted for by the difference in the advertized cathode efficiencies. The width of the measured time distributions certainly eliminates concern about other sources of timing uncertainties influencing the photocathode yield measurement.

The crossover timing technique for determining the photoelectron yield has proven to be extremely useful because the measurement can be made with standard electronic modules without using a light pulser, and without having to dismantle the photomultiplier.

CHAPTER IV

TIMING CHARACTERISTICS OF THE SCINTILLATOR AND PHOTOMULTIPLIER SYSTEM

In this chapter the various sources of time variance associated with single photons and single photoelectrons which were discussed separately in Chapters II and III are considered as integral parts of a scintillator and photomultiplier system. The method used in the system analysis is to determine the system's time response to single detected photons, and then by the method of order statistics to determine the system's response to an impulse function of excited states in the crystal. The final part of the analysis is to calculate the time distribution for a system composed of a NaI(Tℓ) crystal and a photomultiplier using the measured parameters of Chapters II and III.

I. SYSTEM'S RESPONSE TO SINGLE DETECTED PHOTONS

Four sources of time variance for the system are shown in Figure 28. Expressions for $f_1(t)$, $f_2(t)$, $f_3(t)$, and $f_4(t)$ were obtained in Chapters II and III. They are

$$f_1(t) = \frac{1}{\tau} e^{-t/\tau} \quad ,$$

$$f_2(t) = \frac{V_0}{4H} e^{-(V_0 t/4H)} \quad ,$$

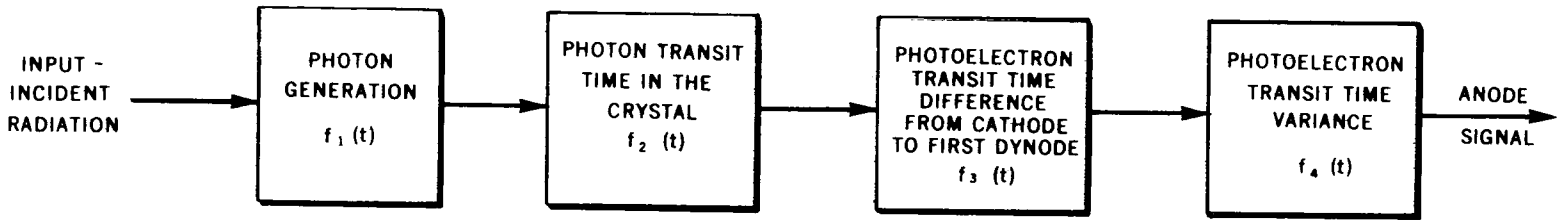


Figure 28. Block diagram of a scintillator and photomultiplier system showing the individual sources of time variance.

$$f_3(t) = \frac{2}{k}\left(e^{-t/k} - e^{-2t/k}\right) \quad ,$$

$$f_4(t) = \frac{t^2}{2k_1^3}\, e^{-t/k_1} \quad . \tag{80}$$

Each of these functions represents a probability-per-unit time that a single electron will experience a delay of t. Therefore, the convolution of the four p.d.f.'s result in the probability-per-unit time that a detected photon will experience a total delay of t from the initial time of the scintillation event to the detection time at the anode. The convolution of a delta input of excited states necessary to produce a single photon with the p.d.f. of the photon generation is

$$f_1(t)_1 = \int_0^t \frac{\delta(x)}{\tau}\, e^{-(t-x)/\tau}\, dx$$

$$= \frac{1}{\tau}\, e^{-t/\tau} \quad , \tag{81}$$

where x is the convolution dummy variable. The function, $f_1(t)_1$, describes the photon generation process. The second convolution is

$$f_{12}(t) = \int_0^t \frac{1}{\tau}\, e^{-(t-x)/\tau} \quad \frac{1}{h'}\, e^{-x/h'}\, dx$$

$$= \frac{1}{h' - \tau}\left(e^{-t/h'} - e^{-t/\tau}\right) \quad , \tag{82}$$

where h' is defined as

$$h' = \frac{4H}{V_0} \quad . \tag{83}$$

Equation (82) represents the scintillator's response, including the photon generation and photon transit time, to a delta function of incident energy. The third convolution is

$$f_{123} = \int_0^t \left[\frac{2}{k(h'-\tau)} \left(e^{-x/k} - e^{-2x/k}\right)\left(e^{-(t-x)/h'} - e^{-(t-x)/\tau}\right) \right] dx$$

$$= ae^{-t/k} + be^{-t/h'} + ce^{-t/\tau} + de^{-2t/k} \quad , \tag{84}$$

where

$$a = \frac{2k}{(k-h')(k-\tau)}$$

$$b = \frac{2h'^2}{(h'-\tau)(k-2h')(k-h')} \quad ,$$

$$c = \frac{-2\tau^2}{(h'-\tau)(k-\tau)(k-2\tau)} \quad ,$$

$$d = \frac{-2k}{(k-2\tau)(k-2h')} \quad .$$

The function $f_{123}(t)$ includes the time distribution of photons in the scintillator and the photoelectron transit time difference for different illumination points on the cathode. The fourth and final convolution is

$$f_{1234}(t) = \int_0^t f_{123}(t-x)\, \frac{x^2}{2k_1^3}\, e^{-x/k_1}\, dx \quad . \tag{86}$$

After the integration is performed, Eq. (86) becomes

$$f_{1234}(t) = \left\{ e^{-t/k_1} \left[\frac{Lt^2}{k_1^2} + \frac{Mt}{k_1} + N \right] + aF^3 e^{-t/k} + \right.$$

$$\left. + bG^3 e^{-t/h'} + cI^3 e^{-t/\tau} + dY^3 e^{-2t/k} \right\} \quad , \tag{87}$$

where,

$$L = -\frac{1}{2}(aF + bG + cI + dY) \quad ,$$

$$M = -(aF^2 + bG^2 + cI^2 + dY^2) \quad ,$$

$$N = -(aF^3 + bG^3 + cI^3 + dY^3) \quad ,$$

$$F = \frac{k}{k - k_1} \quad ,$$

$$G = \frac{h'}{h' - k_1} \quad ,$$

$$I = \frac{\tau}{\tau - k_1} \quad ,$$

$$Y = \frac{k}{k - 2k_1} \quad .$$

Equation (87) is the probability-per-unit time that a photon will be detected at time t after the initial time of generation. The probability distribution function for the system will also be needed for ordering the events. The distribution function is

$$F_{1234}(t) = \int_0^t f_{1234}(x)\, dx \quad . \tag{88}$$

The result of the integration in Eq. (88) is

$$F_{1234}(t) = \left\{ e^{-t/k_1} [Pt^2 + Qt + T] + Se^{-t/k} + Ue^{-t/h'} + \right.$$

$$\left. + Ve^{-t/\tau} + We^{-2t/k} + 1 \right\} \quad , \tag{89}$$

where

$$P = - \frac{L}{k_1} \quad ,$$

$$Q = - (2L + M) \quad ,$$

$$S = -AF^3k \quad ,$$

$$T = - (2L + M + N)k_1 \quad ,$$

$$U = -bG^3h' \quad ,$$

$$V = - cI^3\tau \quad ,$$

$$W = \frac{-dY^3k}{2} \quad .$$

The subscripts on $f_{1234}(t)$ and $F_{1234}(t)$ will be omitted and the functions will be referred to hereafter as $f(t)$ and $F(t)$ respectively.

The remaining step in the analysis is to apply the order statistics developed in Chapter II to determine the distribution of the time ordered photoelectrons. The analysis to this point applies only to the system's response to single detected photons. With the aid of order statistics the system's response to several photons will be determined.

II. INFLUENCE OF THE INDIVIDUAL PARAMETERS ON THE TIME RESOLUTION OF THE SYSTEM

The general order equation for the $j^{\underline{th}}$ photoelectron is

$$g_j(t_j) = \frac{R!}{(j-1)!(R-j)!}\,[1 - F(t_j)]^{R-j}[F(t_j)]^{j-1} f(t_j) \quad , \qquad (12)$$

where R is the total number of photoelectrons resulting for one event, $F(t_j)$ is the probability distribution function given by Eq. (89) and $f(t_j)$ is the p.d.f. given by Eq. (87). When the expressions for $F(t_j)$ and $f(t_j)$ are substituted into Eq. (12), the result is a rather complicated algebraic expression. For this reason, a computer program was written which calculates a sufficient number of points so that the p.d.f. can be constructed. After the function is constructed, a subroutine of the main program calculates the FWHM of the p.d.f. A listing of the complete program is included in Appendix D. With the aid of the computer program, the influence of individual parameters on the system's response is easily determined.

The Influence of Crystal Size on Time Resolution

In Chapter III the results of the Monte Carlo computer calculation of photon transit times inside the crystal were presented. The p.d.f. representing the photon transit times inside the crystal is approximated by

$$f_2(t) = \frac{1}{\sigma} e^{-t/\sigma} \quad . \tag{38}$$

The standard deviation for the nonspecular boundary condition is

$$\sigma = \frac{4H}{v_0} \quad , \tag{41}$$

where v_0 is the velocity of light in the crystal, H is the height of the crystal, and the constant is deduced from Figure 15, page 47, of Chapter II. The time variance is independent of the radius of the crystal for the range of height-to-radius ratios shown in Figure 17, page 49. Therefore, calculation of the time resolution as a function of the crystal height is sufficient for demonstrating the effect of crystal size on the system's time resolution.

The shape of a typical p.d.f. is shown in Figure 29 for a crystal one inch high and for a typical set of RCA-8575 photomultiplier parameters. The calculated p.d.f. is a close approximation to a normal distribution.

The time resolution versus crystal height is presented for two sets of parameters in Figure 30. For curve B the photomultiplier parameters are such that they contribute an insignificant amount to the

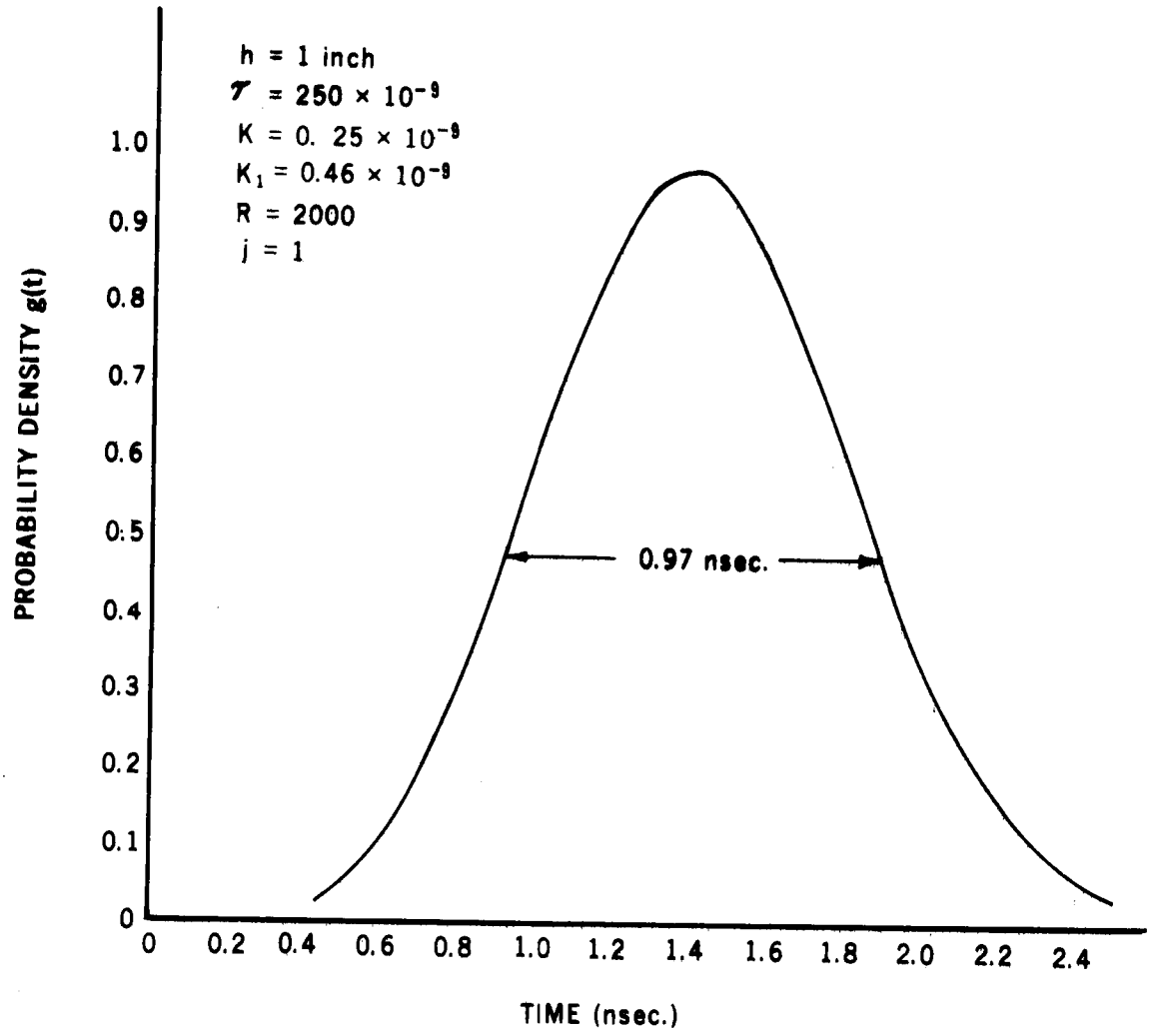


Figure 29. Typical shape of a time distribution function calculated for the RCA-8575 photomultiplier and a crystal height of one inch.

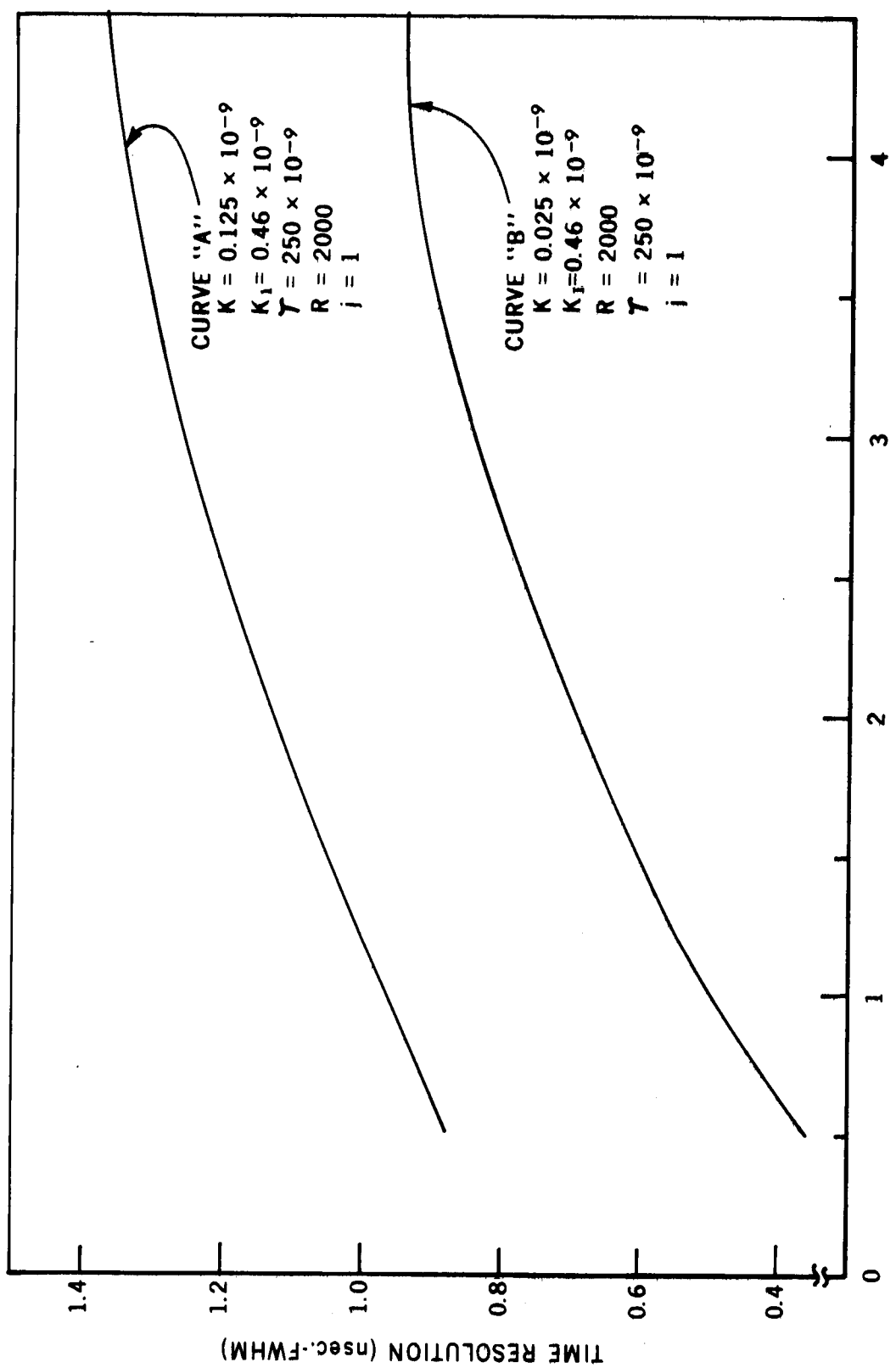


Figure 30. Calculated time resolution versus crystal height.

system's overall time resolution. Therefore, curve B can be interpreted as the effect of crystal size on the time resolution for an almost ideal photomultiplier. The time resolution for this set of parameters is degraded almost a factor of two by going from a 1-inch crystal to a 4-inch crystal. Curve A represents a more realistic set of photomultiplier parameters. The crystal size has less effect for this set of parameters, but the degradation is still more than 30 percent in going from a 1-inch to a 4-inch crystal.

The Influence of the Difference in Photoelectron Transit Times for Different Generation Points on the Cathode

The measurement of the time delay as a function of distance from the center of the photocathode was presented in Chapter III, Section I, for three types of photomultipliers. The relation between delay and position on the photocathode was approximated by

$$|X| = (1 - e^{-t/k}) \quad , \tag{44}$$

where X is the normalized distance from the center of the photomultiplier and t is the time delay. This relationship (Eq. 44) was transformed to the probability that photons incident on the cathode will be delayed a time t. The resulting p.d.f. is

$$f_3(t) = \frac{2}{k} (e^{-t/k} - e^{-2t/k}) \quad . \tag{91}$$

A value of 0.125×10^{-9} for k represents a typical RCA-8575 tube as shown in Figure 20, page 56. For the large (110 millimeter) tube

shown in Figure 22, page 58, the value of the constant is approximately 0.33×10^{-9}.

In Figure 31 the time resolution of the first photoelectron is plotted for two sets of parameters. For curve B the scintillator is assumed to be extremely thin (0.06 inches) and the photoelectron transit time parameter, k , is assumed to be negligibly small. The time resolution (curve B) is degraded approximately 20 percent going from a 42 to a 110 millimeter photocathode. For a typical set of parameters, represented by curve A, the effect of the geometry is reduced to less than 10 percent from 42 to 110 millimeter photocathode.

The Influence of the Fluctuation in Photoelectron Transit Times Due to Initial Velocity Differences

The transit time distribution of electrons from the cathode to the anode was measured for two types of photomultipliers and presented in Chapter III. A reasonable approximation to the measured distribution is

$$f_4(t) = \frac{t^2}{2k_1^3} e^{-t/k_1} \quad . \tag{53}$$

The relationship between the measured FWHM of the distribution and k_1 is given by

$$k_1 = \frac{\Delta t_{(FWHM)}}{3.395} \quad . \tag{54}$$

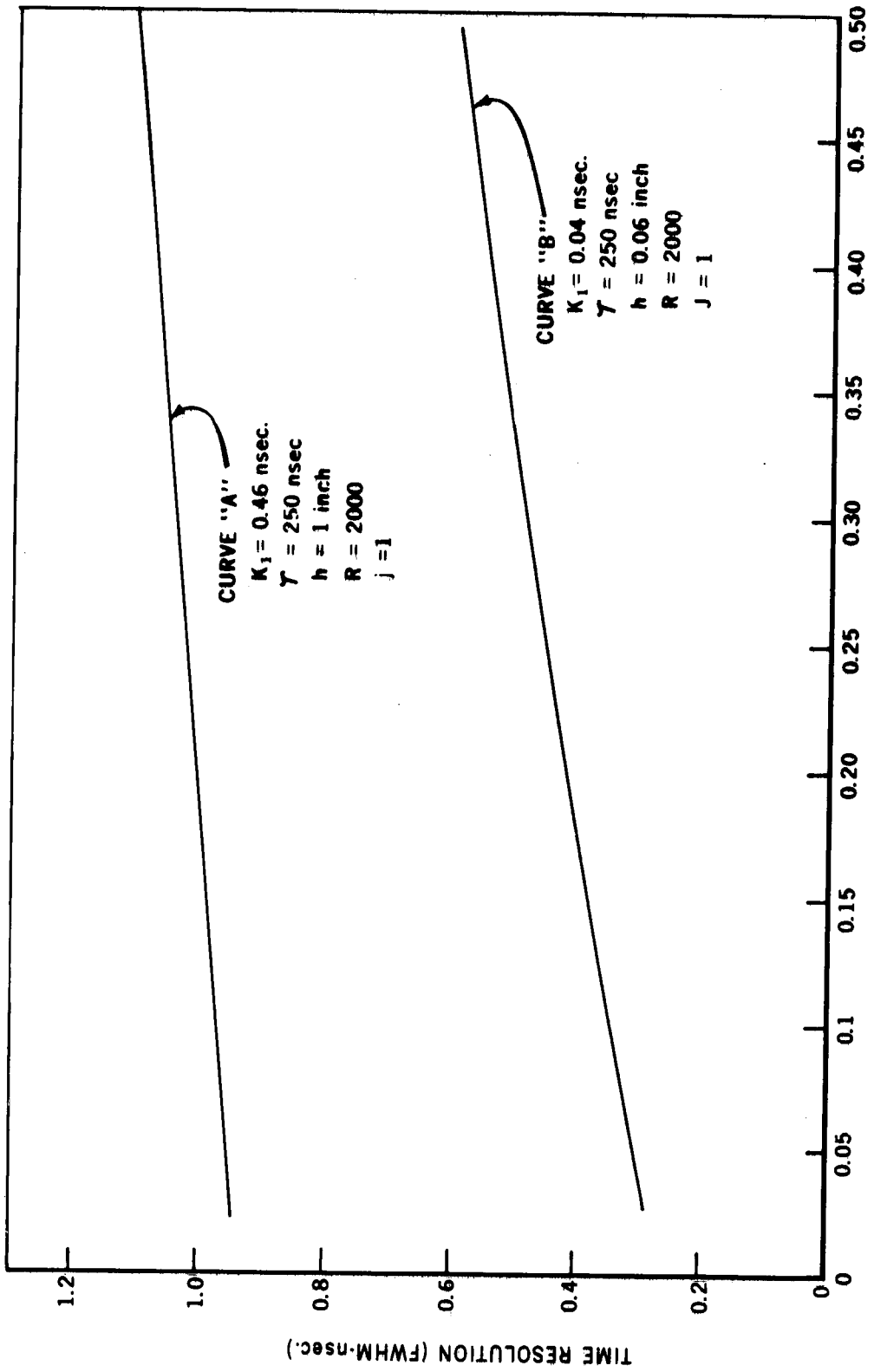


Figure 31. Calculated time resolution versus the photocathode transit time difference parameter, K.

A typical value of k_1 for an RCA-8575 photomultiplier is 0.46×10^{-9} corresponding to the FWHM resolution of 1.56 nsec. In Figure 32, curve B represents the case in which the variance due to the photocathode geometry and crystal size can be neglected. Curve A of Figure 32 represents a typical set of parameters for the RCA-8575 tube and a 1-inch NaI(Tℓ) crystal. The time resolution of the system is degraded by a factor of approximately two by the fluctuation in the initial velocity of photoelectrons for a typical system.

The Influence of the Photoelectron Yield on the Time Resolution

The photoelectron yield is influenced primarily by the efficiency of the photocathode in converting a quantum of light energy to electrons. More specifically the yield includes only those photoelectrons which are detectable at the anode of the photomultiplier. Therefore, the combination of the collection efficiency of the dynodes and the quantum efficiency of the photocathode determines the photoelectron yield. The yield, which is referred to as the parameter R in the general order equation, was measured and the results were presented in Chapter III for the RCA-8575 and the XP-1020 photomultipliers. For the RCA-8575 the yield was 2950 photoelectrons corresponding to a 511 keV gamma and only 1200 photoelectrons at the same energy for the XP-1020. The calculated resolution as a function of the yield is shown in Figure 33. The dashed line is the calculated optimum time resolution for a single exponential p.d.f. system.

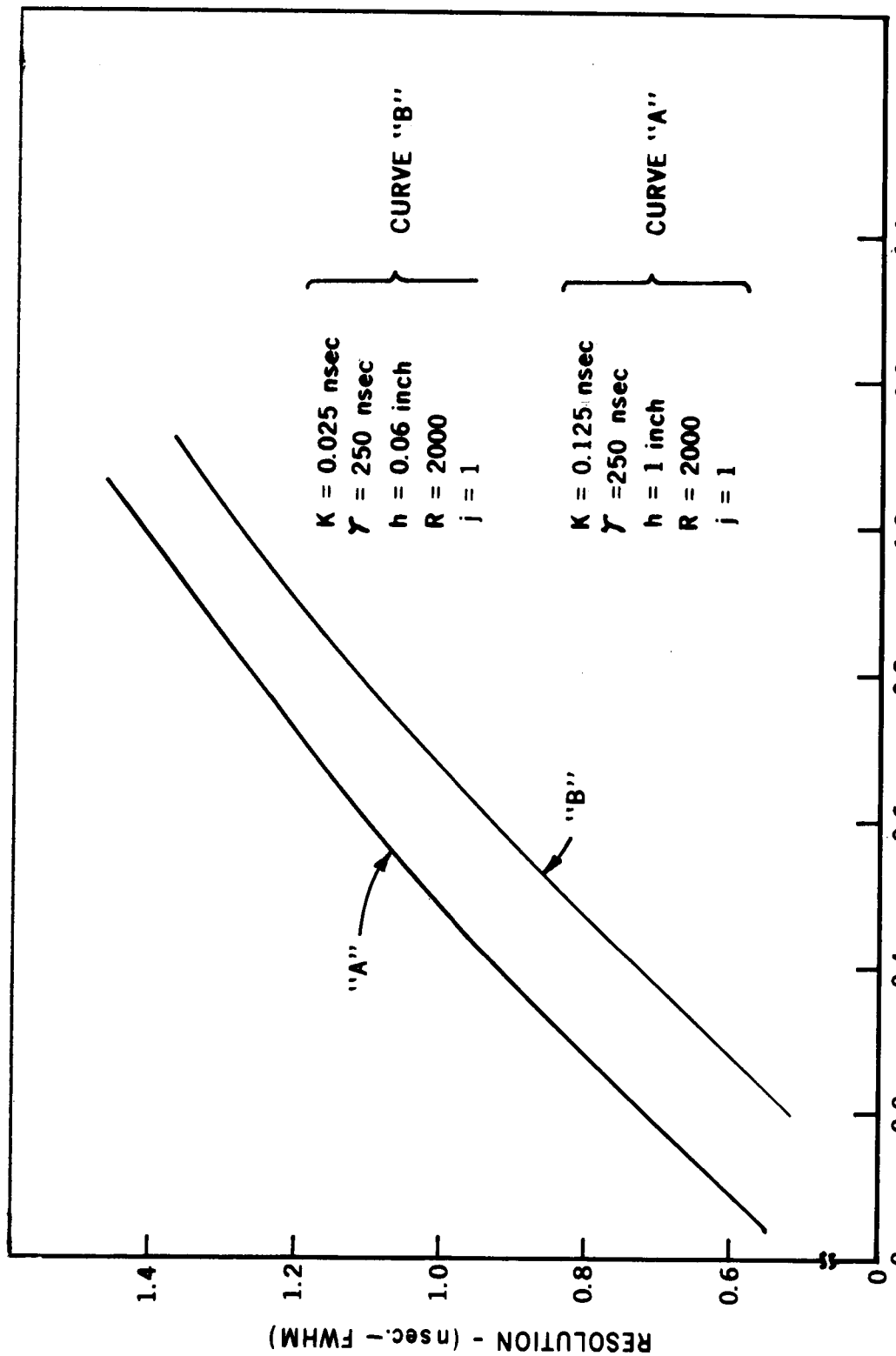


Figure 32. Calculated time resolution versus the transit time parameter K_1.

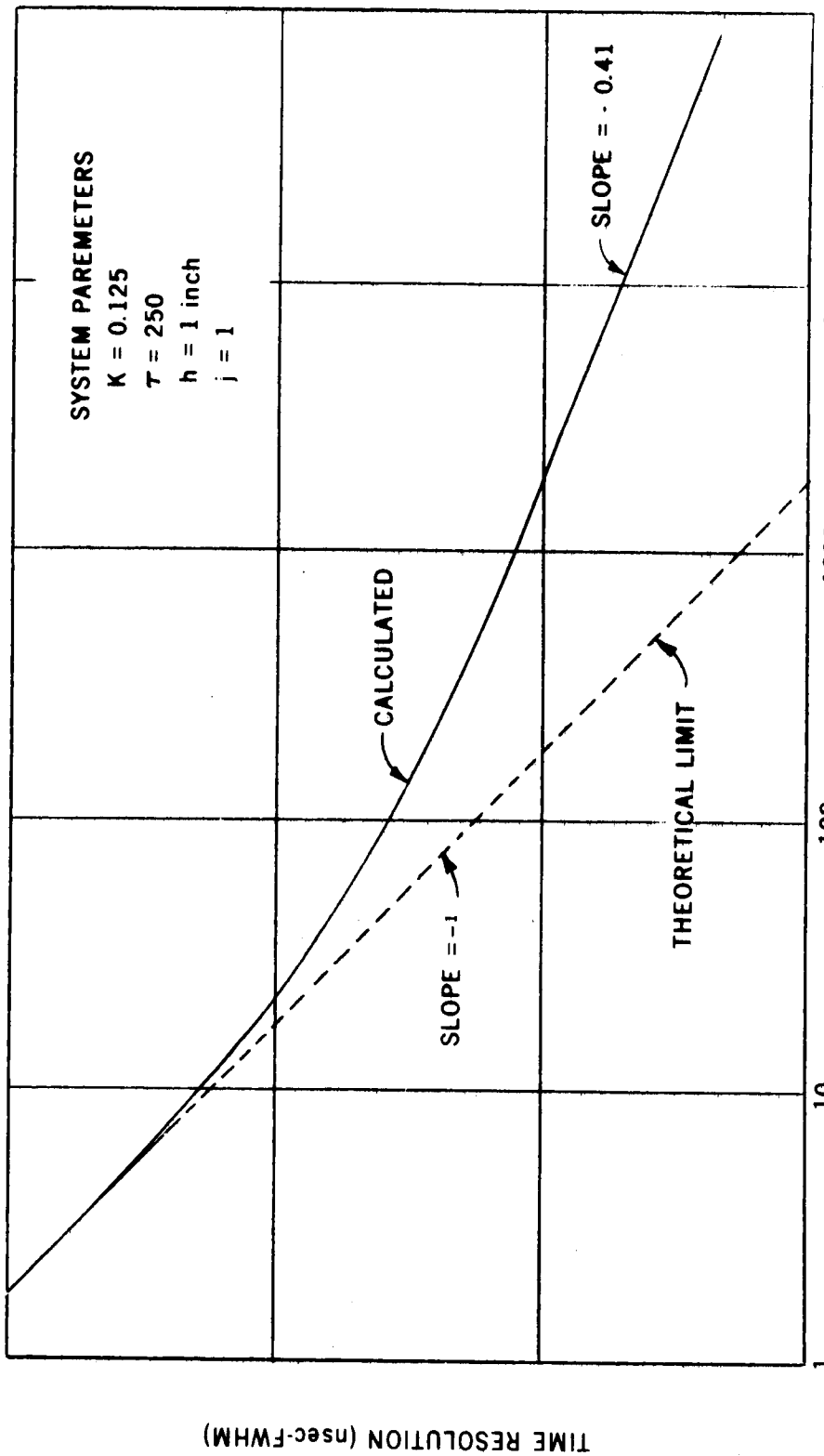


Figure 33. Calculated time resolution versus the photoelectron yield.

The Influence of the Detection Level on Time Resolution

Several experimenters[24,34] have found that timing on the first photoelectron does not produce the optimum resolution when using fast (1 to 3 nsec) scintillators. In general, the optimum has been found experimentally for the fast scintillators to be between 5 and 10 percent of the total electrons. Braunsfurth and Korner[21] observed the optimum detection level for two NaI(Tℓ) crystals to be 0.006 R or 0.6 percent of the total photoelectrons.

The calculated time resolution versus the photoelectron level is shown in Figure 34 for four different photoelectron yields. The calculation predicts an optimum at less than 0.2 percent of the total electrons. This predicted optimum is lower than the optimum measured by Braunsfurth and Korner. Since the calculated time resolution versus detection level (Figure 34) changes very slowly in the range of j/R equal to 0.2 to 0.6 percent, a small second order effect could account for the observed discrepancy. For example, the amplitude variation of the anode pulses, which was not accounted for in the calculations, could be responsible for the discrepancy. The assumption that the $j^{\underline{th}}$ photoelectron can be identified and isolated from the other photoelectrons by the electronic discriminator is, in fact, not completely justified beyond the first photoelectron. Detection of the first electron will be discussed in more detail in the next section.

The optimum photoelectron level for time resolution is strongly influenced by the decay time of the scintillator. The optimum level is plotted as a function of the decay constant of the scintillator in

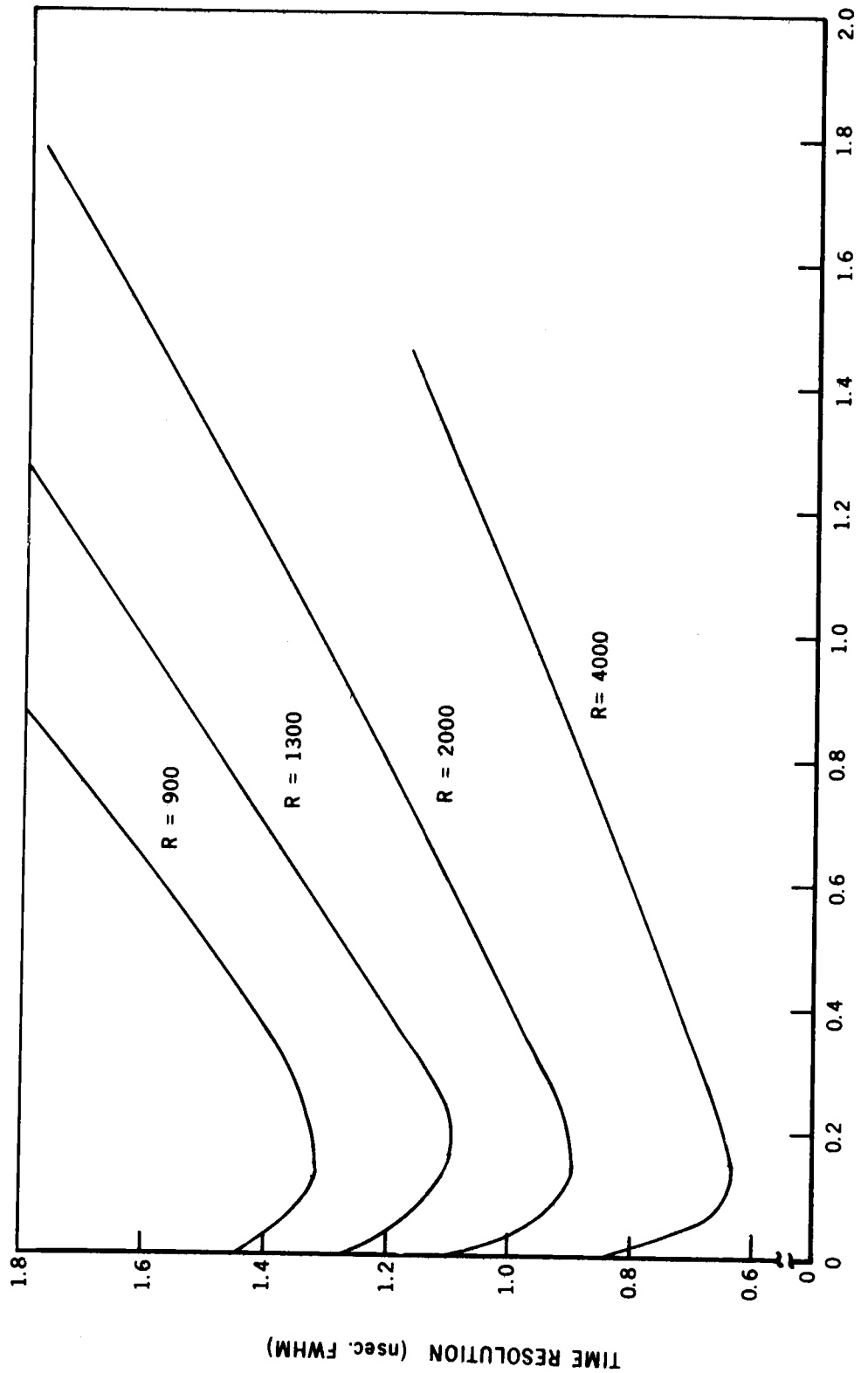


Figure 34. Calculated time resolution versus photoelectron level.

Figure 35. The optimum level for decay constants in the range of 1 to 3 nsec is slightly less than 10 percent. This agrees very well with the experimental results recently reported by Gatti et al.[35] for a scintillator of 1.6 nsec decay constant.

III. TIME RESOLUTION MEASUREMENT TECHNIQUES

In the calculation of the time resolution the assumption is made that any anode pulse resulting from a single photoelectron can be detected without interference from any other photoelectron. Detection of completely isolated photoelectrons is very difficult to achieve since the photoelectrons may occur only a few hundred picoseconds apart. Detection of the anode pulse resulting from the first photoelectron can be achieved with more isolation than any other photoelectron because of the absence of interference from previous photoelectrons. The level discriminator must be extremely sensitive so that the anode pulse resulting from the second photoelectron does not interfere with the detection of the first photoelectron does not interfere with the detection of the first photoelectron. Complete isolation and detection of the first photoelectron is impractical, but sufficient isolation can be achieved so that the time resolution calculations are within the accuracy of the measurements.

The problems of noise pulses below the single electron level becomes important since the discriminator must be very sensitive. The measured noise spectra of a typical RCA-8575 photomultiplier is shown in Figure 36. At the single photoelectron pulse height, the integral noise count rate is approximately 6,000 counts/sec. The count rate exceeds 14,000 counts/sec. at channel number one or at 1/12 the single electron

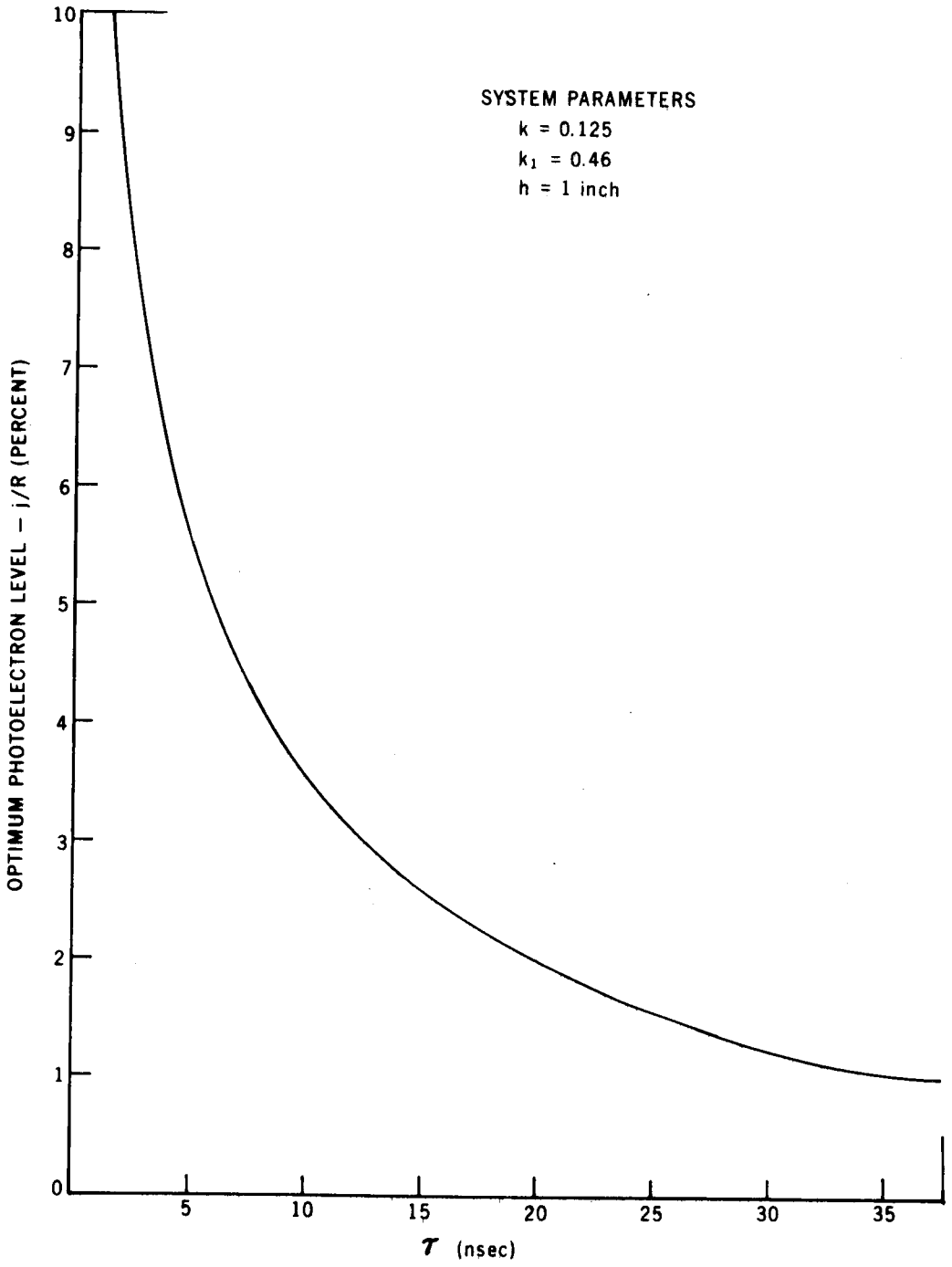


Figure 35. The optimum photoelectron detection level versus the scintillator decay time.

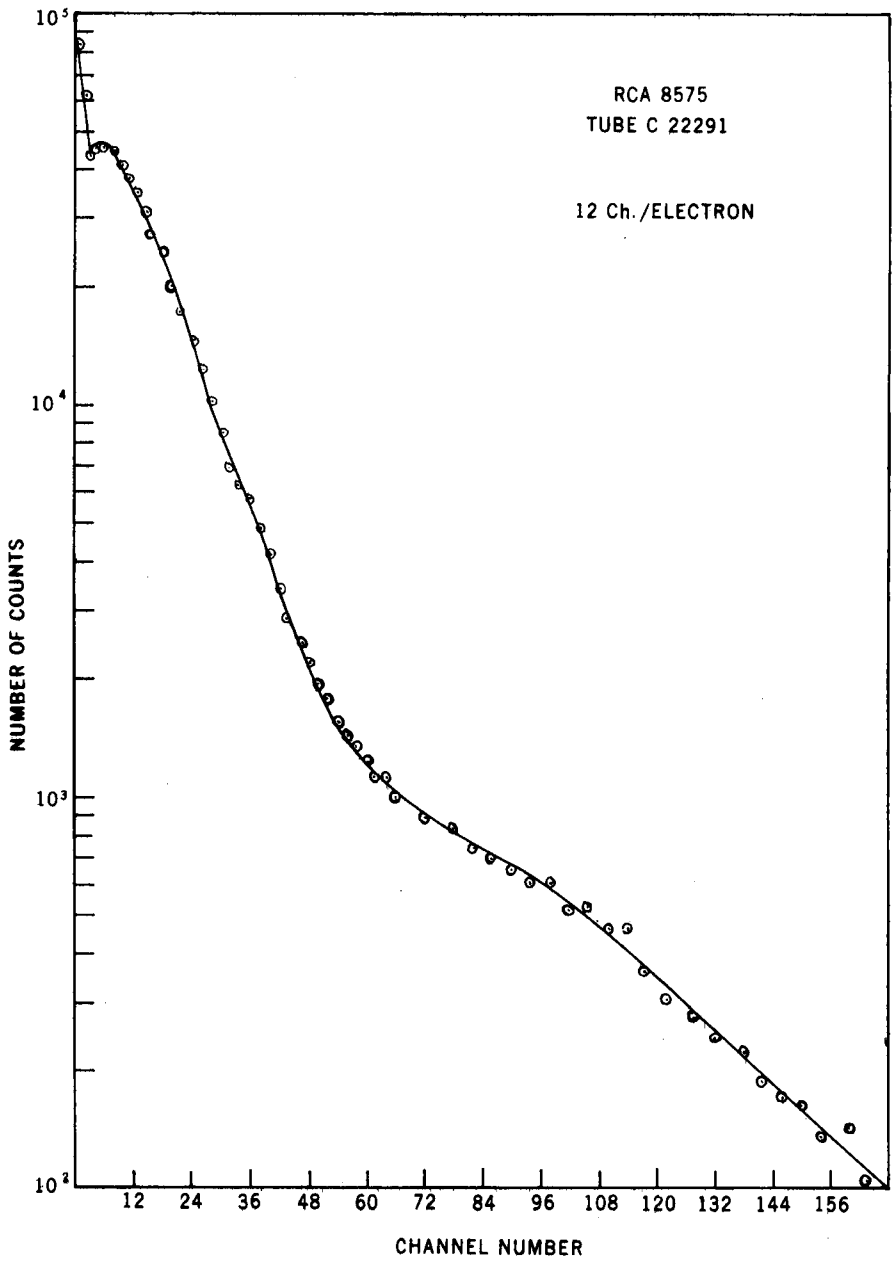


Figure 36. A measured amplitude noise spectrum for a typical RCA-8575 photomultiplier.

height. The single electron noise is a result of a combination of thermal emission and emission due to ion bombardment of the cathode.

The high noise count-rate creates the necessity for signal recognition to eliminate timing on single electron noise pulses. A two-level discriminator scheme was developed which eliminates the triggering due to the noise pulses. A block diagram is shown in Figure 37 of the system which is composed of a high-level discriminator, a low-level discriminator, and a tunnel-diode gate circuit. The low-level discriminator is set to trigger on pulses substantially below the single electron pulse height while the high-level discriminator is set to trigger higher than the single electron pulse height. A small problem is created because the signal from the high-level discriminator occurs later in time than does the low-level signal. To solve this problem, the low-level discriminator output pulse is delayed so that the two signals are approximately in coincidence. The exact amount of time delay depends on the level at which the high-level discriminator is set to trigger, but this delay should always be sufficient to insure that the signal from the high-level discriminator appears at the gate input before the low-level signal appears. The gate is designed so that only the first low-level discriminator pulse occurring in coincidence with a high-level discriminator pulse is allowed to pass through to the output. The gate remains closed for a period of time after the first low-level discriminator pulse and until the high-level discriminator pulse disappears. The reason for this dead time is to eliminate the multiple triggering of the low-level discriminator from reaching the output.

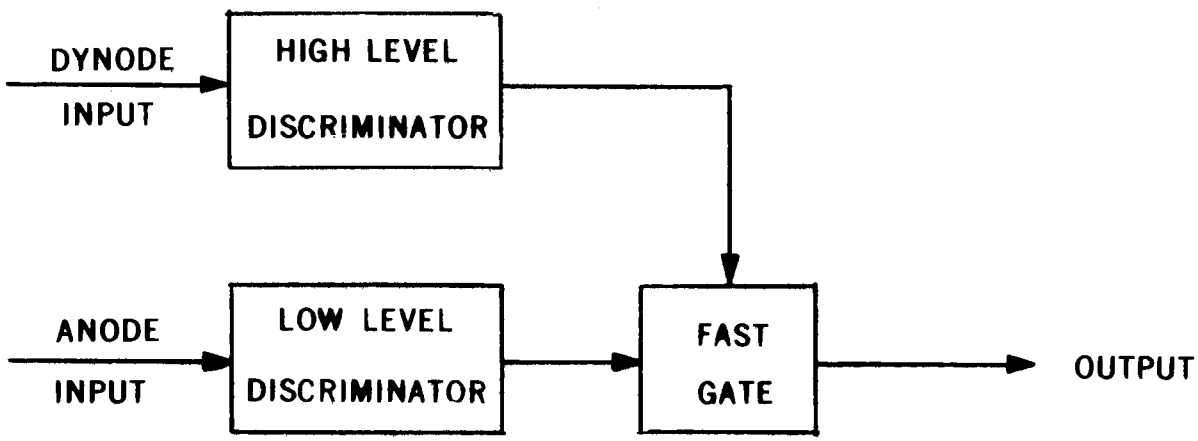


Figure 37. Block-diagram of a two-level recognization scheme.

A schematic diagram of the two-level discriminator system is shown in Figure 38. The low-level discriminator input is connected to the anode of the photomultiplier and the high-level discriminator input is connected to a dynode. The low-level input is composed of two tunnel diodes, TD1 and TD2, both of which are biased in a monostable state. The general design considerations for the tunnel-diode circuit is outlined in a previous publication.[28] The signal from TD2 activates a current switch composed of transistors Q1 through Q4. The current pulse at the collector of Q3 is delayed and routed to the tunnel-diode gate (TD4). The current pulse appearing at TD4 is approximately 10 nsec wide with an amplitude of approximately 30 ma.

The positive dynode signal is inverted through the field-effect transistor Q5. The cut-off bias of the field-effect transistor is controlled by the high-level sensitivity potentiometer. The cut-off bias controls the minimum input signal level that will switch TD3 from the low-voltage to the high-voltage state. After the tunnel-diode switches, it remains in the high-voltage state until the input signal decreases to an amplitude equal to the tunnel diode valley voltage. When TD3 switches to the high voltage state, Q6 begins to conduct current and the collector current of Q7 is turned off. A current pulse from the low-level discriminator can now switch TD4 from the low-level to the high-level state since the negative bias current of Q7 has been removed. TD4 remains in the high-voltage state as long as Q7 is switched off. The negative voltage transition of TD4 is differentiated by a 180pf capacitor and used to activate the current switch Q8, Q9 and Q10. The output at the collector

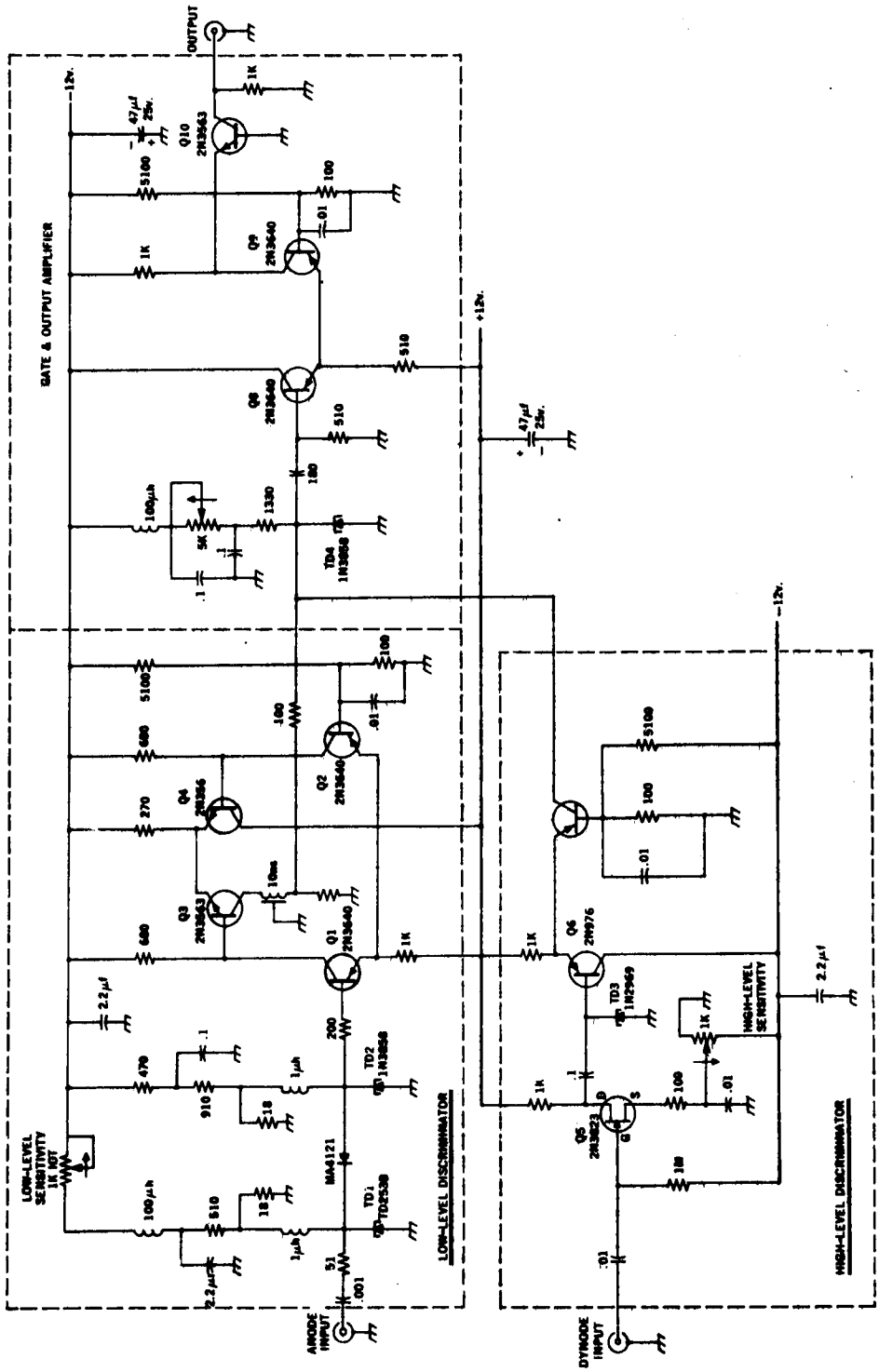


Figure 38. Schematic of a two-level electronic discriminator.

of Q10 is a current pulse with a 20 nsec width and an amplitude of 12 ma.

The low-level sensitivity potentiometer which controls the current through the input tunnel diode is calibrated in units of photoelectrons for each photomultiplier used in the experiments. The calibration is achieved by gating a multichannel analyzer with the pulses from the discriminator. The linear signal from the $10^{\underline{th}}$ dynode of the photomultiplier is routed to the pulse-height analyzer. The analyzer is calibrated in photoelectrons per channel by measuring the number of photoelectrons corresponding to a particular pulse-height channel. If a pulse height is large enough to trigger the discriminator, the analyzer is gated on and that particular energy pulse is analyzed. The least channel containing energy information is recorded for different settings of the sensitivity potentiometer. Therefore, since each channel corresponds to a particular number of photoelectrons, the potentiometer can be calibrated in units of the minimum number of photoelectrons necessary to trigger the discriminator.

IV. EXPERIMENTAL RESULTS

A block diagram of the system used for measuring the time resolution of the NaI(Tℓ) scintillator and photomultiplier is shown in Figure 39. The radiation source is Na^{22} which produces two 511 keV gamma rays in coincidence. One gamma ray is detected in the Naton scintillator and the other in the NaI(Tℓ) scintillator. The fast decaying Naton scintillator, when used with the ORTEC[36] zero crossover

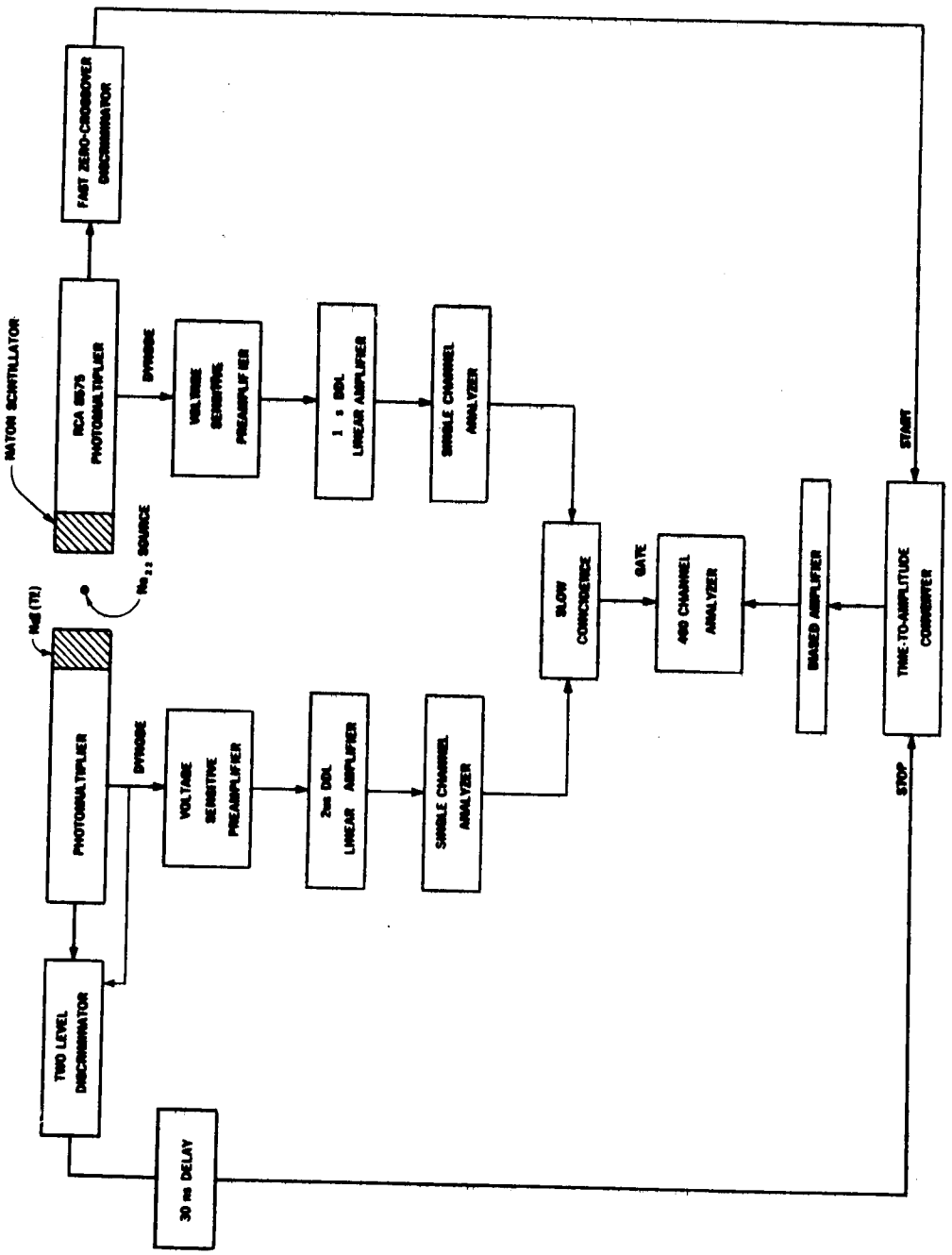


Figure 39. System for measuring the time resolution of the NaI(Tℓ) scintillator and photomultiplier system.

discriminator, produces a time resolution better than 200 picoseconds at an energy of 511 keV. To obtain the resolution of 200 picoseconds the pulse height must be restricted to approximately a 10 percent range in the vicinity of the Compton edge of the 511 keV gamma ray. The 10 percent range restriction is accomplished by amplifying and routing a dynode signal to a single channel analyzer. The analyzer produces a logic pulse if the dynode signal is within the selected range. The energy range on the NaI(Tℓ) scintillator channel is restricted by the same method.

If an event occurs in both the NaI(Tℓ) and Naton scintillator within the selected pulse height ranges, a coincidence pulse is generated which opens the main analyzer gate. When a start signal from the Naton is followed by a stop signal from the NaI(Tℓ) within the time range of the time-to-amplitude converter and during the main analyzer gate open time, the output of the converter is analyzed and stored in the memory of the analyzer. Since the Naton scintillator channel has a resolution of better than 200 picoseconds, the resulting analyzer display is essentially the statistical distribution in time of the NaI(Tℓ) pulse appearing at the anode of the photomultiplier.

Two photomultiplier tubes, an RCA-8575 and an XP-1020, were used for all the experiments. The time delay as a function of incident light position on the cathode and the single electron transit time corresponds to curves of Figures 21 and 22, pages 57 and 58, and Figures 25 and 26, pages 67 and 68, respectively. The measured photoelectron yield for the two tubes were 5.8 and 2.4 photoelectrons per keV respectively.

Four 1-1/2 inch diameter NaI(Tℓ) crystals, in addition to several larger diameter crystals, were supplied by Harshaw Chemical Company. The crystals range in height from 1/4 inch to 4 inches and were all cut from the same ingot. The crystals were carefully cut from the ingot and packed in Al_2O_3 abrasive powder. The resulting interface for the experimental crystals is a single nonspecular type surface. The nonspecular boundary condition was considered in the photon transit time calculations of Chapter II.

The purpose of the first series of experiments is to determine the effect of crystal height on the overall time resolution of the system. No particular emphasis is placed on obtaining the optimum time resolution, instead the emphasis is on knowing the important parameters of the system for each experiment. Before the time resolution for a particular size crystal was measured, the photoelectron yield was carefully determined using the cross-over timing method described in Chapter III. The discriminator in the NaI(Tℓ) channel was adjusted to 1/10 the mean single-electron pulse height so that the timing was performed on the first photoelectron reaching the anode. The operating conditions of the test photomultiplier were recorded so that the single-electron transit time distribution and the transit time difference due to cathode geometry could be measured after the timing experiments are performed. The time spectrum for each of the four crystals are shown in Figures 40 through 43. The solid curve in each figure is the calculated distribution for the specified set of parameters. The calculated distribution fits the experimental data extremely well for all four crystals. The calculated

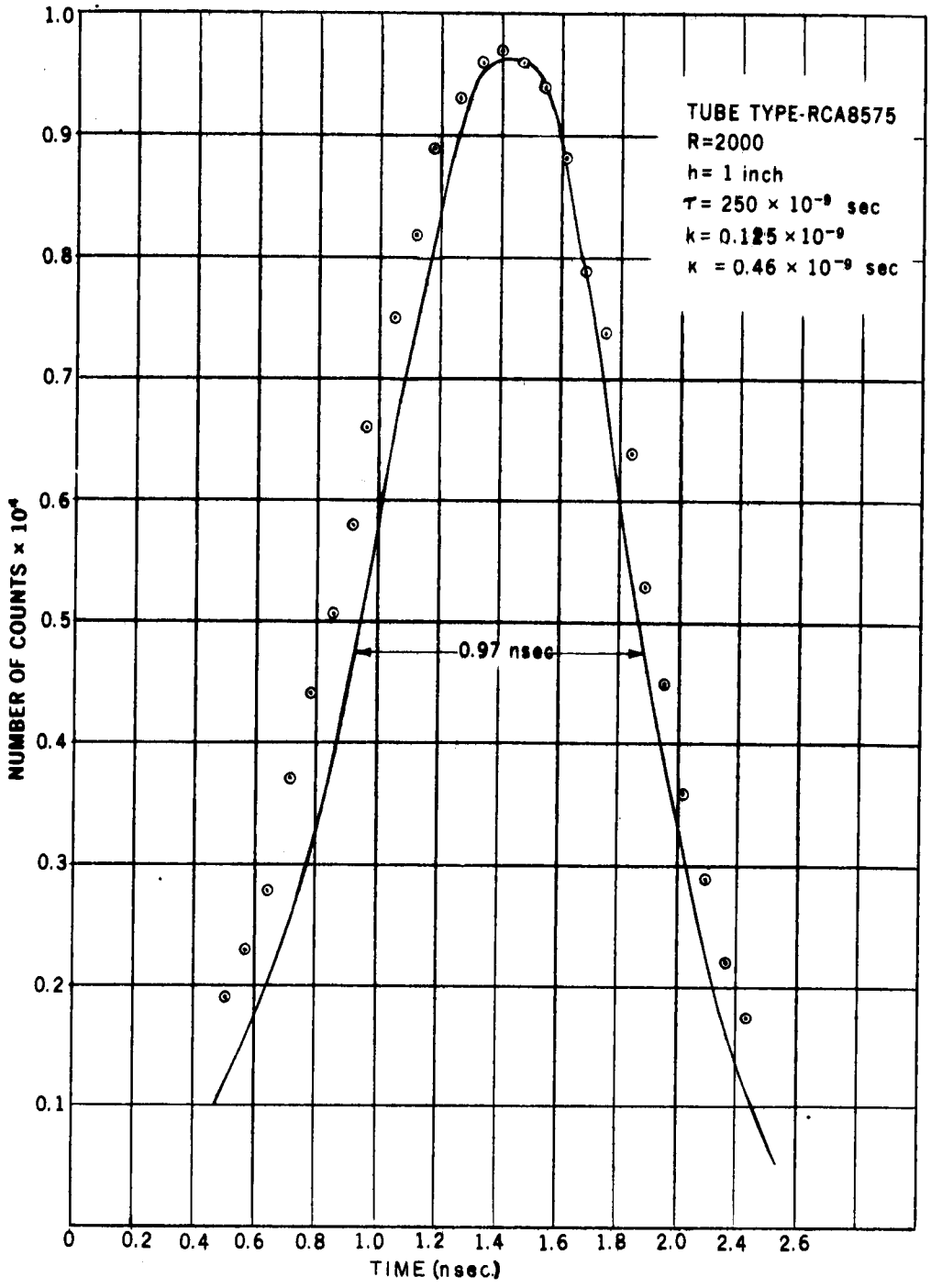


Figure 40. Comparison of the measured and calculated time distribution for a crystal with h = 1.

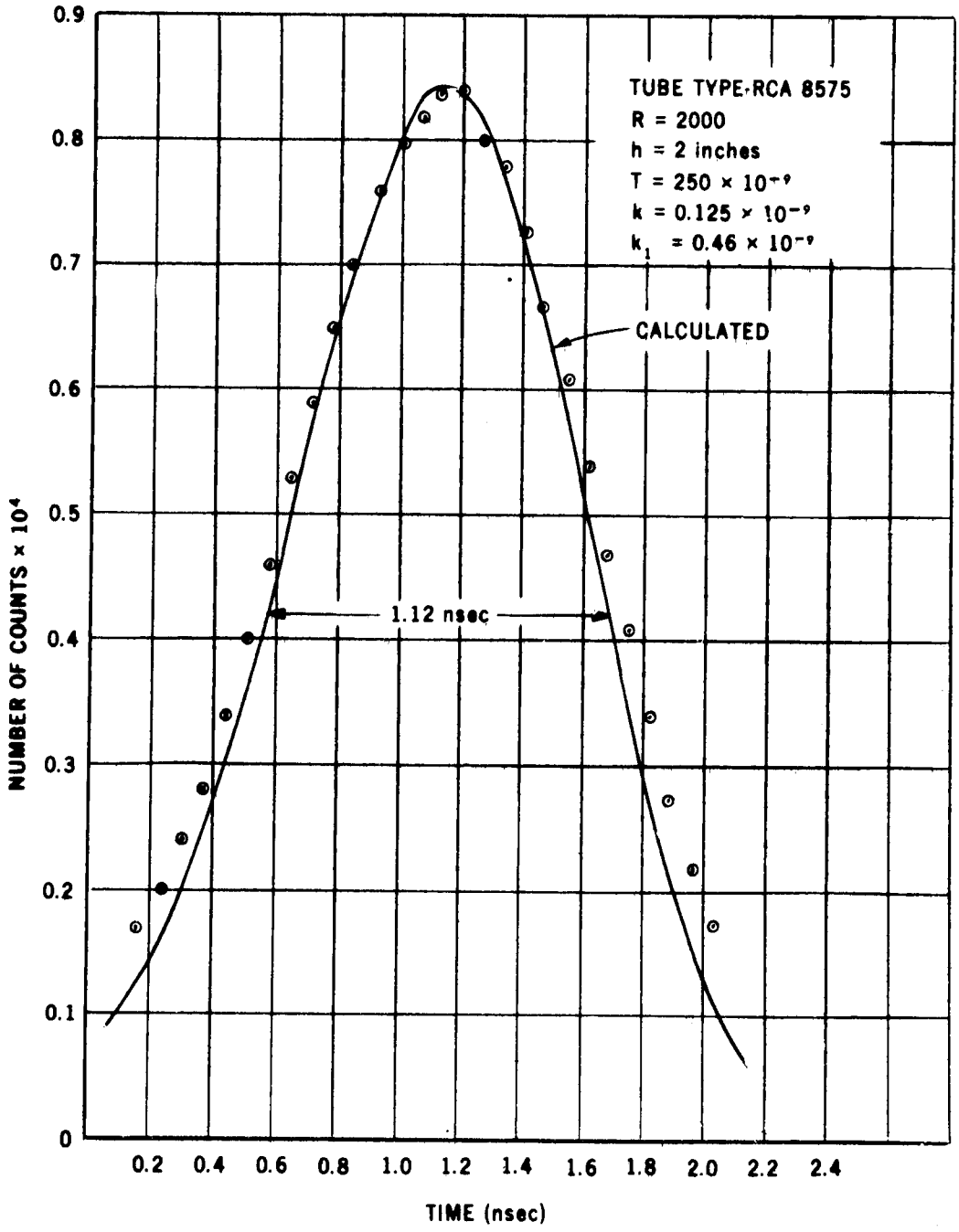


Figure 41. Comparison of the measured and calculated time distribution for a crystal with h = 2.

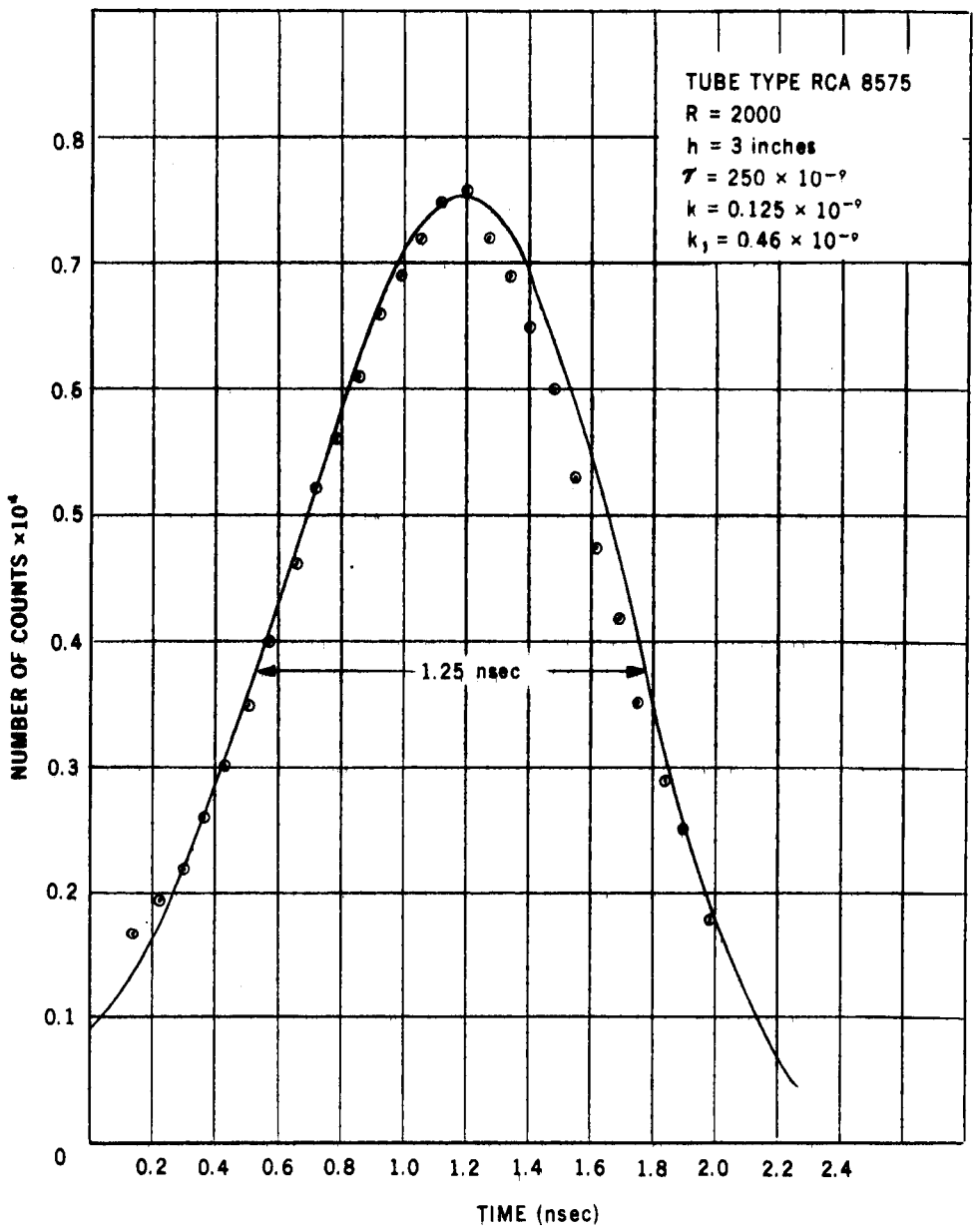


Figure 42. Comparison of the measured and calculated time distribution for a crystal with h = 3.

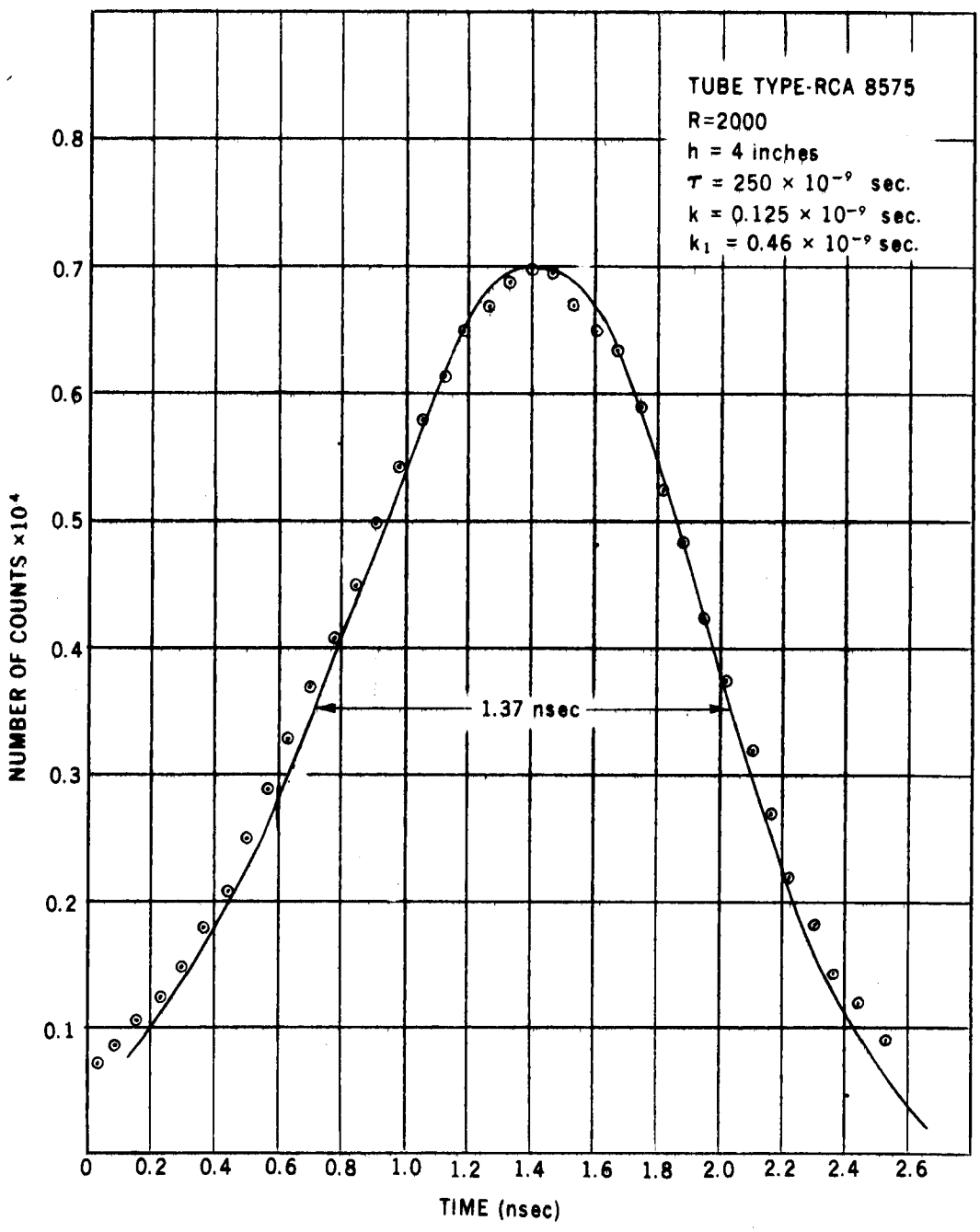


Figure 43. Comparison of the measured and calculated time distribution for a crystal with h = 4.

and experimental time resolution versus crystal height curves is plotted in Figure 44. The data of Figures 44 and 45 were taken with the RCA-8575 and XP-1020 photomultipliers respectively using the same set of crystals.

The purpose of the second experiment was to determine the effect of the photoelectron yield on the overall time resolution. To study the effect of the yield on the time resolution, the photoelectron level on which the timing was performed, was changed by varying the selected pulse height. The pulse height was selected by routing the $10^{\underline{th}}$ dynode signal through a shaping amplifier and to a single channel analyzer as shown in Figure 39, page 109. The experimental results are shown in Figure 46 where the time resolution is plotted as a function of the number of photoelectrons produced at the photocathode. The solid curve is the calculated resolution and the points are derived from the experiment.

The purpose of the third experiment was to determine the time resolution as a function of the photoelectron detection level. To perform this experiment the low level side of the two level discriminator (Figure 38, page 107) was calibrated in photoelectron units as described in a previous section. The calibration is shown in Figure 47 for the RCA-8575 photomultiplier used in this experiment. The results of the experiment are shown in Figure 48. Although a definite optimum photoelectron detection level can not be established from these data, comparison of the calculated time resolution with the data points of Figure 48 suggests that more precise time measurements might indicate an optimum.

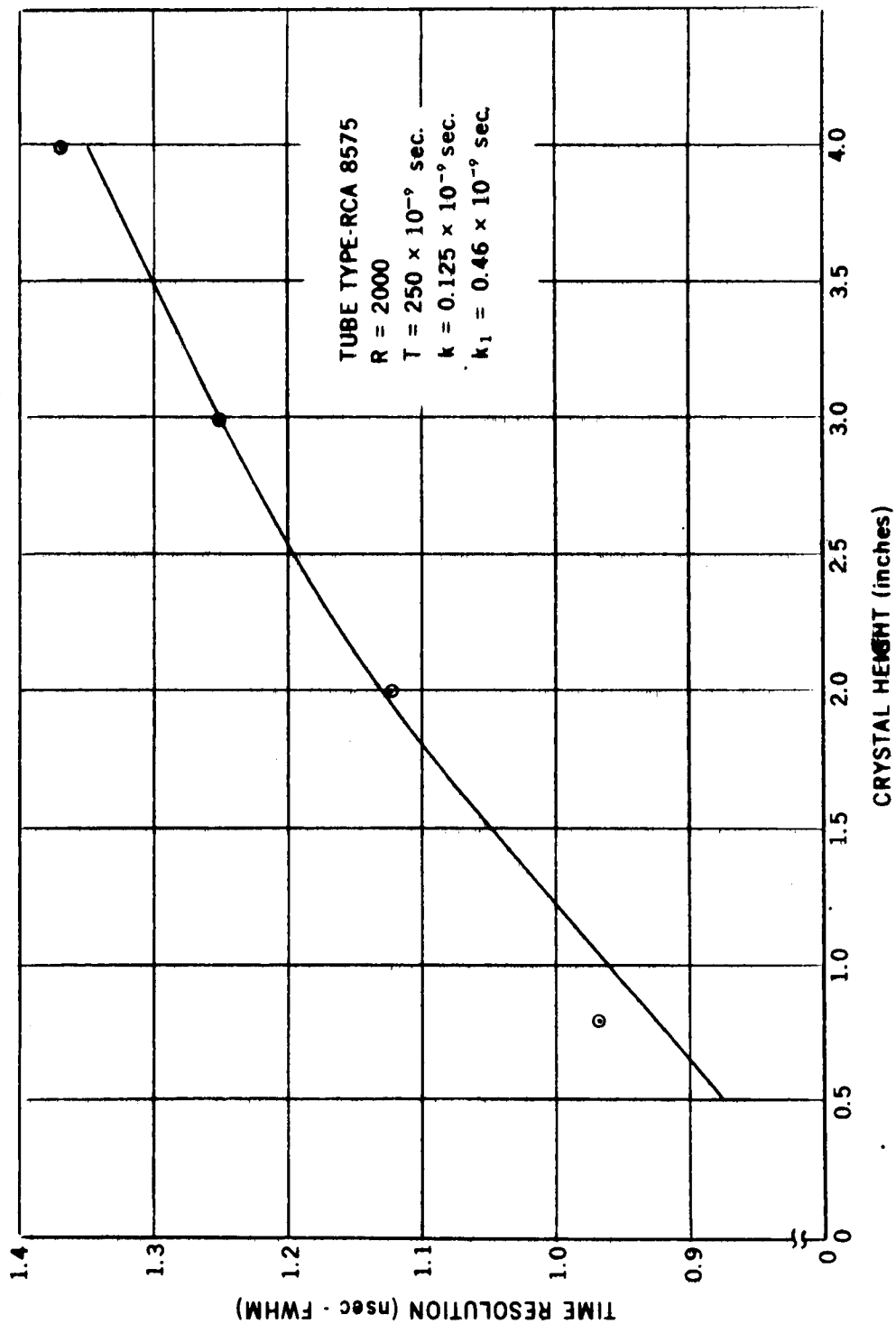


Figure 44. Time resolution versus crystal height using the RCA-8575 photomultiplier.

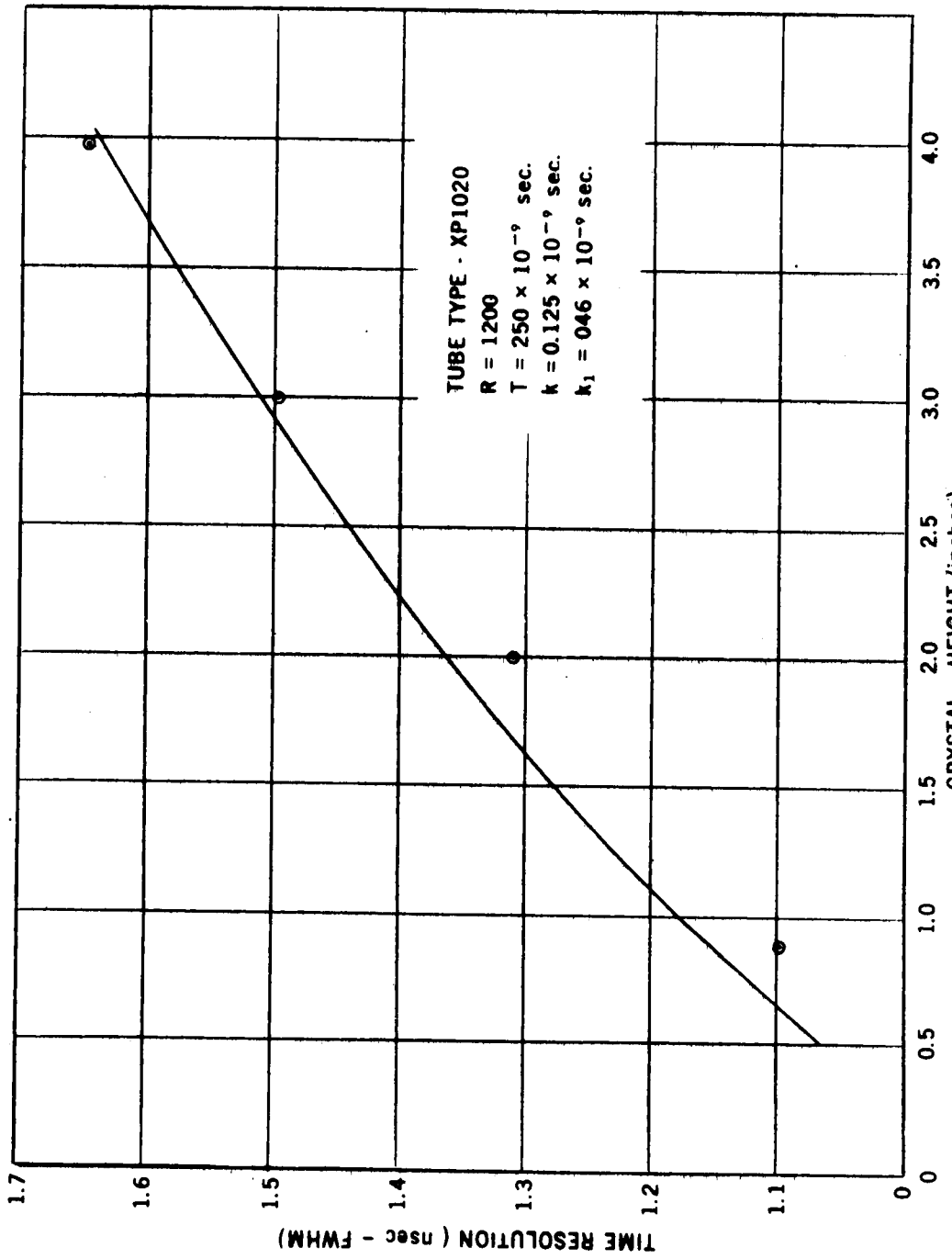


Figure 45. Time resolution versus crystal height using the XP-1020 photomultiplier.

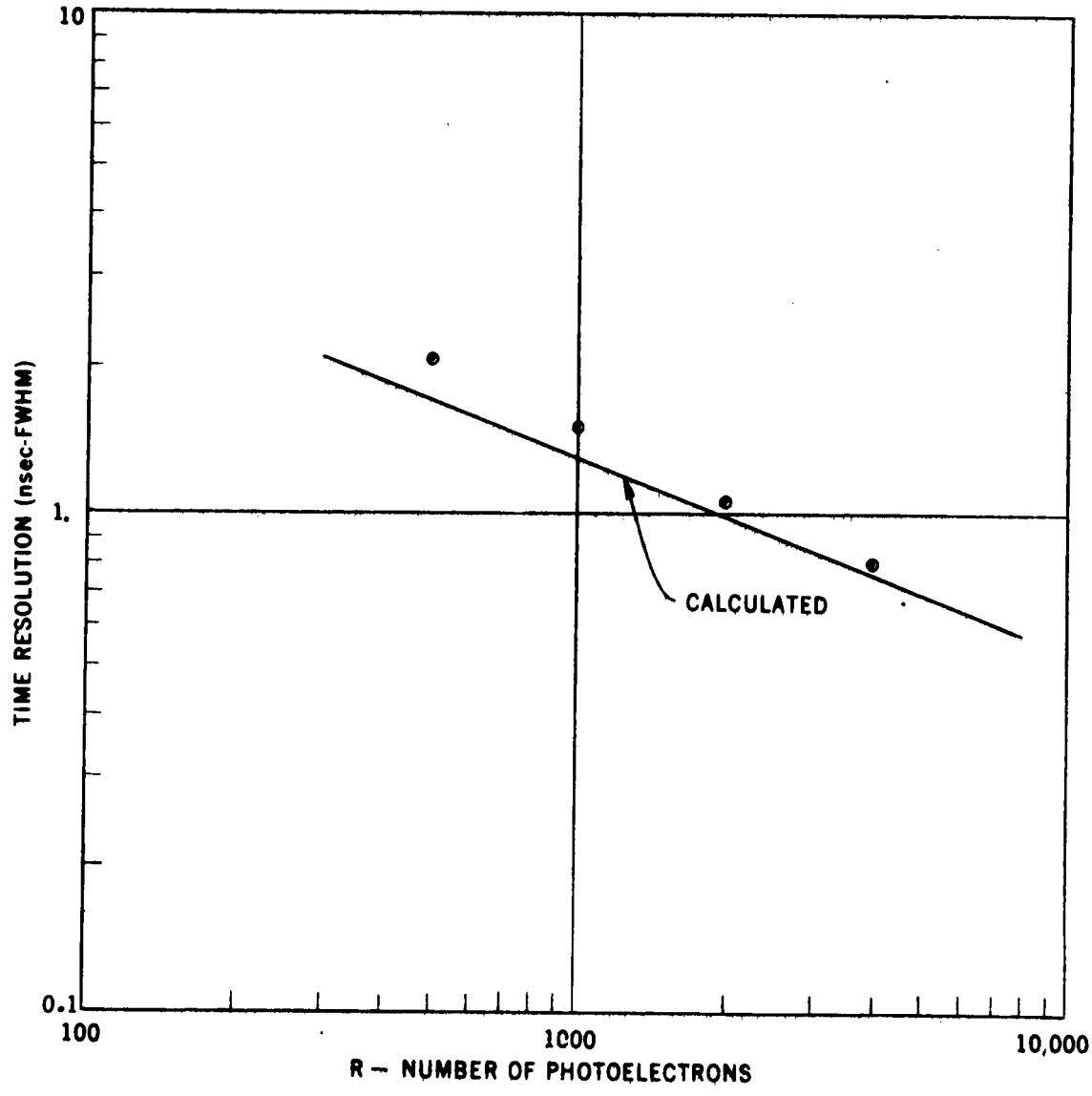


Figure 46. Comparison of the measured and calculated time resolution as a function of photoelectron yield.

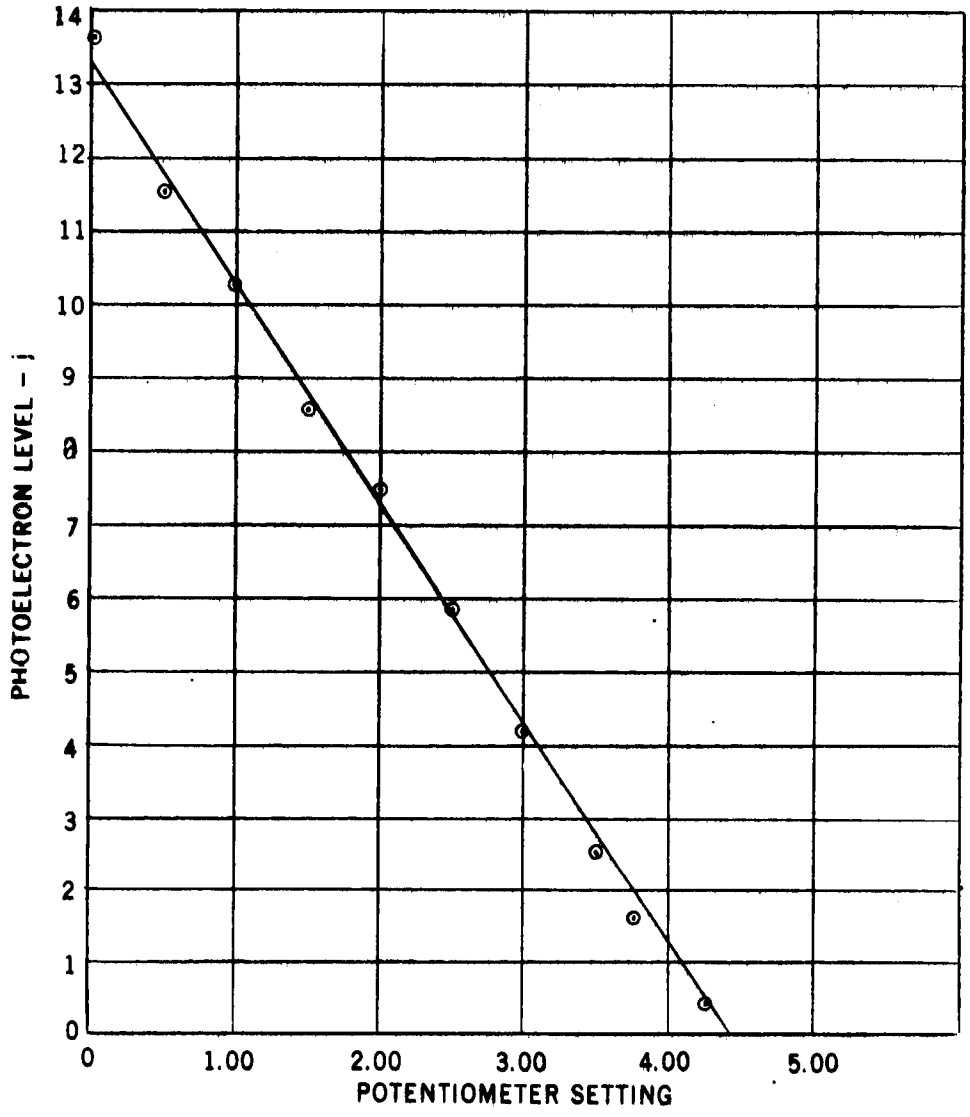


Figure 47. Photoelectron level versus potentiometer setting for the low level discriminator.

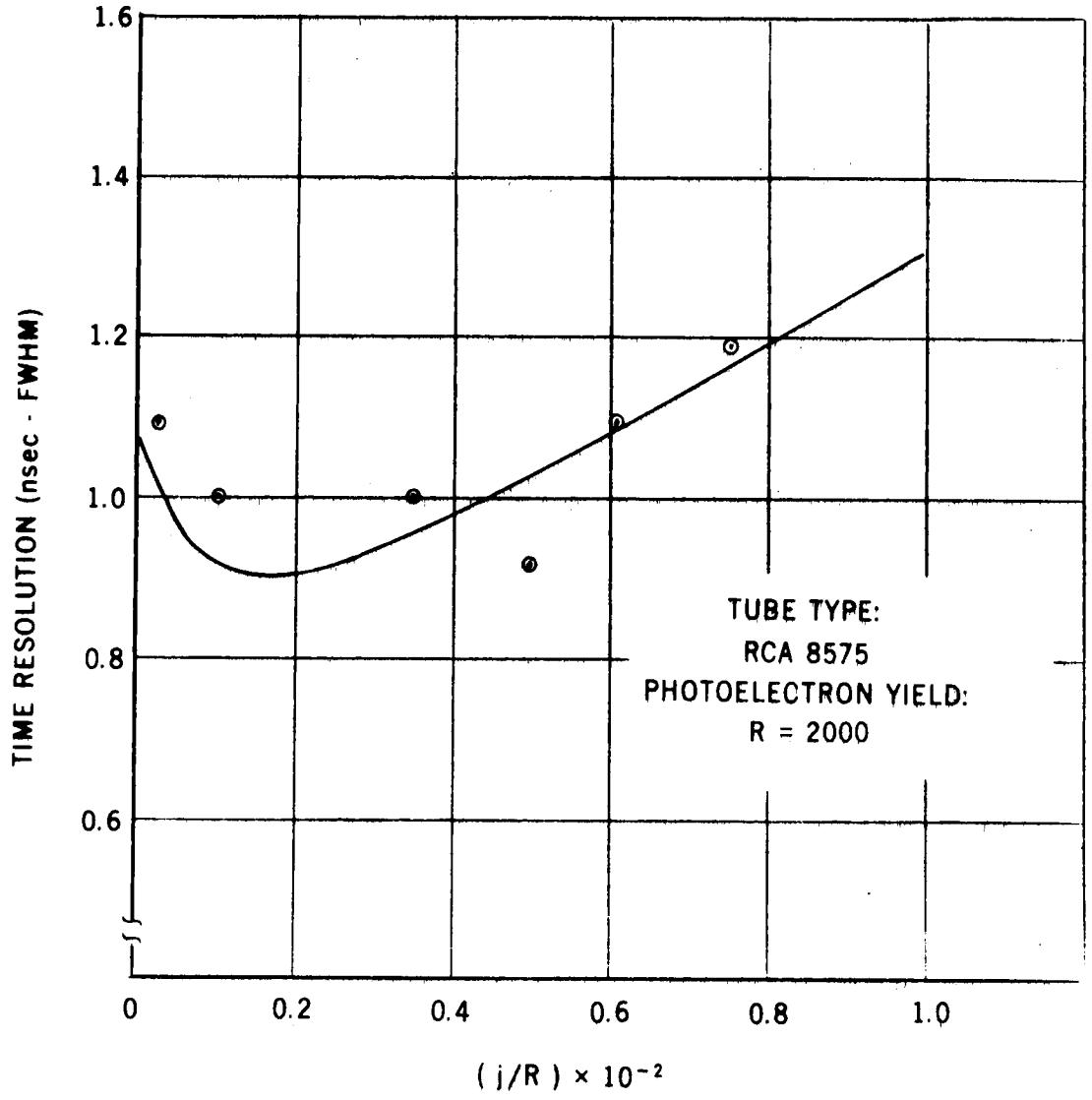


Figure 48. Comparison of calculated and measured time resolution as a function of photoelectron level.

Braunsfurth and Korner[21] report an experimental optimum at a slightly higher j/R ratio than is calculated using the proposed model. The optimum for their system was found to be at a j/R of 0.006, but again their experimental curve of resolution versus detection level was very flat in the region of interest which caused some difficulty in locating the exact optimum. The fact that no optimum was observed in the experimental data suggests that the model needs to be refined. The model could be refined to include such effects as single electron pulse-height variations and timing uncertainties due to the method of processing. However, such extensions of the model are beyond the scope of this thesis. Modifications of the model will be discussed in more detail in the next chapter. A theoretical treatment of time resolution of scintillation detectors, published by Sigfridsson[37] in September of 1967, also predicts an optimum photoelectron detection level.

CHAPTER V

SUMMARY AND SUGGESTIONS FOR FURTHER STUDY

I. SUMMARY

The statistical concepts needed to describe the timing characteristics of a photomultiplier-scintillator system have been presented. The idea of characterizing the system by its response to a single photon was presented in Chapter II. To emphasize this idea, a simple single-exponential system was studied in detail. Such a system consists of a scintillation event being detected and amplified by an ideal photomultiplier. The procedure was presented in Chapter II, Section II, for obtaining an unbiased estimator which contains all the information about the initial time of such a scintillation event.

In Chapter II the photon transit time distribution was calculated by means of a Monte Carlo computer program. The calculations revealed some interesting points about the time distribution. In general the distribution was found to closely approximate an exponential in time with a variance independent of the crystal diameter but linearly dependent on the height of the crystal. The variance in the time distribution was found to increase by a factor of two as the ratio of the indices of refraction of the crystal to the photomultiplier window was decreased from 0.98 to 0.89. This illustrates the need for an almost perfect optical match at the exit interface to obtain good timing. The variance

was found to be less for the nonspecular surface condition than for a specular surface with a nonspecular backing.

In Chapter III the photomultiplier's response to a single photon was investigated. This included measuring the transit time from cathode to the anode for several photoelectron generation points on the cathode. The transit time as a function of distance from the center of the cathode was transformed to a probability per unit time that a photoelectron would be delayed a time t. In order to make this transformation a knowledge of the spatial distribution of photons on the cathode was necessary. This information was obtained from the calculation of the photon transit time inside the crystal. The resulting distribution in time was approximated by the sum of two exponentials.

Also in Chapter III the photoelectron transit time variation, excluding the cathode geometry effect, was investigated. The single electron transit time distribution between the cathode and anode was measured for two types of photomultipliers. For both types of photomultipliers the distribution had the same general shape. Since it is very difficult to separate the cathode-to-first dynode transit time variations from the transit time variation between dynodes, a calculation was made to determine the relative contribution of the two sections to the overall time variance. With the assumption that the first dynode stage has a mean gain of four, the contribution of the first to second dynode transit time to the total transit time variance was calculated to be approximately 15 percent. Also in Chapter III an experimental technique was described which makes it very convenient to measure the photoelectron yield from

a NaI(Tℓ) scintillator. Using this technique a typical measured yield for the RCA-8575 photomultiplier was 5.8 photoelectrons per keV, and for the XP-1020 was 2.4 photoelectrons per keV.

In Chapter IV all the investigated sources of single electron time-variance were convoluted to obtain a probability density function for the entire system. After the rather complex density function was derived for single electron events, the statistical order equation developed in Chapter II was applied to determine the distribution of the time ordered pulses appearing at the anode of the photomultiplier. For a specified set of system parameters and a particular photoelectron level, the final equation is the probability-per-unity time that the photoelectrons will be detected at the anode at time t. Therefore, the width of the distribution is a measure of the time resolution of the system for the conditions specified.

The results of the calculations for five important system parameters are presented. The transit time difference due to cathode geometry has the least influence on the time resolution of any of the five parameters considered. The transit time spread between cathode and anode contributes more than any other single parameter. Changing the crystal height from 1 inch to 4 inches causes approximately a 30 percent decrease in the time resolution. The time resolution as a function of photoelectron level was shown to exhibit an optimum at a j/R of approximately 0.15 percent. The effect of the optimum is shown to increase as the total number of photoelectrons increase and as the scintillation decay time of the crystal decreases. The time resolution is shown to

be strongly influenced by the photocathode yield or the number of photoelectrons produced in a scintillation event. The resolution varies as $R^{-0.41}$ compared to the theoretical limit of R^{-1} for a single exponential distribution.

Several experiments were performed to determine the accuracy of the calculations. In Chapter IV the measured time resolution as a function crystal height was shown to agree, with only slight error, with the calculations. The most comforting part of this experiment was that the calculated shapes of the time distributions agreed very well with the measured distributions. The time resolution was measured for several photoelectron levels and found to agree in general with the calculations although the accuracy was not expected to be very good. The resolution as a function of the number of photoelectrons produced was also measured and found to agree extremely well with the calculations except for a slope that is slightly too large.

II. SUGGESTIONS FOR FURTHER STUDY

The calculations using the proposed model has been shown to describe the NaI(Tℓ) scintillator-photomultiplier system with acceptable engineering accuracy. When the scintillator decay time is reduced to a nanosecond or slightly larger, the photoelectrons will appear at the anode two orders of magnitude closer together than they do for a NaI(Tℓ) event. For this reason, the identification of the photoelectron level becomes impossible with the speed of existing photomultipliers and electronic discriminators. In such a case the time resolution at any

photoelectron level is expected to be strongly influenced by both the amplitude and time spread of nearby photoelectrons. Thus, the most needed extension is to include in the present model the influence of the single electron pulse shape. This can be done by measuring the transit time distribution in time and in amplitude. The result would be a two dimensional statistical analysis of the system which would apply to any type of signal processing at the anode of the photomultiplier.

In Chapter II a procedure was presented to determine whether or not a particular measurement contained all the information about the initial time of the scintillation event. It was found that all such information was contained in the measurement of the arrival time of the first photoelectron for a system that could be described by single exponential distribution function. For a more complex system, such as the one of Chapter IV, all the time information is not contained in the first photoelectron. In fact, even the best single time measurement is not at the first photoelectron. The necessary question to ask is how much time information is contained in such a complex distribution with no constraints on the processing. The solution will probably suggest either multiple time sampling of an event or nonlinear processing or possibly a combination of the two. A study in this area would, no doubt, be very profitable in the field of fast timing.

The third and final suggestion for further study pertains to the crystal shape and boundary conditions. As was pointed out by the calculations in Chapter II, a crystal with only a nonspecular surface has better time characteristics than a crystal with a specular surface and

a nonspecular backing. Experiments should be devised to determine the validity of this calculation and also determine the optimum shape of the crystal.

LIST OF REFERENCES

LIST OF REFERENCES

1. J. B. Marion and J. L. Fowler, Fast Neutron Physics, Part I, Interscience Publishers, Inc., New York, 1960.

2. E. R. Rae and E. M. Bowery, Proc. Phys. Soc. (London) 66A, 1073 (1953).

3. R. B. Day and D. A. Lind, Bull. Am. Phys. Soc. 2, 32 (1957).

4. L. E. Beghian, G. H. R. Kegel, and R. P. Scharenberg, "Fast Sodium Iodide Spectrometer and Its Application to Millimicrosecond Time Measurement," Rev. Sci. Instr. 29, 753-757 (Sept. 1958).

5. G. H. Narayan and J. R. Prescott, "Line-widths in NaI(Tℓ) Scintillation Counters for Low Energy Gamma-Rays," NS-13 (3), 132-137 (June 1966).

6. Harshaw Scintillation Phosphors, Second Edition, The Harshaw Chem. Co., 1962.

7. R. Nutt and J. A. Biggerstaff, "A Gamma-Ray Detector Using an Array of NaI(Tℓ) Scintillators," Instrumentation and Controls Division Annual Progress Report, ORNL-4219, 1-3 (1967).

8. L. G. Hyman, R. M. Schwarcz and R. A. Schluter, "Study of High Speed Photomultiplier Systems," Rev. Sci. Instr. 35, 393-406 (March 1964).

9. E. Gatti and V. Svelto, "Theory of Time Resolution in Scintillation Counters," Nucl. Inst. and Meth., 4, 189-201 (April 1959).

10. M. A. El-Wahab and J. V. Kane, "An Analytic Treatment for Scintillation Counter Time Resolution Functions," Nucl. Instr. and Meth. 15, 15-22 (November 1962).

11. E. Gatti and V. Svelto, "Revised Theory of Time Resolution in Scintillation Counters," Nucl. Instr. and Meth. 30, 213-223 (May 1964)

12. J. H. Hammersley, Monte Carlo Method, John Wiley and Sons, New York; Methuem, London, 1964.

13. W. J. Price, Nuclear Radiation Detection, McGraw Hill Book Co. New York, 1964.

14. L. M. Bollinger and G. E. Thomas, "Measurement of the Time Dependence of Scintillation Intensity by a Delayed-Coincidence Method," Rev. Sci. Instr. 32, 1044 (1961).

15. F. J. Lynch, "Improved Timing with NaI(Tℓ)," IEEE TRANS. on Nucl. Sc. NS-13 (3), 140-147 (1966).

16. W. J. Van Sciever, "Energy Transfer and the Role of Thallium Dimers in the NaI(Tℓ) Scintillation Process." IEEE TRANS. on Nucl. Sc. NS-3 (4), 39 (1956).

17. S. S. Wilks, Mathematical Statistics, John Wiley & Sons, New York, 1962.

18. R. V. Hogg, and A. T. Craig, Introduction to Mathematical Statistics, Second Edition, The Macmillan Company, New York, 1965.

19. R. Post, "Resolving Time of Scintillator Counters," Nucleonics, 10 (6), 56 (Jan. 1952).

20. M. Cocchio and A. Roto, "Light Collection on a Photocathode from a Cylindrical Scintillator," Nucl. Instr. and Meth. 46, 136-140 (April 1966).

21. J. Braunsfurth and H. J. Korner, "Resolving Time Properties of NaI Scintillators," Nucl. Instr. and Meth. 34, 140-150 (March 1965).

22. V. O. Vyazemskiy, I. I. Lomonosov, A. N. Pisarevskiy, Kh. V. Protopopov, V. A. Ruzin, and E. D. Teterin, Stsintillyatsionnyi Metod V Radiometrii, State House for Atomic Energy Gosatomizdat, Moscow, 1961.

23. G. Pietri, "Progress in Photomultiplier Tubes for Scintillation Counting and Nuclear Physics," IRE TRANS. on Nucl. Sc., NS-9 (3), 150-156 (Sept. 1962).

24. G. Bertolina, V. Mandl, A. Rota and M. Cocciti, "Time Resolution Measurements with the XP1020 Photomultiplier" Nucl. Instr. and Meth. 42, 109-117 (January 1966).

25. G. Bertonin, M. Coochi, V. Mandl and A. Rota, "Time Resolution Measurements with Fast Photomultipliers" IEEE TRANS. on Nucl. Sc. NS-13 (3), 119-126 (June 1966).

26. Q. A. Kerns, F. A. Kirsten and G. C. Cox, "Generator of Nanosecond Light Pulses for Phototube Testing," Rev. Sci. Instr. 30, 31-36, (Jan. 1959).

27. M. Birk, Q. A. Kerns and R. F. Tusting, "Evaluation of the C-70045A High-Speed Photomultiplier," unpublished UCRL Report, 11147 (Feb. 1964).

28. R. Nutt, "Optimum Design of Sensitive Tunnel Diode Discriminators," IEEE TRANS. on Nucl. Sc. NS-14 (1), 110-115 (Feb. 1967).

29. G. R. Kerns, "Photomultiplier Single-Electron Time Spread Measurements," IEEE TRANS. on Nucl. Sc. NS-14 (1), 449-554 (Feb. 1967).

30. P. Onno and R. E. Bell, "Dependence of Line Widths of Scintillation Counters on Integrating Time Constant," Nucl. Instr. and Meth. 17, 149-150 (June 1962).

31. C. J. Borkowski and R. L. Clark, "Gamma-Ray Energy Resolution with NaI(Tℓ) Scintillation Spectrometers," Rev. of Sc. Instr. 24, 1046-1050 (June 1953).

32. J. B. Birks, Theory and Practice of Scintillation Counting, Macmillan Company, New York, 1964.

33. A. Houdayer, S. K. Mark, and R. E. Bell," Direct Measurement of the Primary Photoelectron Yield in Sodium Iodide Scintillation Counters," Nucl. Instr. and Meth. 59, 319-321 (Nov. 1968).

34. G. Present, A. Schwarzschild, I. Spirn and N. Wotherspoon, "Fast Delayed Coincidence Technique: The XP1020 Photomultiplier and Limits of Resolving Times Due to Scintillator Characteristics," Nucl. Instr. and Meth. 31, 71-76 (Jan. 1964).

35. E. Gatti and V. Svelto, "Review of Theories and Experiments of Resolving Time with Scintillation Counters," Nucl. Instr. and Meth. 43 (1), 248-268 (March 1966).

36. ORTEC Catalog 1001, Pg. 110-111.

37. B. Sigfridsson, "Theoretical Analysis of Time Resolution in Scintillation Detectors," Nucl. Instr. and Meth. 54, 13-28 (Sept. 1967).

APPENDIXES

APPENDIX A

CALCULATION OF THE VARIANCE OF THE Jth PHOTOELECTRON FOR A SINGLE EXPONENTIAL DISTRIBUTION FUNCTION

The variance of the (j+1)th photoelectron is given by,

$$\sigma^2_{j+1} = (\overline{t^2_{j+1}}) - (\bar{t}_{j+1})^2 \quad . \tag{92}$$

As was defined in the development of $\bar{t}$ let,

$$x_{j+1} = \frac{1}{\tau} t_{j+1} \quad , \tag{93}$$

so that,

$$\sigma^2_{j+1} = \tau^2 \left[\overline{x^2_{j+1}} - (\bar{x}_{j+1})^2 \right] \quad . \tag{94}$$

Since the mean $\bar{x}$ has already been calculated and is given by Eq. (25), it is necessary only to calculate the second moment $(\overline{x^2_{j+1}})$. By definition

$$\overline{x^2_{j+1}} = \int_0^\infty x^2 \, g_{j+1}(x_{j+1}) dx \quad . \tag{95}$$

The distribution $g_{j+1}(x_{j+1})$ is obtained from Eq. (16) by replacing j with j+1 and t/τ with X_{j+1}. Eq. (95) becomes

$$\overline{X^2_{j+1}} = \frac{R!}{(j-1)!(R-j)!\tau} \int_0^\infty X^2_{j+1}\, e^{-(R-j)x_{j+1}} \left(1 - e^{-X_{j+1}}\right)^j dx$$

$$= \frac{R!}{(j-1)!(R-j)!\tau} \int_0^\infty X^2_{j+1}\, e^{-RX_{j+1}} \left(e^{X_{j+1}} - 1\right)^j dx$$

$$= \frac{1}{A(R,j)} \int_0^\infty X^2_{j+1}\, e^{-RX_{j+1}} \left(e^{X_{j+1}} - 1\right)^j dx$$

$$= \frac{C(R,j)}{A(R,j)} \quad , \tag{96}$$

where,

$$C(R,j) = \int_0^\infty X^2_{j+1}\, e^{-RX_{j+1}} \left(e^{X_{j+1}} - 1\right)^j dx \quad , \tag{97}$$

and

$$A(R,j) = \frac{\tau(j-1)!(R-j)!}{R} \quad . \tag{98}$$

The integral $C(R,j)$ can be expressed as

$$C(R,j) = \int_0^\infty X^2 \left(e^X - 1\right)^j e^{-RX} dx \quad . \tag{99}$$

The subscripts are dropped in Eq. (99) since they are not needed. Integrating by parts yields,

$$C(R,j) = X^2(e^X - 1)^j\left(\frac{-1}{R} e^{-RX}\right)\Big|_0^\infty + \frac{2}{R}\int_0^\infty X(e^X - 1)^j\, e^{-RX} dx +$$

$$+ \frac{j}{R}\int_0^\infty X^2 \left(e^X - 1\right)^{j-1} e^{-(R-1)X} dx \quad ,$$

$$C(R,j) = \frac{2}{R} B(R,j) + \frac{j}{R} C(R-1,j-1) \quad , \tag{100}$$

where $B(R,j)$ is defined in Eq. (20). Eq. (100) can be further expanded by integrating $C(R-1,j-1)$ by parts. The result is

$$C(R,j) = \frac{2}{R} B(R,j) + \frac{j}{R} \left[\left(\frac{2}{R-1}\right) B(R-1,j-1) + \frac{j-1}{R-1} C(R-j,j-2) \right]$$

$$= 2 \left\{ \frac{B(R,j)}{R} + \frac{j}{R(R-1)} B(R-1,j-1) + \frac{j-1}{2(R-1)} C(R-1,j-1) \right\} \quad . \tag{101}$$

If the procedure outlined between Eq. (99) and (101) is repeated j times,

$$C(R,j) = 2 \left\{ \frac{B(R,j)}{R} + \frac{j}{R(R-1)} B(R-1,j-1) + \ldots + \frac{j!(R-k-1)!}{(j-k)!R!} B(R-k,j-k) \right.$$

$$\left. + \ldots + \frac{1}{2} \frac{j!}{R!} (R-j)! \, C(R-j,0) \right\} \quad . \tag{102}$$

But,

$$C(R-j,0) = \int_0^\infty X^2 \, e^{-(R-j)X} \, dx \quad .$$

Also by Eq. (23),

$$B(R,j) = A(R,j) \sum_{P=0}^{j} \frac{1}{R-P} \quad . \tag{23}$$

Substituting (R-1) for R and (j-1) for j in Eq. (23) yields,

$$B(R-1,j-1) = A(R,j) \sum_{P=0}^{j-1} \frac{1}{R-P-1} \quad . \tag{103}$$

Also, if (R-k) and (j-k) are substituted for R and j respectively in Eq. (23), the result is

$$B(R-k,j-k) = A(R,j) \sum_{P=0}^{j-k} \frac{1}{R-P-k} \quad . \tag{104}$$

The expression C(R,j) given by Eq. (102) can be expressed as,

$$C(R,j) = 2 \sum_{k=0}^{j} \left[B(R-k,j-k) \frac{j!(R-k-1)}{(j-k)!R!} \right]$$

$$= 2 \sum_{k=0}^{j} B(R-k,j-k) \frac{1}{(R-k)} \quad . \tag{105}$$

Substituting Eq. (104) into Eq. (105) yields,

$$C(R,j) = 2A(R,j) \sum_{k=0}^{j} \left[\left(\frac{1}{R-k}\right) \sum_{p=k}^{j} \frac{1}{R-P} \right] \quad . \tag{106}$$

The ratio of C(R,j) to A(R,j) is, by Eq. (96), the second moment. Therefore,

$$\overline{X_{j+1}^2} = 2 \sum_{k=0}^{j} \left(\frac{1}{R-k}\right) \sum_{P=k}^{j} \left(\frac{1}{R-P}\right) \quad . \tag{107}$$

The time variance of the $(j+1)^{th}$ photoelectron is

$$\sigma^2_{j+1} = \tau^2 \left[\overline{X^2_{j+1}} - (\overline{X}_{j+1})^2 \right] . \tag{108}$$

Combining Eq. (25) of the text with Eq. (107) and (108) yields

$$\sigma^2_{j+1} = \tau^2 \left\{ \left[\sum_{k=0}^{j} \left(\frac{1}{R-k}\right) \sum_{P=k}^{j} \frac{2}{R-P} \right] - \left(\sum_{P=0}^{j} \frac{1}{R-P} \right)^2 \right\}$$

$$= \tau^2 \left\{ \sum_{k=0}^{j} \left[\frac{1}{R-k} \sum_{P=k}^{j} \frac{2}{R-P} \right] - \left[\sum_{k=0}^{j} \frac{1}{R-k} \right] \left[\sum_{k=0}^{j} \frac{1}{R-k} \right] \right\} . \tag{109}$$

The variance can be simplified by factoring Eq. (109). The result is

$$\sigma^2_{j+1} = \tau^2 \left\{ \sum_{k=0}^{j} \left[\frac{1}{R-k} \left(2 \sum_{P=k}^{j} \left(\frac{1}{R-P}\right) - \sum_{k=0}^{j} \frac{1}{R-k} \right) \right] \right\}$$

$$= \tau^2 \left\{ \sum_{k=0}^{j} \left[\frac{1}{R-k} \left(\sum_{P=k}^{j} \frac{1}{R-P} - \sum_{P=0}^{k-1} \frac{1}{R-P} \right) \right] \right\}$$

$$= \tau^2 \left\{ \sum_{k=0}^{j} \left(\frac{1}{R-k}\right)^2 \right\} . \tag{110}$$

In the limit of large R and R-j the variance can be expressed in integral form as follows:

$$\sigma^2_{j+1} = \tau^2 \int_{R-j}^{R} \left(\frac{1}{q} \right) dq = \frac{\tau^2 j}{R(R-j)} \quad . \qquad (111)$$

This expression for the variance is used in Chapter II.

APPENDIX B

COMPUTER PROGRAM LISTING FOR THE PHOTON TRANSIT TIME CALCULATIONS

The Monte Carlo program "Scatter" was written in Fortran for the IBM 360/75 Computer at Oak Ridge National Laboratory. The program computes the statistical photon path length distribution for a cylindrical crystal. The photon path length is then transformed to transit time. There are two main programs. Program number one considers the boundary to be composed of a specular surface with a nonspecular backing. Program number two considers the boundary to be a nonspecular surface only. All subroutines for the programs are also listed.

```
      PROGRAM SCATTER
C  PROGRAM ≠ 1, SIDES AND TOP ASSIGNED INDEX OF REFRACTION.
      COMMON /STATS/NANNULI,WL(50),WTLNTHS(50),TRWTS(50),NRAYS(50),
     1TWTS(50),LSQS(50),BASEWTLH,BASEWTS,KASERAYS,TBASEWTS,BASELSQS,
     2TBASEWTL
      COMMON /WORK/RAD,HT,NISO,NSOURCE,REFINDEX,XLIMIT,XO,YO,ZO,X1,Y1,Z1
     1,ALPHA,BETA,GAMMA,LNTH,DIST,WT,WTTRANS,BOTT,TOP,XLIM
      COMMON /POINT?XSOURCE,YSOURCE,ZSOURCE
      COMMON /BAR?LNTHSIZE(2000),BARSIZE,MAX
      DIMENSION AZ(500),WWT(500),DS(500),AX(500),AY(500)
      DIMENSION ICO(3)
      TYPE REAL*8 LNTH,LSQS,LNTHSQ,LNTH2,LNTH3SQ
      IMPLICIT REAL*8 (A-H,O-Z)
      DATA XLIM/1 .OD-9/
    3 CONTINUE
C  RAD = CYLINDER RADIUS.  HT = CYLINDER HEIGHT.
C  REFINDEX = INDEX OF REFRACTION OF BASE.
C  XLIMIT = LOWER LIMIT ON WEIGHT.
C  ATTEN = ATTENUATION FACTOR.
C  NISO = NUMBER OF PHOTONS FROM EACH SOURCE POINT.
C  NANNULI = NUMBER OF ANNULI.
```

```
C  NSOURCE = NUMBER OF SOURCE POINTS (XO,YO,ZO).
C  BARSIZ  = BARSIZE FOR HISTOGRAM.
C  NR = NO OF TIMES TO SPIN RANDOM NO GENERATOR
      READ 9,RAD,HT,REFINDEX,XLIMIT,REFSD,NISO,NANNULI,NSOURCE,BARSIZE,
     1NR
    9 FORMAT (5D10.4,3I4,D5.2,I4)
      DO 1 I=1,NR
    1 A = FLTRNF(0)
      ZMAX=HT/2.
      DO 75 IIII=1,NSOURCE
      READ 11,XO,YO,ZO
   11 FORMAT (3D10.4)
      DO 5 K=1,50
      WTLNTHS(K)=TRWTS(K)=TWTS(K)=LSQS(K)=WL(K) = 0.
    5 NRAYS(K)=0
      BASEWTLH=BASEWTS=TBASEWTS=BASELSQS=TBASEWTL=0.
      KASERAYS=0
      RADSQ = RAD*RAD
      REFINDEY = REFSD
      NPART = 0
      AA = DARSIN(REFINDEY)
      ALPTEST = -DCOS(AA)- .02
      DSUMCUT = 0.
      NCOL = 0
      MVCT = 0
      WM = 0.
      DO 2 II=1,3
    2 ICO(II) = 0
      XSOURCE=XO
      YSOURCE=YO
      ZSOURCE=ZO
      MAX=0
      DO 12 N=1,2000
   12 LNTHSIZE(N)=0
      DO 80 M=1,NISO
      WT=1.
      J = 0
      LNTH=DIST=0.
      X1=XSOURCE
      Y1=YSOURCE
      Z1=ZSOURCE
      IC = 1
      MOVE=0
C
C  GTISO RETURNS THREE DIRECTION COSINES CHOSEN RANDOMLY
C
   10 CALL GTISO (ALPHA,BETA,GAMMA)
C
C  IF THE Z-AXIS POINT IS AT THE TOP OF THE CYLINDER GAMMA MUST BE NEG.
```

```
C
      IF (Z1 .LE. (ZMAX-XLIM))GO TO 40
   15 IF (GAMMA .GT. 0) GAMMA=-GAMMA
      GO TO 40
C
C  INTRSCT DETERMINES THE POINT OF INTERSECTION OF THE DIRECTION VECTOR
C  WITH THE CYLINDER WALL
C
   40 CALL INTRSCT
C
C  FIND NEW STASTICAL WEIGHT OF PHOTON
C
      WTTRANS = 0.0
      MOVE=MOVE+1
C
C  INCREMENT TOTAL DISTANCE TRAVELED BY SINGLE PHOTON
C
      IF(MOVE .LT. 500)GO TO 42
      MVCT = MVCT + 1
      WM = WM + WT
      ICO(IC) = (ICO(IC) + 1
      PRINT 250,X1,Y1,Z1,X0,Y0,Z0,ALPHA,BETA,GAMMA,BOTT,TOP,WT
  250 FORMAT(1H0,9E10.3,2F5.1,F8.3)
      GO TO 60
   42 DIST=DIST+  LNTH
      NCOL = NCOL +1
      IF(BASEWTS.GT.0.98) GO TO 65
C
C  IF POINT OF INTERSECTION IS ON BOTTOM OF CYLINDER CALL REFLECTX,
C  OTHERWISE CONTINUE FOLLOWING IT ON ITS MERRY WANDERINGS
C  REFLECTX COMPUTES THE ANGLES AND WEIGHTS OF THE REFLECTED AND
C  TRANSMITTED (IF ANY) RADIATION FROM THE BASE
C
   47 IF(BOTT)50,4,50
    4 IF(TOP)25,26,25
   26 SGAM = GAMMA
    6 US = X1/RAD
      VS = Y1/RAD
      GAMMA = -DABS(US*ALPHA + VS*BETA)
    8 RTEMP = REFINDEX
      REFINDEX = REFINDEY
      CALL REFLECTX
      REFINDEX=RTEMP
      IF(WTTRANS-XLIMIT)29,29,33
   33 J = J+1
      AZ(J) = Z1
      DS(J) = DIST
      WWT(J) = WTTRANS
   29 IF(WT-XLIMIT)60,60,31
   31 ALPHA = -ALPHA
```

```
      BETA = -BETA
      GAMMA - SGAM
      GO TO 40
   25 RTEMP = REFINDEX
      REFINDEX = REFINDEY
      SGAM = GAMMA
      GAMMA = -GAMMA
      CALL REFLECTX
      REFINDEX = RTEMP
      GAMMA = -SGAM
      IF(WTTRANS-XLIMIT)28,28,27
   27 J = J+1
      AX(J) = X1
      AY(J) = Y1
      AZ(J) = Z1
      DS(J) = DIST
      WWT(J) =  WTTRANS
   28 IF(WT-XLIMIT)60,60,40
   50 CALL REFLECTX
      GO TO 28
   60 IF(J)65,65,11
   11 Z1 = AZ(J)
      IF(Z1.LE.(ZMAX-XLIM))GO TO 999
      X1 = AX(J)
      Y1 = AY(J)
  998 CALL GTISO(ALPHA,BETA,GAMMA)
      IF(GAMMA.GT.0.0)GAMMA = -GAMMA
      IF(GAMMA.GT.ALPTEST)GO TO 998
      IC = 2
      GO TO 997
  999 X1 = RAD
      IC = 3
      Y1 = 0.0
   41 CALL GTISO(ALPHA,BETA,GAMMA)
      IF(ALPHA.GT.0.0)ALPHA = -ALPHA
      IF(ALPHA.GT.ALPTEST)GO TO 41
  997 DIST = DS(J)
      WT = WWT(J)
      NPART = NPART + 1
      MOVE = 1
      J = J-1
      GO TO 40
   65 CALL XOUT
   80 CONTINUE
   70 CALL STATOUT
      PRINT 100,NCOL,NPART
  100 FORMAT(1HO,6HNCOL =,I8,5X,7HNPART =,I8)
   75 PRINT 101,MVCT,WM,(ICO(I),*=1,3)
  101 FORMAT(1HO,I10,E12.4,3I10)
      GO TO 3
      END
```

```
      PROGRAM SCATTER
C  PROGRAM ≠ 2, ISOTROPIC.
      COMMON /STATS/NANNULI,WL(50),WTLNTHS(50),TRWTS(50),NRAYS(50),
     1TWTS(50),LSQS(50),BASEWTLH,BASEWTS,KASERAYS,TBASEWTS,BASELSQS,
     2TBASEWTL
      COMMON /WORK?RAD,HT,NISO,NSOURCE,REFINDEX,XLIMIT,XO,YO,ZO,X1,Y1,Z1
     1,ALPHA,BETA,GAMMA,LNTH,DIST,WT,WTTRANS,BOTT,TOP,XLIM
      COMMON /POINT/XSOURCE,YSOURCE,ZSOURCE
      COMMON /BAR/LNTHSIZE(2000),BARSIZE,MAX
      TYPE REAL*8 LNTH,LSQS
      IMPLICIT REAL*8 (A-H,O-Z)
      DATA XLIM/1.0D-9/
    3 CONTINUE
C  RAD = CYLINDER RADIUS.  HT = CYLINDER HEIGHT.
C  REFINDEX = INDEX OF REFRACTION OF BASE.
C  XLIMIT = LOWER LIMIT ON WEIGHT.
C  ATTEN = ATTENUATION FACTOR.
C  NISO = NUMBER OF PHOTONS FROM EACH SOURCE POINT.
C  NANNULI = NUMBER OF ANNULI.
C  NSOURCE = NUMBER OF SOURCE POINTS (XO,YO,ZO).
C  BARSIZE = BARSIZE FOR HISTOGRAM.
      READ 9,RAD,HT,REFINDEX,XLIMIT,ATTEN,NISO,NANNULI,NSOURCE,BARSIZE
    9 FORMAT (5D10.4,3I4,D5.2)
      ZMAX=HT/2.
      DO 70 I=1,NSOURCE
      READ 11,XO,YO,ZO
   11 FORMAT (3D10.4)
      DO 5 K=1,50
      WTLNTHS(K)=TRWTS(K)=TWTS(K)=LSQS(K)=WL(K) = 0.
    5 NRAYS(K)=0
      BASEWTLH=BASEWTS=TBASEWTS=BASELSQS=TBASEWTL=0.
      KASERAYS=0
      XSOURCE=XO
      YSOURCE=YO
      ZSOURCE=ZO
      MAX=0
      DO 12 N=1,2000
   12 LNTHSIZE(N)=0
      DO 60 M=1,NISO
      WT=1.
      LNTH=DIST=0.
      X1=XSOURCE
      Y1=YSOURCE
      Z1=ZSOURCE
      MOVE=0
C
C  GTISO RETURNS THREE DIRECTION COSINES CHOSEN RANDOMLY
C
   10 CALL GTISO (ALPHA,BETA,GAMMA)
```

```
C
C  IF THE Z-AXIS POINT IS AT THE TOP OF THE CYLINDER GAMMA MUST BE NEG.
C
      IF (Z1 .LE. (ZMAX-XLIM))GO TO 17
   15 IF (GAMMA .GT. 0) GAMMA=-GAMMA
      GO TO 40
C
C  IF INITIAL MOVE FROM SOURCE POINT JUMP TO INTRSCT
C
   17 IF (MOVE .EQ. 0) GO TO 40
C
C  OTHERWISE IN ORDER TO BE CERTAIN DIRECTION CHOSEN IS BACK INTO THE
C  CYLINDER, AFTER FINDING LENGTH OF CORD, CHOSE THE POINT (RADIUS,0,Z1)
C  AS THE NEW INTERSECTION POINT AND MAKE THE CHOSEN ALPHA NEGATIVE
C
   20 X1=RAD
      Y1=0.
      IF (ALPHA .GT. 0) ALPHA =-ALPHA
C
C  INTRSCT DETERMINES THE POINT OF INTERSECTION OF THE DIRECTION VECTOR
C  WITH THE CYLINDER WALL
C
   40 CALL INTRSCT
C
C  FIND NEW STASTICAL WEIGHT OF PHOTON
C
      MOVE=MOVE+1
      WT=WT-WT*ATTEN*LNTH
C
C  INCREMENT TOTAL DISTANCE TRAVELED BY SINGLE PHOTON
C
      DIST=DIST+WT*LNTH
C
C  IF WEIGHT IS LESS THAN LOWER TOLERANCE FORGET ABOUT THIS PHOTON
C
      IF (WT .LT. XLIMIT) GO TO 60
C
C  IF POINT OF INTERSECTION IS ON BOTTOM OF CYLINDER CALL REFLECTX,
C  OTHERWISE CONTINUE FOLLOWING IT ON ITS MERRY WANDERINGS
C
   47 IF (BOTT .NE. 1) GO TO 10
C
C  REFLECTX COMPUTES THE ANGLES AND WEIGHTS OF THE REFLECTED AND
C  TRANSMITTED (IF ANY) RADIATION FROM THE BASE
C
   50 CALL REFLECTX
      IF (WT .GE. XLIMIT) GO TO 40
C
C  XOUT AND STATOUT THE STATISTICAL OUTPUT
C
```

```
   60 CALL XOUT
   70 CALL STATOUT
      GO TO 3
      END



      SUBROUTINE INTRSCT
C
C.....................................................................
C
C  INTRSCT DETERMINES THE INTERSECTION OF A LINE AND A FINITE CYLINDER
C
C.....................................................................
C
      COMMON /WORK/RAD,HT,NISO,NSOURCE,REFINDEX,XLIMIT,X0,Y0,Z0,X1,Y1,Z1
     1,ALPHA,BETA,GAMMA,LNTH,DIST,WT,WTTRANS,BOTT,TOP,XLIM
      TYPE REAL*8 LNTH
      IMPLICIT REAL*8 (A-H,O-Z)
      ZMAX-HT/2.0
      CSNS1-ALPHA
      CSNS2=BETA
      CSNS3=GAMMA
      X0=X1
      Y0=Y1
      Z0=Z1
      NFLAG=0
      BOTT=TOP=0.0
      XSQRD=X0*X0
      YSQRD=Y0*Y0
      RSQRD=RAD*RAD
      RX=RSQRD-XSQRD
      RY=RSQRD-YSQRD
      IF (CSNS1   .NE. 0.0) GO TO 32
   31 X1=X0
      IF (CSNS2   .EQ. 0.0) CALL ERROR
  303 Y1=DSIGN(1.0,CSNS2  )*DSQRT(RX)
      Z1=Z0 + (CSNS3  *(Y1-Y0))/CSNS2
      GO TO 21
   32 IF (CSNS2   .NE. 0.0) GO TO 34
   33 X1=DSIGN (1,0,CSNS1  )*DSQRT(RY)
      Z1=Z0 + (CSNS3  *(X1-X0))/CSNS1
      GO TO 21
   34 AB=CSNS1  *CSNS2
      CHECK=XSQRD + YSQRD
      BSQRD=CSNS2  *CSNS2
      ASQRD=CSNS1  *CSNS1
      ASQBSQ=ASQRD + BSQRD
```

```
      SQX=AB*2.0*YO
      IF(CHECK.LT.XLIM)GO TO 35
      IF((RAD/CHECK) .LE. XLIM) TO TO 36
   35 XT-BSQRD*XO - AB*YO
      TEMP=ASQRD*RY +BSQRD*RX + SQX*XO
      TEMP1=DSQRT(TEMP)*CSNS1
   22 X1=(XT+TEMP1)/ASQBSQ
      DX=X1-XO
   24 CONTINUE
      Y1=YO + (CSNS2  *DX)/CSNS1
      Z1=ZO + (CSNS3  *DX)/CSNS1
C  CHECK DIRECTION WITH SCALAR PRODUCT
      DY=Y1-YO
      DZ=Z1-ZO
      VECTOR=DX*CSNS1  +DY*CSNS2  *DZ*CSNS3
      IF (VECTOR .GT. 0.0) GO TO 21
   37 TEMP1=-TEMP1
      NFLAG=NGLAG + 1
      IF (NFLAG .LE. 1) GO TO 22
   38 CALL ERROR
C  IF XO,YO,ZO ARE ON BOUNDARY-PERIMETER OF CIRCLE
      36 X1=((BSQRD-ASQRD)*XO-SQX)/ASQBSQ
      NFLAG=NFLAG + 1
      DX=X1-XO
      GO TO 24
   21 PLANE=Z1-ZMAX
      IF (PLANE .LE. 0.0 .AND. DABS(PLANE) .GT. (2.0*ZMAX-XLIM))GO TO 39
  300 IF ((PLANE*XLIM) .LE. 0.0) GO TO 1
  301 Z1=ZMAX
      TOP=1.0
      GO TO 23
   39 Z1=-ZMAX
      BOTT=1.0
   23 DZB=Z1-ZO
      Y1=YO + (CSNS2  *DZB)/CSNS3
      X1=XO + (CSNS1  *DZB)/CSNS3
    1 LNTH=(XO-X1)**2 +(YO-Y1)**2 + (ZO-Z1)**2
      LNTH=DSQRT(LNTH)
      RETURN
      END
```

```
      SUBROUTINE REFLECTX
C
C.....................................................................
C
C  REFLECTX DETERMINES WHAT HAPPENS WHEN A PHOTON IS INCIDENT TO THE BASE.
C  IF THE ANGLE OF INCIDENCE (MEASURED FROM THE Z-AXIS) IS GREATER THAN
C  THE CRITICAL ANGLE ALL OF THE RADIATION IS REFLECTED BACK INTO THE
C  CYLINDER.  IF THE ANGLE OF INCIDENCE IS EQUAL TO THE CRITICAL ANGLE
C  THE PHOTON IS ASSUMED LOST AND IS DROPPED.  IF THE ANGLE OF INCIDENCE
C  IS LESS THAN THE CRITICAL ANGLE PART OF THE RADIATION IS REFLECTED
C  BACK INTO THE CYLINDER AND FOLLOWED AGAIN, AND PART IS TRANSMITTED
C  THROUGH THE BOTTOM AND REGISTERS ON THE COUNTER.  THE APPROPRIATE
C  WEIGHTS OF THE REFLECTED AND TRANSMITTED RADIATION ARE COMPUTED IN
C  THIS SUBROUTINE.
C
C.....................................................................
C
      COMMON /WORK/RAD,HT,NISO,NSOURCE,REFINDEX,XLIMIT,XO,YO,ZO,X1,Y1,Z1
     1,ALPHA,BETA,GAMMA,LNTH,DIST,WT,WTTRANS,BOTT,TOP,XLIM
      TYPE REAL*8 LNTH
      IMPLICIT REAL*8 (A-H,O-Z)
      GAMMA=-GAMMA
      THETAI=DARCOS(GAMMA)
      REFANGLE = DARSIN(REFINDEX)
      ATHETA=THETAI
      IF (ATHETA .LT. 0) ATHETA=-ATHETA
      IF ( ATHETA .GT. REFANGLE) GO TO 100
      STHI = DSIN(THETAI)
      THETAT=DARSIN(STHI/REFINDEX)
      TIMTT=THETAI-THETAT
      TIPTT=THETAI+THETAT
      WTI=WT
      WT=(WT/2.0)*(DTAN(TIMTT)**2/DTAN(TIPTT)**2 + DSIN(TIMTT)**2/DSIN(T
     1IPTT)**2)
      IF ( ATHETA .EQ. REFANGLE) GO TO 100
      WTTRANS=WTI-WT
      IF(BOTT.EQ.0.0)100,2
    2 CALL OUT
  100 CONTINUE
      RETURN
      END
```

```
      SUBROUTINE OUT
      COMMON /STATS?NANNULI,WL(50),WTLNTHS(50),TRWTS(50),NRAYS(50),
     1TWTS(50),LSQS(50),BASEWTLH,BASEWTS,KASERAYS,TBASEWTS,BASELSQS,
     2TBASEWTL
      COMMON /WORK?RAD,HT,NISO,NSOURCE,REFINDEX,XLIMIT,X0,Y0,Z0,X1,Y1,Z1
     1,ALPHA,BETA,GAMMA,LNTH,DIST,WT,WTTRANS,BOTT,TOP,XLIM
      COMMON /BAR/LNTHSIZE(2000),BARSIZE,MAX
      TYPE REAL*8 LNTH,LSQS
      IMPLICIT REAL*8 (A-H,O-Z)
      RHO=DSQRT(X1*X1 + Y1*Y1)
      XANNULI=NANNULI
      RINC=RAD/XANNULI
      NULI=RHO/RINC + 1.0
      IF (NULI .GT. NANNULI) NULI=NANNULI
      DIST1 = DIST*WTTRANS
      WTLNTHS(NULI)=WTLNTHS(NULI)+DIST1
      TRWTS(NULI)=TRWTS(NULI)+WTTRANS
      NRAYS(NULI)=NRAYS(NULI)+1
      BASEWTLH=BASEWTLH+DIST1
      BASEWTS=BASEWTS+WTTRANS
      KASERAYS=KASERAYS+1
      CONTINUE
      RETURN
      ENTRY XOUT
      DO 40 I=1,NANNULI
      IF (TRWTS(I) .LE. 0.0) GO TO 40
      TWTS(I)=TWTS(I)+TRWTS(I)
      LSQS(I)=LSQS(I)+WTLNTHS(I)**2/TRWTS(I)
      WL(I)=WL(I)+WTLNTHS(I)
      TRWTS(I)=WTLNTHS(I)=0.0
   40 CONTINUE
      DBAR = BASEWTLH/BASEWTS
      K=XFIXF(DBAR/BARSIZE) + 1
      LNTHSIZE(K)=LNTHSIZE(K)+1
      IF (K .GT. MAX) MAX=K
      TBASEWTS=TBASEWTS + BASEWTS
      IF(BASEWTS.EQ.0.0) RETURN
      BASELSQS=BASELSQS =(BASEWTLH*BASEWTLH)/BASEWTS
      TBASEWTL=TBASEWTL + BASEWTLH
      BASEWTS=BASEWTLH=0.0
      RETURN
      END
```

```
      SUBROUTINE STATOUT
      COMMON /STATS?NANNULI,WL(50),WTLNTHS(50),TRWTS(50),NRAYS(50),
     1TWTS(50),LSQS(50),BASEWTLH,BASEWTS,_ASERAYS,TBASEWTS,BASELSQS,
     2TBASEWTL
      COMMON /WORK/RAD,HT,NISO,NSOURCE,REFINDEX,XLIMIT,X0,Y0,Z0,X1,Y1,Z1
     1,ALPHA,BETA,GAMMA,LNTH,DIST,WT,WTTRANS,BOTT,TOP,XLIM
      COMMON /POINT?XSOURCE,YSOURCE,ZSOURCE
      COMMON /DO/XNTHSIZE,YMAX
      COMMON /BAR?LNTHSIZE(2000),BARSIZE,MAX
      DIMENSION P(2000),SIZE(2000),XNTHSIZE(2000),DBAR(50),AVW(50),
     1SIGMAS(50),PROB(50)
      DIMENSION JOUT(2000),N(2000)
      DATA K,NOTH/1H*,1H /
      TYPE REAL*8 LNTH,LSQS
      TYPE REAL M
      IMPLICIT REAL*8 (A-H,O-Z)
      SUM=WTSQS=0.0
   23 DO 40 I=1,NANNULI
      IF (RNAYS(I) .EQ. 0) GO TO 40
   30 DBAR(I)=WL(I)/TWTS(I)
      XRAY=NRAYS(I)
      AVW(I)=TWTS(I)/XRAY
      SIGMAS(I)=(LSQS(I)/TWTS(I)=DBAR(I)**2)
      IF (SIGMAS(I) .LT. 0.0) GO TO 40
   31 SIGMAS(I)=DSQRT(SIGMAS(I))
      PROD=AVW(I)*DBAR(I)
      WTSQS = WTSQS + PROD*DBAR
   40 CONTINUE
      DBARBASE=TBASEWTL/TBASEWTS
      BASERAYS=KASERAYS
      AVWBASE=TBASEWTS/BASERAYS
      SIGBASE =       ((BASELSQS/TBASEWTS)-DBARBASE*DBARBASE)
      IF(SIGBASE.LT.  0.0) SIGBASE = 0.0
      SIGBASE = DSQRT(SIGBASE)
      PROBBASE=0.0
      DO 46 I=1,NANNULI
      PROB(I)=TWTS(I)/TBASEWTS
   46 PROBBASE=PROBBASE+PROB(I)
      WRITE (51,101) RAD,HT,REFINDEX,NANNULI,NISO,NSOURCE,XLIMIT,TBASEW
     1TS
  101 FORMAT (1H1,20HRADIUS OF CYLINDER =,F9.5,10X,20HHEIGHT OF CYLINDER
     1 =,F9.5,10X,29HINDEX OF REFRACTION OF BASE =,F8.5/1X,18hNUMBER OF
     2ANNULI =,I3,18X,19HNUMBER OF PHOTONS =,I4,16X,25HNUMBER OF SOURCE
     3POINTS =,I3/1X ,23HLOWER LIMIT ON WEIGHT =,D12.4,4X,34HTOTAL WEIGH
     4T EXISTED THROUGH BASE =,D12.4)
      WRITE (51,987)XSOURCE,YSOURCE,ZSOURCE
  987 FORMAT (1X,4HX0 =,F6.3,3X,4HY0 =,F6.3,3X,4HZ0 =,F6.3 //)
      WRITE (51,102) (I,PROB(I),DBAR(I),SIGMAS(I),NRAYS(I),AVW(I),I=1,
     1NANNULI)
```

```
102 FORMAT (1X,99HANNULUS    EXIT PROBABILITY    EFFECTIVE DISTANCE
   1 DEVIATION    ANNULAR ENERGY    WEIGHT PER EXIT//(1X,I5,8X,D12.5,
   29X,D12.5,5X,D12.5,8X,I5,11X,D12.5))
    WRITE (51,103) PROBBASE,DBARBASE,SIGBASE,KASERAYS,AVWBASE
103 FORMAT (2X,4HBASE,8X,E12.5,9X,E12.5,5X,E12.5,7X,I6,11X,E12.5)
 24 XBRAYS = NISO
    WRITE (51.7)
    DO 12 I=1,MAX
    X=I
    XNTHSIZE(I)=LNTHSIZE(I)
    SNTHSIZE(I)=XNTHSIZE(I)/XBRAYS
    JOUT(I)=XNTHSIZE(I)*100./BARSIZE
    SIZE(I)=(X-.5)*BARSIZE*XNTHSIZE(*)
    SUM=SUM+SIZE(I)
 12 P(I)=X*BARSIZE
    IF(MAX.GT.24)GO TO 11
    DO 10 I=MAX+1,24
    P(I) = 0.0
 10 XNTHSIZE(I) = 0.0
 11 IN=0
    DO 20 I=1,MAX
    IF (JOUT(I) .GT. IN) IN=JOUT(I)
 20 CONTINUE
    JSCALE=1
    IF (IN.GT. 25) JSCALE=(IN + 24)/25
    DO 500 I=1,MAX
500 N(I)=NOTH
    NAX=MAX
@$& IF (JOUT(NAX) .GE. 1) 249,248
248 NAX=NAX-1
    GO TO 247
249 CONTINUE
    IN=IN/JSCALE
    DO 250 I-1,IN
    M=IN-I+1
    DO 70 J=1,NAX
    IF (JOUT(J)/JSCALE .GE. M) N(J)=K
 70 CONTINUE
275 IF (NAX .GT. 39) GO TO 279
     IF (BARSIZE .EQ. .5) GO TO 279
    M=M8JSCALE*BARSIZE
    WRITE (51,3) P(I),XNTHSIZE(I),M,(N(J),J=1,NAX)
    GO TO 250
279 IF (NAX .GT. 79) NAX=79
    M=M*JSCALE*BARSIZE
    WRITE (51,2) P(I),XNTHSIZE(I),M,(N(J),J=1,NAX)
250 CONTINUE
    IN=IN+1
    WRITE (51,6) P(IN),XNTHSIZE(IN)
    IN=IN+1
    N=5
```

```
      IF (BARSIZE .#Q. 2.) N=10
      IF (BARSIZE .EQ. .1) N=1
      DO 9 I=1,17
    9 NRAYS(I)=(I-1)*N
      IF (BARSIZE .EQ..1) GO TO 884
      IF (BARSIZE .EQ. .5) GO TO 884
      IF (NAX .GT. 39) GO TO 883
  884 WRITE (51,1) P(IN),XNTHSIZE(IN),(NRAYS(I),I=1,8)
      GO TO 886
  883 WRITE (51,8) P(IN),XNTHSIZE(IN),(NRAYS(I),I=1,17)
  886 IN=IN+1
      DO 300 I=IN,MAX
  300 WRITE (51,5) P(I), XNTHSIZE(I)
      WRITE (51,14) SUM
    1 FORMAT (1X,F5.1,4X,F7.5,14X,6HCLASS ,8(I2,8X))
    2 FORMAT (1X,F5.1,4X,F7.5,16X,F4.1,2X,79(A1))
    3 FORMAT (1X,F5.1,4X,F7.5,16X,F4.1,3X,39(A1,1X))
    5 FORMAT (1X,F5.1,4X,F7.5)
    6 FORMAT (1X,F5.1,4X,F7.5,20X,                83H----------
     1----------                                              )
    7 FORMAT (//1X,5HCLASS,3X,9HFREQUENCY,15X,86HPER CENT----------
     1----------                                              )
    8 FORMAT (1X,F5.1,4X,F7.5,14X,6HCLASS ,17(I2,3X))
   14 FORMAT (/1X,38HSUM OF MIDPOINTS AND NUMBER IN CLASS =,E12.5)
  100 RETURN
```

```
      SUBROUTINE GTISO(U,V,W)
C  ISOTROPIC UNIT VECTOR  COVEYOU METHOD
      IMPLICIT REAL*8 (A-H,O-Z)
    1 Z=FLTRNF(Q)
      ZSQ=Z*Z
      X = (2.0*FLTRNF(0)-1.0)*.687369
      XSQ=X*X
      Y = .687369*(2.0*FLTRNF(0)-1.0)
      YSQ = Y*Y
      XYSQ=YSQ+XSQ
      D=XYSQ+ZSQ
      A = D*D-Z
      IF(A.GE.0.)GO TO 1
    2 ZD = (Z+Z)/D
      U=ZD*X
      V=ZD*Y
      W=(ZSQ-XYSQ)/D
      RETURN
      END
```

```
SUBROUTINE GTISU (U,V,W)
IMPLICIT REAL*8 (A-H,O-Z)
R = FLTRNF(0)
RHO = DSQRT(1.-R)
PHI=(2.0*FLTRNF(X)-1.0)*3.1415926536
U=RHO*DCOX(PHI)
V=RHO*DSIN(PHI)
RETURN
END
```

APPENDIX C

CALCULATION OF THE WEIGHT OF THE REFLECTED AND TRANSMITTED LIGHT OF AN UNPOLARIZED PLANE WAVE

The intensity of light reflected and refracted at an interface is needed in the calculation of photon transit times inside a cylindrical crystal. The calculation of the intensity or, for the single photon case, the weight associated with the reflected and refracted light proceeds as follows. The wave is first assumed to be polarized such that the electric field is parallel to the plane of incidence and the intensity or weight of the reflected wave is calculated. The wave is then assumed to be polarized such that the electric field is perpendicular to the plane of incidence. Since natural or unpolarized light has equal parallel and perpendicular components, the reflected weight is given by

$$W_R = \frac{1}{2} W_1 + \frac{1}{2} W_2 \quad , \tag{112}$$

where W_1 and W_2 are the reflected weights associated with the parallel and perpendicular polarized waves respectively. In Figure 49 the electric field is parallel to the plane of incidence and the magnetic field is perpendicular.

The electric and magnetic fields in the incident, the reflected, and the refracted wave trains must obey the usual boundary conditions, namely, the tangential components must be continuous across the interface. Let the maximum values of the electric and magnetic intensities

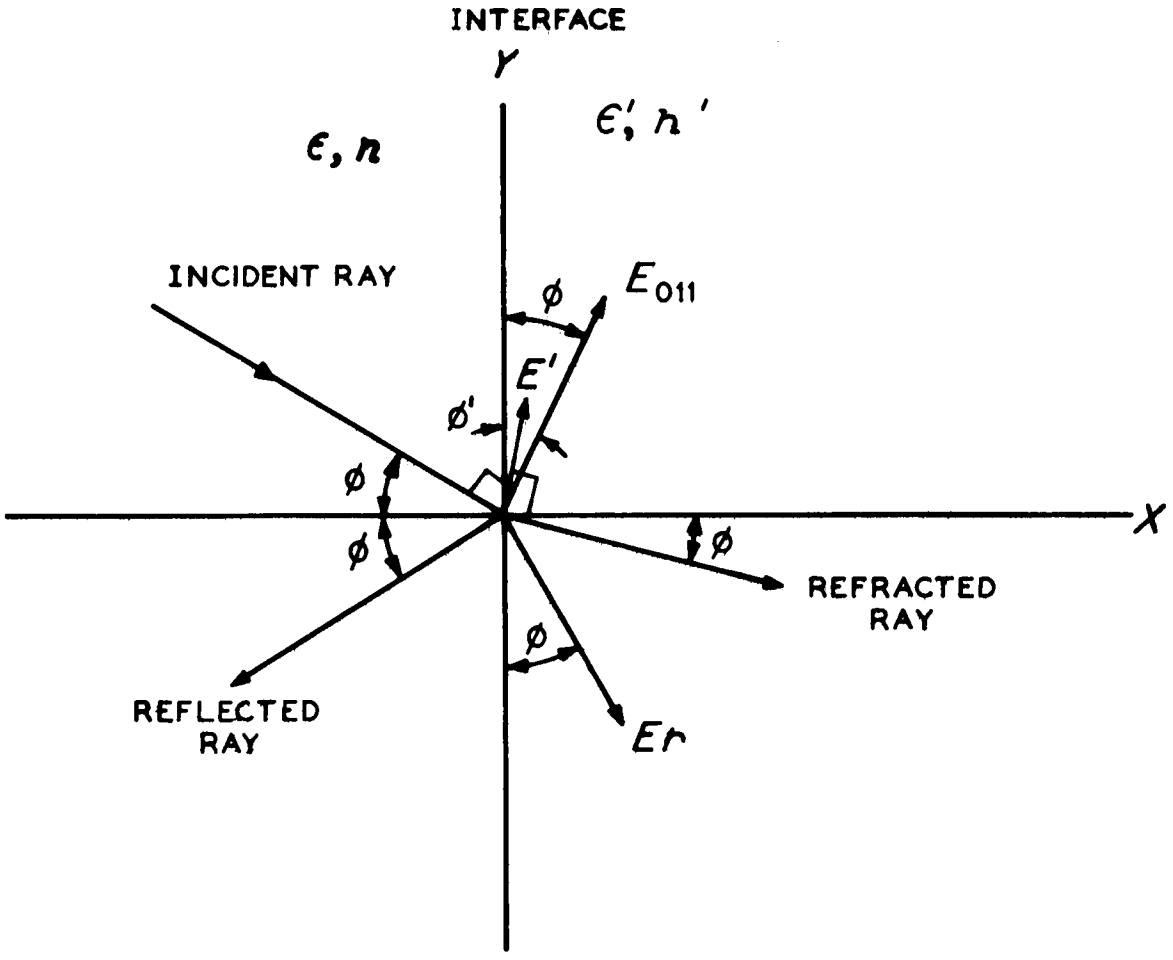


Figure 49. Reflection and refraction of a plane polarized wave with electric field parallel to the incident plane.

of the incident, reflected and refracted wave be represented by E_{o11} and H_o, E_r and H_r and E' and H' respectively. The tangential component of electric field is continuous or

$$E_{o11} \cos \phi - E_r \cos \phi = E' \cos \phi' \quad . \tag{113}$$

where the angles ϕ and ϕ' are defined in Figure 49.

The components of the magnetic field are already tangent to the interface so that

$$H_o + H_r = H' \quad . \tag{114}$$

From the general laws of electromagnetic theory, the relations between the electric and magnetic fields are,

$$\sqrt{\varepsilon}\, E_{o11} = \sqrt{\mu}\, H_o \quad ,$$

$$\sqrt{\varepsilon}\, E_r = \sqrt{\mu}\, H_r \quad ,$$

$$\sqrt{\varepsilon'}\, E' = \sqrt{\mu'}\, H' \quad . \tag{115}$$

Substituting Eq. 115 into 114 yields

$$\eta\, E_{o11} + \eta\, E_r = \eta'\, E' \quad ,$$

where

$$\eta \equiv \frac{\varepsilon}{\varepsilon_o} \quad , \text{ and } \quad \eta' \equiv \frac{\varepsilon'}{\varepsilon_o} \quad . \tag{116}$$

Another general law to be used is

$$\eta \sin \phi = \eta' \sin \phi' \quad . \tag{117}$$

Combining Eqs. 113, 116 and 117 yields,

$$E_r = \frac{\tan(\phi - \phi')}{\tan(\phi + \phi')} \; E_{o11} \quad . \tag{118}$$

Thus, for the electric field parallel to the incident plane, the ratio of reflected to incident intensity is

$$\frac{I_r}{I_{o11}} = \frac{E_r^2}{E_{o11}^2} = \frac{\tan^2(\phi - \phi')}{\tan^2(\phi + \phi')} \quad . \tag{119}$$

The development is rather elementary in electromagnetic theory, and is included here for completeness only. The development for a perpendicular electric field is very similar and will not be included. The ratio of reflected to incident intensity for the perpendicular case is

$$\frac{I_r}{I_{o\perp}} = \frac{E_r^2}{E_o^2} = \frac{\sin^2(\phi - \phi')}{\sin^2(\phi + \phi')} \quad . \tag{120}$$

As previously stated (Eq. 112) if the light is unpolarized, the perpendicular and parallel components will be equal so that

$$I_o = \frac{1}{2} I_{o\perp} + \frac{1}{2} I_{o11} \quad .$$

$$W_r = \frac{I_r}{I_o} = \frac{1}{2} \frac{\sin^2 (\phi - \phi')}{\sin^2 (\phi + \phi')} + \frac{1}{2} \frac{\tan^2 (\phi - \phi')}{\tan^2 (\phi + \phi')} \quad . \qquad (121)$$

This equation is used in the photon transit calculations (Appendix B) to determine the weight of reflected light at the interfaces of the crystal. The transmitted weight is determined by

$$W_T = 1 - W_r$$

where W_T is the transmitted weight and W_r is the reflected weight.

APPENDIX D

COMPUTER PROGRAM LISTING FOR THE PHOTOMULTIPLIER-SCINTILLATOR ORDER STATISTICS

The following computer program "Photom" was written in fortran for the IBM 1604 Computer at the Oak Ridge National Laboratory. The Program computes the distribution $g_j(t_j)$ given by Eq. (12) of the text. In addition to the calculation of $g_j(t_j)$ for a given set of system parameters, the subroutine "Half m" calculates the full-width at half maximum (FWHM) of the time distribution. The calculations are stored on magnetic tape by the IBM 1604 computer. From the tape a plot of $g_j(t_j)$ is made using a "magnetic tape plotting program" with the Control Data 160 Computer at Oak Ridge National Laboratory.

```
      PROGRAM PHOTOM
C     PHOTOMULTIPLIER CURVE DISTRIBUTION CALCULATION FOR R, NUTT/BY MOM,
      COMMON GJTJ,MAXT,FMAX,TSTEP,T,PAX,PBX,PCX,PDX,FOA,FOB,FOC,FTA,FTB,
     1FTC,FTD,S,U,V,W,TPB
      DIMENSION P(6),GJTJ(1000),X(3)
C     FIRST CARD CONTAINS TMAX,TSTEP,CUTLOW, AND CUTUP, FORMAT(4F10.0)
C     FIRST DATA CARD PUNCHED IN THIS ORDER, K,K1,TAU,H,R,AND J.
C     READ IN AS P(1) THRU P(6) FORMAT(6E10.0)
C     SECOND CARD, PZER,PSTEP,KP AND KN FORMAT(2E10.U,2I5)
C     TMAX=UPPER TIME LIMIT IN NANOSECONDS.
C     TSTEP=TIME INCREMENT IN NANOSECONDS.
C     CUTLOW=PERCENT OF FULL MAX FOR LOWER CUTOFF.
C     CUTUP=PERCENT OF FULL MAX FOR UPPER CUTOFF.
C     PZER=INITIAL VALUE OF VARIABLE.
C     PSTEP=INCREMENT OF THE VARIABLE.
C     KP=DESIGNATES WHICH P(X) IS THE VARIABLE.
C     KN=NUMBER OF TIMES VARIABLE IS TO BE INCREMENTED.
      KK=0
```

```
      READ 300,TMAX,TSTEP,CUTLOW,CUTUP
  300 FORMAT(4F10.0)
      MT=TMAX/TSTEP
C     MT MUST BE LESS THAN OR EQ. TO 1000 TO RETAIN GIVEN DIMENSION.
    1 READ 100,P
  100 FORMAT(6F10.0)
      IF(P(3))9,9,7
    7 READ 105,PZER,PSTEP,KP,KN
  105 FORMAT(2F10.0,215)
      P(KP)=PZER
      CRJ=P(5)
      DO 5 NA=1,KN
      A=2.*P(1)/((P(1)-P(4))*(P(1)-P(3)))
      B=2.*P(4)*P(4)/((P(4)-P(3))*(P(1)-2.*P(4))*(P(1)-P(4)))
      C=-2.*P(3)*P(3)/((P(4)-P(3))*(P(1)-P(3))*(P(1)-2.*P(3)))
      D=-2.*P(1)/((P(1)-2.*P(3))*(P*1)-2.*P(4)))
      F=P(1)/(P(1)-P(2))
      IF(P(4)-P(2))30,5,30
   30 G=P(4)/(P(4)-P(2))
   25 XI=P(3)/(P(3)-P(2))
      Y=P(1)/(P(1)-2.*P(2))
      DO 8 NN-1,3
      A=A*F
      B=B*G
      C=C*XI
      D=D*Y
    8 X(NN)=A+B+C+D
      XL=-X(1)/2.
      XM=-X(2)
      XN=-X(3)
C
C     AT END OF LOOP A=A*F**3, B=B*G**3,C=C8XI**3 AND D=D*Y**3
C
      XP=-XL/P(2)
      Q=-(2.*XL+XM)
      S=-A*P(1)
      U=-B*P(4)
      V=-C*P(3)
      W=-D*P(1)/2.
      R=-(1.+S+U+V+W)
      FMAX=-10.
      PAX=1,/P(1)
      PBX=1,/P(2)
      PCX=1,/P(3)
      PDX=1./P(4)
      KK=KK+1
      T=0.U
      IF(P(6)-1.01)4,4,3
    3 CRJ=CRJ*(P*5)-P(6)+1.)/(P(6)-1.)
```

```
  4 DO 50 NB=1,MT
    T=T+TSTEP
    IF(T-TMAX)20,20,21
 21 PRINT 200,KK
200 FORMAT(1HO,23HTIME DIMENSION EXCEEDED,5X,4HCASE,I4,9H DELETED.)
    GO TO 5
 20 TSQ=T*T
    CALL DSIDE(P(1),P(2),P(3),P(4))
    ALPHA=EXPF(TPB)
    FITJ=ALPHA*(TSQ*XP+Q*T)+1.-ALPHA+FOA+FOB+FOC
    IF(FITJ)35,40,45
 40 PRINT 275,KK
275 FORMAT(1HO,35(1H*),26HFITJ= ZERO, EXECUTION CASE,I4,9H DELETED.,
   135(1H*))
    GO TO 50
 35 PRINT 250,KK
250 FORMAT(1HO,25(1H*),31HWARNING--FITJ COMPUTED NEGATIVE,7H (CASE ,I3
   1,26H) SIGN CHANGED TO POSITIVE,25(1H*))
    PRINT 400,F1TJ,T,P(2),XP,Q,R,S,U,P(4),V,P(3),W,P(1),A
400 FORMAT(2(7X,7E15.5/))
    FITJ=ABSF(FITJ)
 45 F2TJ=ALPHA*(TSQ*XL/(P(2)*P(2))+T*XM/P(2))+FTA+FTB+FTC+FTD
    GJTJ(NB)=CRJ*(1,-F1TJ)**(P(5)-P(6))*F1TJ**(P(6)-1.)*F2TJ
    IF(FMAX-GJTJ(NB))10,10,11
 10 FMAX=GJTJ(NB)
    GO TO 50
 11 IF(GJTJ(NB)-CUTUP*FMAX)12,50,50
 12 MAXT=NB
    GO TO 80
 50 CONTINUE
 80 DO 60 NO=1,MAXT
    IF(GJTJ(NO)-CUTLOW*FMAX)60,65,65
 60 CONTINUE
    MINT=1
    GO TO 75
 65 MINT=NO
 75 T=MINT*TSTEP
    WRITE OUTPUT TAPE 5,101,KK,P
101 FORMAT(4HCASE,I3,3X,2HK=,F5,3,3X,3HK1=,F5,3,3X,4HTAU=,F6,1,3X,2HH=
   1,F5,3,3X,2HR=,F6,1,3X,2HJ=,F5,1)
    WRITE OUTPUT TAPE 5,102,FMAX,T,TSTEP
102 FORMAT(3F10.4)
    CALL HALFM(KK)
    WRITE OUTPUT TAPE 5,104,(GJTJ(IA),IA=MINT,MAXT)
104 FORMAT(8F10.4)
    WRITE OUTPUT TAPE 5,125
125 FORMAT(3H-1.)
  5 P(KP)=P(KP)+PSTEP
    GO TO 1
  9 END FILE 5
```

```
      END FILE 5
      REWIND 5
      CALL EXIT




      SUBROUTINE HALFM(KK)
      COMMON G,J,FMAX,TSTEP
      DIMENSION G(1000)
      HMAX=FMAX/2.
      DO 3 L=1,J
      IF(G(L)-HMAX)3,4,5
    3 CONTINUE
      PRINT 100,KK
  100 FORMAT(//47X,20HERROR IN HALFM, CASE,I3)
      RETURN
    4 TONE=TSTEP*L
      GO TO 9
    5 TU=TSTEP*L
      TL=TSTEP*(L-1)
      B=(G(L)-G(L-1))/(TU-TL)
      A=G(L)-B*TU
      TONE=(HMAX-A)/B
    9 M=J+1
      DO 6 N=1,J
      M=M-1
      IF(G(M)-HMAX)6,7,8
    6 CONTINUE
      PRINT 101,KK
  101 FORMAT(//47X,17HHALFM ERROR, CASE,I3)
      RETURN
    7 TTWO=TSTEP*M
      GO TO 10
    8 TL=TSTEP*M
      TU=TSTEP*(M+1)
      B=(G(M+1)-G(M))/(TU-TL)
      A=G(M)-B*TL
      TTWO=(HMAX-A)/B
   10 WIDTH=TTWO-TONE
      WRITE OUTPUT TAPE 5,102,WIDTH
  102 FORMAT(28H FULL WIDTH AT HALF MAXIMUM=,F10,4,14H  NANOSECONDS.)
      RETURN
      END
```

```
      SUBROUTINE DSIDE(PA,PB,PC,PD)
      COMMON GZ,JZ,FZ,TZ,T,PAX,PBX,PCX,PDX,FOA,FOB,FOC,FTA,FTB,FTC,FTD,S
     1,U,V,W,TPB
      DIMENSION GZ(1000)
      TPA=-T/PA
      TPB=-T/PB
      TPC=-T/PC
      TPD=-T/PD
      IF(PB-PA)1,2,2
    1 FTA=S*EXPF(TPB)/PA*(EXPF(-T*(PBX-PAX))-1.)
      GO TO 3
    2 FTA=S*EXPF(TPB)/PA*(1.-EXPF(-T*(PAX-PBX)))
    3 IF(PB-PD)4,5,5
    4 BET=U*EXPF(TPD)
      BETA=EXPF(-T*(PBX-PDX))
      FTB=BET/PD*(BETA-1.)
      FOA=BET*(1.-BETA)
      GO TO 6
    5 BET=U*EXPF(TPB)
      BETA=EXPF(-T*(PDX-PBX))
      FTB=BET/PD*(1.-BETA)
      FOA=BET*(BETA-1.)
    6 IF(PB-PC)7,8,8
    7 BET=V*EXPF(TPC)
      BETA=EXPF(-T*(PBX-PCX))
      FTC=BET/PC*(BETA-1.)
      FOB=BET*(1,-BETA)
      GO TO 9
    8 BET=V*EXPF(TPB)
      BETA=EXPF(-T*(PCX-PBX))
      FTC=BET*(1,-BETA)
      FOB=BET*(BETA-1.)
    9 IF(PB-(PA/2.))10,11,11
   10 BET=W*EXPF(2.*TPA)
      BETA=EXPF(-T*(PBX-2.*PAX))
      FTD=2,*BET*(BETA-1.)
      FOC=BET*(1,-BETA)
      GO TO 12
   11 BET=W*EXPF(TPB)
      BETA=EXPF(-T*(2.*PAX-PBX))
      FTD=2.*BET*(1.-BETA)
      FOC=BET*(BETA-1.)
   12 RETURN
      END
```

```
C     MAGNETIC TAPE PLOTTING PROGRAM.
      COMMON TMIN,G,GMAX,GMIN,TITLE,WIDTH
      DIMENSION TITLE(12),WIDTH(12),X(8)
      GMIN=0.0
    1 READ INPUT TAPE 3,1,TITLE
    1 FORMAT(12A6)
      IF(XEOF(K))9,2,9
    2 READ INPUT TAPE 3,2,GMAX,TMIN,TSTEP
    2 FORMAT(3F10.4)
      GMAX=GMAX+.1*GMAX
      READ INPUT TAPE 3,1,WIDTH
      CALL LINPLT(1)
    3 READ INPUT TAPE 3,4,X
    4 FORMAT(8F10,4)
      DO 5 I=1,8
      IF(X(I))1,3,4
    4 G=X(I)
      CALL LINPLT(0)
    5 TMIN=TMIN+TSTEP
      GO TO 3
    9 X=EXITF(1)
      END
```

```
      SUBROUTINE LINPLT(N)
      COMMON AINFO,FINFO,FMAX,FMIN,TITLE,WIDTH
      DIMENSION K4(31),TITLE(12),KA(4),WIDTH(12)
      IF(FMAX-FMIN) 1000,1000,9
 1000 WRITE TYPE 100
  100 FORMAT (1HO//23HERROR SUBROUTINE LINPLT //)
      PAUSE 77
      RETURN
    9 IF (N) 1,1,2
    2 PRINT 101,TITLE
  101 FORMAT(14H1 LINEAR PLOT 12A6)
      PRINT 3,WIDTH
    3 FORMAT(2H  ,12A6)
      PRINT 4
    4 FORMAT(//14H  TIME    GJTJ/)
B   99 K4(1)=34012766
B      K4(2)=05730133
B      K4(3)=66107304
B      K4(4)=33017054
B      K4(5)=01120170
B      K4(31)=54742020
       DO 3 I=6,30
```

```
B    3 K4(I)=20202020
B      KA(1)=60202020
B      KA(2)=20602020
B      KA(3)=20206020
B      KA(4)=20202060
       RETURN
     1 IF (FINFO-FMIN) 6,7,8
     6 PRINT 102,AINFO,FINFO
   102 FORMAT(1X,F5,1,F8,4,1H*100X1H*)
       RETURN
     7 PRINT 103,AINFO,FINFO
   103 FORMAT(1X,F5,1,F8,4,1H+100X1H*)
       RETURN
     8 IF (FINFO-FMAX) 4,5,6
     5 PRINT 104,AINFO,FINFO
   104 FORMAT(1X,F5,1,F8,4,1H*100X1H+)
       RETURN
     4 PLUS=100.*(FINFO-FMIN)/(FMAX=FMIN)
       IPLUS=PLUS
       NIND=IPLUS/4+6
       NX=IPLUS-4*(NIND-6)+1
       K4(NIND)=KA(NX)
       PRINT K4,AINFO,FINFO
B      K4(NIND)=20202020
       RETURN
       END
```

VITA

Ronald Nutt was born in Hohenwald, Tennessee, on April 24, 1938. He attended elementary school in that city and was graduated from Lewis County High School in 1956. The following September he entered The University of Tennessee. While at The University of Tennessee he worked as a co-op student with the Tennessee Valley Authority. In June, 1961, he received a Bachelor of Science degree in Electrical Engineering. In the summer of 1961, he accepted a graduate assistantship at The University of Tennessee and began study toward a Master's degree. He received this degree in August, 1962. At this time he went to work for the Oak Ridge National Laboratory.

In September, 1963, he accepted a teaching position in Electronics and re-entered the Graduate School at The University of Tennessee. He has been employed at the Oak Ridge National Laboratory since September, 1965. He received the Doctor of Philosophy degree with a major in Electrical Engineering in March, 1969. At this time he assumed a position as Senior Research Engineer with ORTEC while remaining with Oak Ridge National Laboratory as a consultant. He is a member of the Eta Kappa Nu, Tau Beta Pi, and Sigma Xi.

He is married to the former Robbie Brooks of Ooltewah, Tennessee, and is the father of three children; Rhonda Gayle, Robert Eve, and Randall Keith.